Different effects of conditional Knock-Out of Stat3 on the sensory epithelium of the Organ of Corti

Unterschiedliche Auswirkungen des konditionellen Knock-Outs von Stat3 im sensorischen Epithel des Cortischen Organs

Doctoral thesis for the doctoral degree “Dr. rer. nat.”

at the Oto-Rhino-Laryngology, University Hospital Würzburg

and the Graduate School of Life Sciences, Julius-Maximilians-Universität Würzburg,

in Section **Neuroscience**

submitted by

Linda Ilse Bieniussa

from

Würzburg

Würzburg, October 2023

Submitted on: ……..……..

Office stamp

Members of the Thesis Committee

Chairperson: PD Dr. Frank Döring

Primary Supervisor: apl. Prof. Dr. med. Kristen Rak

Supervisor (Second): Prof. Dr. med. Dr. h.c. Rudolf Hagen

Supervisor (Third): apl. Prof. Dr. rer. nat. Robert Blum

Supervisor (Fourth): Prof. Dr. rer. nat. Rudolf Martini

Affidavit/Eidesstattliche Erklärung

Affidavit

I hereby confirm that my thesis entitled "**Different effects of conditional Knock-Out of Stat3 on the sensory epithelium of the Organ of Corti**" is the result of my own work. I did not receive any help or support from commercial consults. All sources and/or materials applied are listed and specified in this thesis.

Furthermore, I confirm that this thesis has not been submitted as part of another examination process neither identical nor in similar form.

Place, Date | Signature

Würzburg,

Eidestattliche Erklärung

Hiermit erkläre ich unter Eid, die vorliegende Dissertation "**Unterschiedliche Auswirkungen des konditionellen Knock-Outs von Stat3 im sensorischen Epithel des Cortischen Organs**" eigenständig, d.h. insbesondere selbstständig und ohne Hilfe eines kommerziellen Promotionsberaters angefertigt und keine anderen, als die von mir angegebenen Quellen und Hilfsmittel verwendet zu haben.

Ich erkläre außerdem, dass die Dissertation weder in gleicher noch in ähnlicher Form bereits in einem anderen Prüfungsverfahren vorgelegen hat.

Ort, Datum | Unterschrift

Würzburg, den

List of Content

1. Abstract

The mammalian cochlea detects sound in response to vibration at frequency-dependent positions along the cochlea duct. The sensory outer hair cells, which are surrounded by supporting cells, act as a signal amplifier by changing their cell length. This is called electromotility. To ensure correct electrical transmission during mechanical forces, a certain resistance of the sensory epithelium is a prerequisite for correct transduction of auditory information. This resistance is managed by microtubules and its posttranslational modification in the supporting cells of the sensory epithelium of the cochlea. Stat3 is a transcription factor, with its different phosphorylation sites, is involved in many cellular processes like differentiation, inflammation, cell survival and microtubule dynamics, depending on cell type and activated pathway. While Stat3 has a wide range of intracellular roles, the question arose, how and if Stat3 is involved in cells of the organ of Corti to ensure a correct hearing.

To test this, Cre/loxp system were used to perform conditional Knock-Out (cKO) of Stat3 in outer hair cells or supporting cells either before hearing onset or after hearing onset. Hearing performances included DPOAE and ABR measurements, while molecular were performed by sequencing. Additionally, morphological examination was used by immunohistochemistry and electron microscopy.

A cKO of Stat3 before and after hearing onset in outer hair cells leads to hearing impairments, whereas synapses, nerve fibers and mitochondria were not affected. Bulk sequencing analyzation of outer hair cells out of cKO mice before hearing onset resulted in a disturbance of cellular homeostasis and extracellular signals. A cKO of Stat3 in the outer hair cells after hearing onset resulted in inflammatory signaling pathway with increased cytokine production and upregulation of NF-kb pathway. In supporting cells, cKO of Stat3 only after hearing onset resulted in a hearing impairment. However, synapses, nerve soma and fibers were not affected of a cKO of Stat3 in supporting cells. Nevertheless, detyronisated modification of microtubules were altered, which can lead to an instability of supporting cells during hearing.

In conclusion, Stat3 likely interact in a cell-specific and function-specific manner in cells of the organ of Corti. While a cKO in outer hair cells resulted in increased cytokine production, supporting cells altered its stability due to decreased detyronisated modification of microtubules. Together the results indicated that Stat3 is an important protein for hearing performances. However, additional investigations of the molecular mechanism are needed to understand the role of Stat3 in the cells of the organ of Corti.

2. Zusammenfassung

Die Cochlea von Säugetieren nimmt Schall als Reaktion auf Vibrationen an frequenzabhängigen Positionen entlang des Cochlea-Kanals wahr. Die sensorischen äußeren Haarzellen, die von Stützzellen umgeben sind, wirken als Signalverstärker, indem sie ihre Zelllänge verändern können. Dies wird als Elektromotilität bezeichnet. Um eine korrekte elektrische Übertragung bei mechanischen Kräften zu gewährleisten, ist ein gewisser Widerstand des sensorischen Epithels eine Voraussetzung für die fehlerfreie Weiterleitung von Hörinformationen. Dieser Widerstand wird durch Mikrotubuli und deren posttranslationalen Modifikationen in den Stützzellen des sensorischen Epithels der Cochlea gewährleistet. Stat3 ist ein Transkriptionsfaktor, der an verschiedenen Phosphorylierungsstellen, sowie je nach Zelltyp und aktiviertem Signalweg an vielen zellulären Prozessen wie Differenzierung, Entzündung, Zellüberleben und Mikrotubuli-Dynamik beteiligt ist. Während Stat3 ein breites Spektrum an intrazellulären Funktionen hat, stellte sich die Frage, wie und ob Stat3 in den Zellen des Cortischen Organ einen Einfluss auf den Hörprozess hat.

Um dies zu testen, wurde das Cre/loxp-System verwendet, um Stat3 in den äußeren Haarzellen oder den Stützzellen entweder vor oder nach Hörbeginn von Mäusen konditional auszuschalten. Um das Hörvermögen zu erfassen, wurden DPOAE- und ABR-Messungen durchgeführt, während molekulare und morphologische Untersuchungen mittels Sequenzierung und Immunhistochemie durchgeführt wurden.

Eine konditioneller Knock-Out von Stat3 vor und nach dem Beginn des Hörens in äußeren Haarzellen führt zu leichten Hörschäden, während Synapsen, Nervenfasern und Mitochondrien nicht betroffen waren. Die Analyse der Sequenzierung von äußeren Haarzellen aus Mäusen mit konditionellem Knock-Out vor dem Beginn des Hörens ergab eine Störung der zellulären Homöostase und der extrazellulären Signale. Ein konditioneller Knock-Out von Stat3 in den äußeren Haarzellen nach Beginn des Hörens führte zu einem früh-entzündlichen Signalweg mit erhöhter Zytokinproduktion und der Hochregulierung des NF-κB-Wegs. In den Stützzellen führte ein kondioneller Knock-Out von Stat3 nur nach dem Beginn des Hörens zu einer Hörbeeinträchtigung. Synapsen, Nervensoma und -fasern waren jedoch von einem konditionellen Knock-Out von Stat3 in Stützzellen nicht betroffen. Dennoch war die detyronisierte Modifikation der Mikrotubuli verändert, was zu einer Instabilität der Stützzellen, insbesondere der Phalangealfortsätze, führte, was wiederum zu einer Instabilität des Epithels während des Hörvorgangs führte.

Zusammenfassend lässt sich sagen, dass ein konditioneller Knock-Out von Stat3 in Zellen des Cortischen Organs zu einer Hörstörung führte. Während ein konditioneller Knock-Out in äußeren Haarzellen eine erhöhte Zytokinproduktion zur Folge hatte, verloren die Stützzellen

ihre Zellstabilität aufgrund einer verminderten detyronisierten Modifikation der Mikrotubuli. Insgesamt deuten die Ergebnisse darauf hin, dass Stat3 ein wichtiges Protein für die Hörleistung ist. Es sind jedoch weitere Untersuchungen des molekularen Mechanismus erforderlich, um die Rolle von Stat3 in den Zellen des Corti-Organs zu verstehen.

3. Introduction

3.1. Anatomy of the cochlea

The inner ear is located in the petrous bone and consist of a bony and membranous labyrinth. It is separated in the vestibular organ and the cochlea. The vestibular organ manages the balance by sacculus and utriculus for linear accelerations, whereas the semicircular canals detect rotational accelerations. The anatomy of the cochlea is separated. The organ of hearing lies on a bony axis, the modiolus, with the membranous cochlear duct in the scala media. Together the cochlea winds 2½ times around the modiolus. The scala media is demarcated apically from the scala vestibuli by Reissner's membrane and basally from the scala tympani by the basilar membrane (Fig. 1). Scala tympani and vestibuli communicate via the helicotrema at the apical tip of the cochlea. Laterally, the cochlear duct is closed by the stria vascularis, which contains capillaries and is responsible for the production of endolymph. It actively secretes K+ ions, establishing a positive endocochlear potential of +85 mV between endolymph and perilymph. The potential between hair cells and the endolymph has a difference of 140 and 155 mV, respectively.

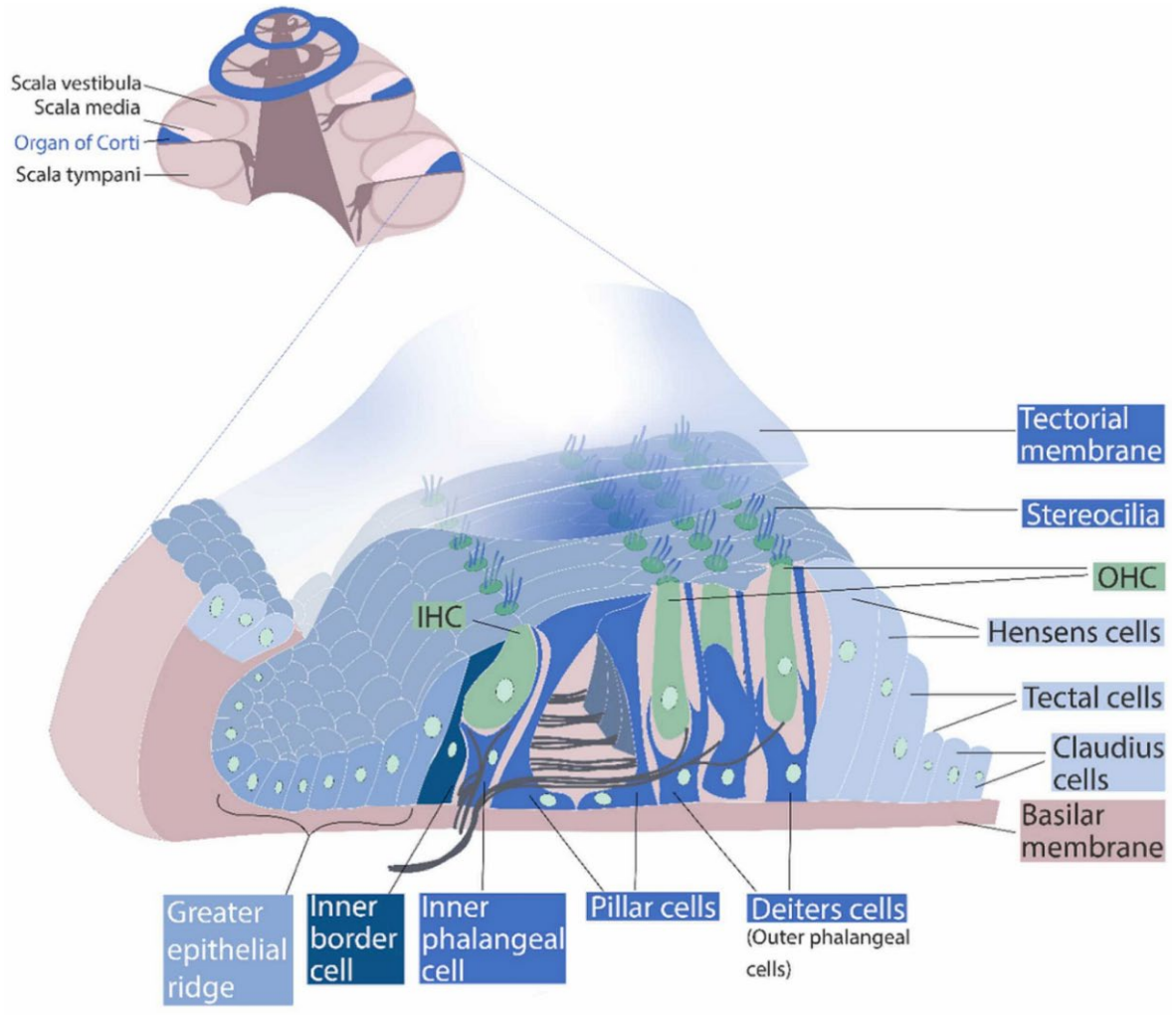

Figure 1: A schematic view of the sensory epithelium of the cochlea.

The cochlea is separated in three different regions, scala media, tympani and vestibuli. Scala vestibuli and scala tympani are filled with endolymph and is the area of the traveling wave, whereas scala media consist of perilymph and includes the organ of Corti. The organ of Corti is a specialized sensory epithelium. It transforms mechanical sound vibrations into electrical neural signals. The organ of Corti itself is placed basilary on the basilar membrane, which is a highly specialized basement membrane, and is limited apically by the tectorial membrane. The organ of Corti consists of one row of inner hair cells (IHCs) and three rows of outer hair cells (OHCs). The hair cells are surrounded by different supporting cells. Deiters cells held OHCs basally like a cup, while inner phalangeal cells brace the IHC. Pillar cells separate and support both the OHCs and the IHCs. Additionally, the organ of Corti is marked off medially by greater epithelial ridge cells and laterally by Hensen's, Tectal and Claudius cells. Adapted from Bieniussa et al. (2023).

The sound transduction takes place in the organ of Corti. Closest to the modiolus, the great epithelial gride, inner boarding cells and the inner phalangeal cells support an inner hair cells (IHC) row. Laterally followed supporting cells are the inner and outer pillar cells (IPC and OPC), which build a tunnel of Corti, where neuronal fibers crossing the tunnel of Corti to the outer hair cells (OHC). The OHCs are arranged in three rows supported by Deiter´s cells (DC). Laterally, the organ of Corti is supported by Hensen, tectal and Claudius cells (Fig. 1). DCs phalangeal process and the cuticular plate of OHCs build together the reticular lamina. On the top of hair cells, actin-rich stereocilia are arranged in bundles of 50 to 100 in increased length in lateral direction connected by tip links. Stereocilia are mobile and embedded basally in the cuticular plate (CP) (Jensen-Smith et al., 2003) and apically, the longest stereocilia are connected in the acellular gelatinous tectorial membrane (TM) (Slepecky et al., 1992).

During development, each hair cell possesses a kinocilium, which is a microtubule-based organelle built around a distinct microtubule axoneme and separated from the extensive microtubule network in the soma. In mice, microvilli and the kinocilium first appear at embryonic day (E) 13.5 and is responsible for the planar cell polarity for the arrangement of stereocilia at the cuticular plate. The development, structure and function of the kinocilium is like other mammalian primary cilia (Satir et al., 2007). Only some of the microvilli surrounding the kinocilium will enlarge and become stereocilia, whereas the remaining ones will be reabsorbed. Stereocilia grow in a defined V-shaped pattern with the kinocilium at the vertex of the "V" (Frolenkov et al., 2004; Kelly et al., 2007) on OHCs, while they form straight lines on IHCs. Kinocilia spontaneously regress postnatally, and entirely disappear until postnatal day (p) 21 (Lim et al., 1985)

3.2. Physiology of hearing

Sound enters the ear through the external auditory canal and causes the eardrum to vibrate. Via the ossicular chain (malleus, incus and stapes), the vibrations are transmitted in the middle ear and finally arrive the oval window. A pressure wave is induced in the perilymph of the scala vestibuli, which also reaches scala media and finally the round window via the elastic membranes. The basilar membrane is the only structure through which there is significant

absorption of sound energy. This changes its structure on its way apically. While it appears relatively narrow and stiff basally, it becomes broader and more flexible in the apical direction. As a result, the wave loses hardly any energy at the base and travels apically like a traveling wave. The amplitude increases to a maximum and flattens out again relatively quickly. Where the maximum occurs depends on the frequency of the incoming sound. High frequencies tend to provoke it at the base of the cochlea, low at the tip. This phenomenon of each location on the basilar membrane being associated with a single frequency is called tonotopy.

The OHCs are based between the basilar membrane and apically to the tectorial membrane. Upon input of a sound event, both membranes move and bending of the connected stereocilia occurs. As a result, mechanical tension is created on tip links, whereupon neighboring non-selective cation channels, named transduction channels, are opened without delay. Due to the endocochlear potential, K^+ ions flow into the hair cells driven by the concentration gradient and trigger depolarization. Depolarization creates a receptor potential that opens voltage-dependent L-type Ca^{2+} channels at the base of the hair cells, which in turn release the transmitter glutamate at synapses and activate auditory neurons (Knirsch et al., 2007). The K^+ ions leave the hair cells again at their base through a passive channel. OHCs are sparsely innervated by afferent fibers, where depolarization has a different effect. They contract due to depolarization and stretch upon hyperpolarization. Thus, they amplify the oscillations of the basilar membrane and make it possible for the OHC to perceive anything at all at sound pressure levels (SPL) below 70 dB (Liberman et al., 2002). Prestin, a protein of transmembrane anion transporters mediating electroneutral exchange of chloride and carbonate across the plasma membrane (Bai et al., 2009; Liberman et al., 2002; Song et al., 2010), produces the amplification. This molecular motor is several orders of magnitude faster than other motor proteins (Liberman et al., 2002) and exert lateral forces that directly influence the physical state of the plasma membrane. The process mechanically contracts and/or elongates OHCs by substitution of chloride by sulphate in the binding pocket of Prestin (Bavi et al., 2021). This process is known as electromotility. The motility generates so-called otoacoustic emissions, which can be measured with a sensitive microphone in the external auditory canal. In this way, the functionality of the OHCs can verified objectively and non-invasively.

3.3. Hearing pathway

The term central auditory pathway refers to specifically somatosensory fibers that extend from the organ of Corti to the primary and secondary auditory cortex in areas 41 and 42 of the temporal lobe (Fig. 2) (gyri temporales transversi). Spiral ganglia of the cochleae (SPG) are bipolar neurons whose processes extend centrally to the nuclei cochleares (NC) in the medulla oblongata and the nuclei olivary system (NOS) for binaural hearing. Via the lemniscus lateralis

(LL) neurons of ipsa- and contralateral side innervate the colliculi inferior (CI). From here, the nerve fibers run via the to the corpus geniculatum mediale (CGM), further to the primary and finally to the secondary auditory cortex (AC) (Fig. 2). Electrical activity of these nuclei of hearing pathway can be detected via auditory brainstem response, a brainstem electroencephalogram. Auditory brainstem response helps diagnose suspected neurologic abnormalities of the 8th cranial nerve as well as the associated auditory pathways and the estimation of hearing sensitivity (Davies, 2016; Young et al., 2020).

The cochlear nerve contains afferent and efferent neuronal fibers. Type I spiral ganglia neurons are bipolar, innervate IHCs exclusively, and account for 95% of the total afferents. The remaining 5% are pseudounipolar type II spiral ganglia and innervate OHCs. The somata of the afferent neurons are located intracochlearly and form the so-called Rosenthal canal (Moralee, 1996; Ota et al., 1980). Cholinergic efferent neuron fibres represent 95 % of the axons crossing the tunnel of Corti (Elliott et al., 2021; Simmons, 2002), the rest consists of type 2 spiral ganglion neurons (Fuchs et al., 2019; Maison et al., 2003). Therefore, OHCs are mainly innervated by myelinated MOC fibres, which belong to the descending neural auditory pathway (Simmons, 2002), which soma are located at the NOS. This area is responsible for time difference and the lateral portion measures the difference of the sound intensity. This binaural hearing not only localizes the location of the sound source, but also fades out noisy signals (Bazwinsky et al., 2003).

The NCs, separated in ventral and dorsal, contains most afferents and is tonotopically structured as the organ of Corti. While the ventral portion receives signals from the apical part of the cochlea and is thus specialized for low frequencies, fibers from the basal cochlea reach the dorsal portion and responsible for the high frequencies (Bourk et al., 1981).

The LL consists of nerve fibers from the NC, the NOS, and the nuclei of the LL itself (Fig. 2). The three nuclei lie posteriorly and are referred to as the LL ventralis, intermedius, and dorsalis based on their location (Cho et al., 2005). The function of the LL is not fully understood, but the ventral nucleus could play a role in the encoding of temporal features of auditory stimuli and the perception of speech.

The CIs form mainly from fibers of the LL and the NOS, but copies of the NCs also advance directly to this midbrain circuit site. Neurons from the NOS and NCs terminate. The CIs represent a kind of collecting station of afferents and consist of a large central, which in turn is subdivided into a dorsomedial and a ventrolateral portion, and a pericentral nucleus (Braun, 2000).

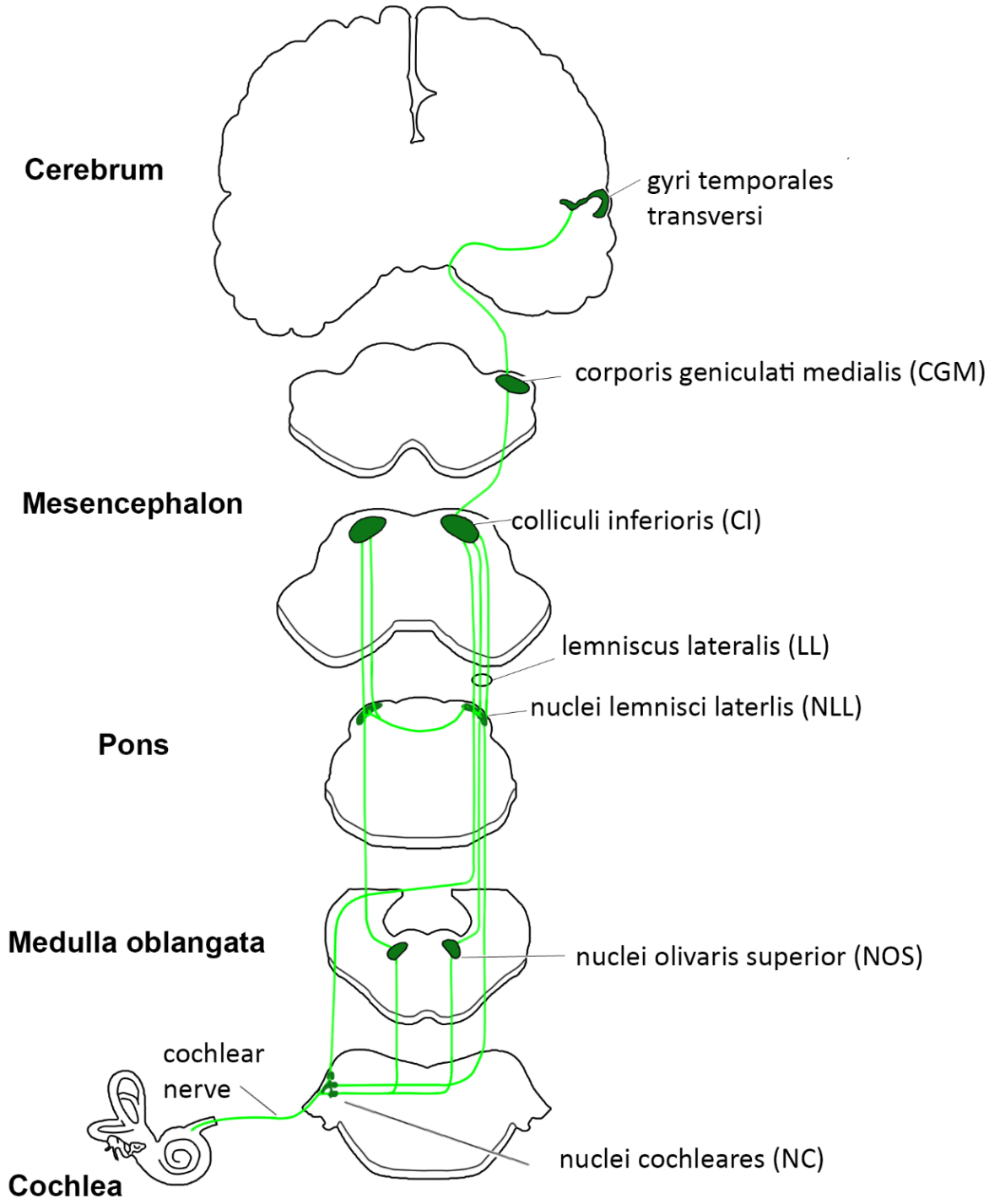

Figure 2: A schematic view of the auditory neuronal pathway.
The hearing pathway starts with the cochlear nerve in the Cochlea, which afferent nerve fibers ends in the nuclei cochleares (NC) and the efferent fibers are located in the nuclei olivaris superior (NOS) in the medulla oblangata. The ipsa- and contralateral fibers are passing the nuclei lemnisci lateralis (NLL) in Pons and innervate together as lemniscus lateralis (LL) the colliculi inferiors (CI) in the mesencephalon through the corporis geniculate medialis (CGM) to the auditory cortex in the cerebrum.

The CGM receive afferents from the CI and the LL and consists of a ventral, medial, and dorsal nucleus. The ventral nucleus, which has a clear tonotopy, projects predominantly to the primary

AC, the other two to adjacent cortical areas (Winer, 1984). Auditory cortex is in the superior temporal gyrus and is divided into a primary and secondary AC, as well as various association areas. These include the anterior, posterior, and ventroposterior areas, as well as the posterior ectosylvian cortex. Neurons in the rostral area of the primary AC respond to high frequencies, while low frequencies are detected by the caudal portion (Liem et al., 2012).

3.4. Stat3

Stat3 is a member of the family of "Signal Transducers and Activators of Transcription", knowing for its comparable DNA binding activity. Therefore, Stat3 is a transcription factor of many cellular processes including cell growth, proliferation, survival (Levy et al., 2002), but also inflammation (Yu et al., 2009), autophagy (You et al., 2015) and apoptosis (Wan et al., 2010) depending on cell types. In mature cochlea, Stat3 is highly expressed in inner and outer hair cells and Deiters cells of the organ of Corti (Wilson et al., 2014), but so far little is known about the function of Stat3 in the sensory epithelia of the cochlea.

The murine *Stat3* gene is located on Chromosome 11 from 100777632-100830447 base pairs (bp) on the minus strand in 24 exons, which mRNA is 74444 bp long. Synonyms for Stat3 are 1110034C02Rik or acute-phase response factor (Aprf).

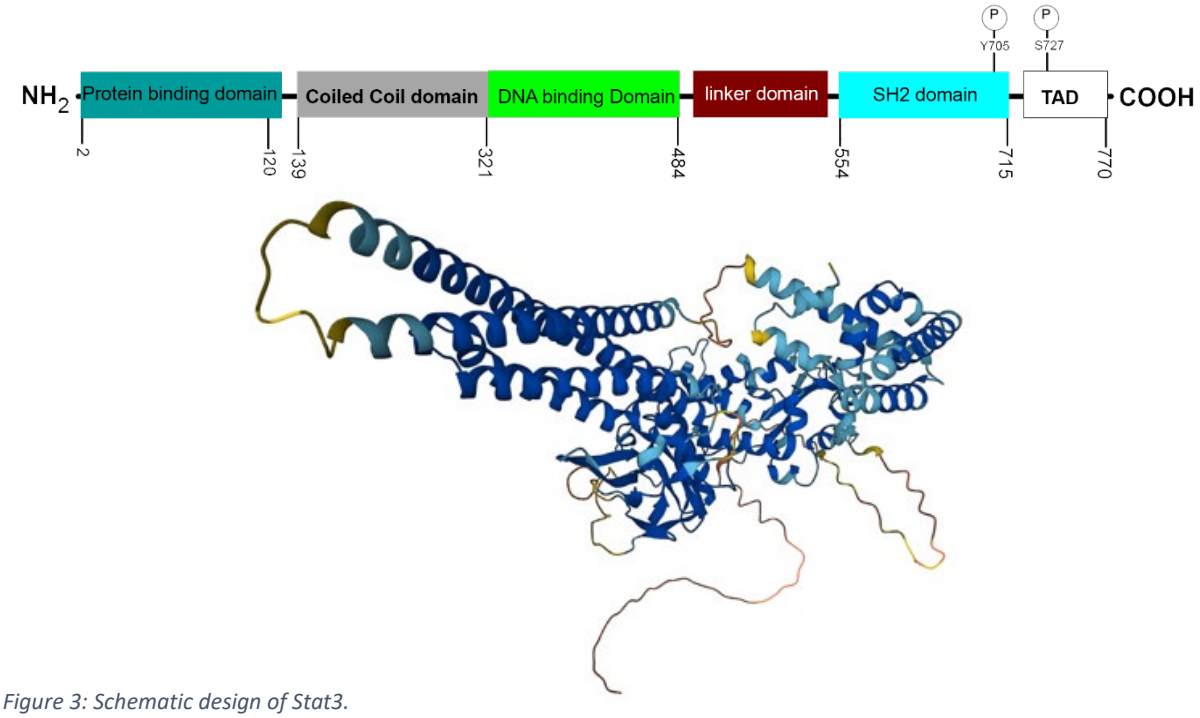

Figure 3: Schematic design of Stat3.
The protein contains a protein-protein binding domain at the N-terminal followed by a coiled coil and a DNA binding domain. After a linker domain, the SH2 domain with the phosphorylation side at tyrosine (Y) at position 705 and a C-terminal with its phosphorylation side at serine (S) 727 are ended the protein Stat3. 3D- construction was made by alphafold.

Activation of Stat3 is elicited by numerous growth factors like EGF, TGFα or IGF-1 acting through protein tyrosine kinase receptors and cytokines like IFNγ, CNTF, but mostly by IL-6. Stat3 plays an important role in IL-6 like cytokine signaling (Stahl et al., 1993; Stahl et al., 1995) via IL-6 transducing receptor chain gp130 (Boulton et al., 1995). Notable features of Stat3 are the typical DNA binding domain, an SH2 domain and a major tyrosine phosphorylation site at Y705 (pY705) as well as at S727 (pS727) (Fig. 3). Probably due to the ubiquitous and wide range of these essential roles, Stat3 has become a major therapeutic target, too. The existence of various important cellular roles, Stat3 exist a bright list of modification, which depends also on its pathway (Diallo et al., 2022). Stat3 is involved in a canonical and non-canonical pathway.

3.4.1. Stat3 as transcription factor

Stat3 is a major player in cell proliferation and differentiation, apoptosis, angiogenesis, and immunity as well as inflammation, autoimmune diseases, stroke, neurodegeneration, traumatic injury (Diallo et al., 2022). Additionally, Stat3 is crucial for several cancer subtypes and acts as a oncogene (Yu et al., 2014).

At the canonical JAK/STAT pathway, phosphorylation of Stat3 at Y705 leads to dimerization of Stat3 via intermolecular pY705-SH2 interactions and reentry in the nucleus via nuclear transport domain. In the nucleus dimerized Stat3 activates its high affinity DNA binding activity (TTCNNNGAA), where the C terminal domains is a transcriptional activation domain (Fig. 5). This DNA binding activity can be inhibited through peptide inhibitor of activated Stat3 (*PIAS3*) (Chung et al., 1997) (Fig. 4). Beside the numerous Stat target genes like *mcl-1, blc2*, and *stat3* itself, it is encoding suppressor of cytokine signaling 3 (*Socs3*) proteins were expressed acting as feedback inhibitors at the receptor level through various mechanisms (Mohr et al., 2012) (Fig. 4).

In addition to pY705-Stat3, unphosphorylated Stat3 (U-Stat3) can also serve as a transcription factor, although it expresses other genes than pY705-Stat3. Predominantly, U-Stat3 is believed to residue in the cytoplasma, while a nuclear transport is ensured with the help of importin α3 and NF-kB (Liu et al., 2005; Yang et al., 2008). U-Stat3 promotes, for example, the expression of *RANTES, MET, MRAS* and *TSD11* gene (Fig. 4) (Yang et al., 2007).

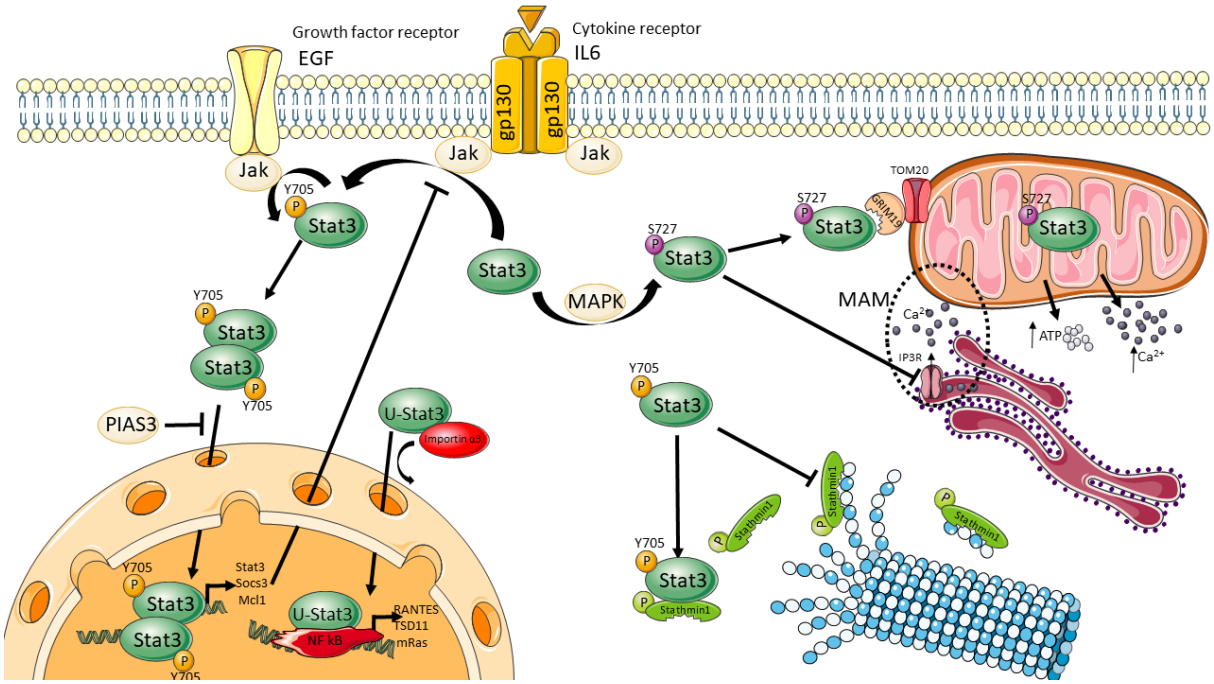

Figure 4: Stat3 pathways and interactions.

In the canonical pathway, Stat3 is phosphorylated at Tyrosine705 (Y705) by JAK, while it dimerizes and enters the nucleus to induce specific gene expression like Stat3 itself, Socs3 as a negative regulator of Jak and several survival, proliferation and proapoptotic genes. The entrance of dimerized pY705-Stat3 can inhibited by Pias3. In the non-canonical signaling, Stat3 is part of several regulation signaling. pY705-Stat3 is a co-regulator of microtubule dynamic in a protein-protein interaction with p-Stathmin1. Another phosphorylation of Stat3 is at the amino acid Serine272 (S727) via MAPK. pS727-Stat3 inhibit the IP3R calcium release at the mitochondria associated endoplasmic reticulum membrane (MAM) and can interact with GRIM19 and TOM20 to entry the mitochondria, where it regulates mitochondria gene expression and the cellular metabolic activity like ATP synthesis, increases mitochondrial Ca^{2+} and inhibition of ROS release. Unphosphorylated Stat3 (U-Stat3) can act as a transcription factor for different genes like pY705-Stat3. Through interaction of importin a3, U-Stat3 is able to reentry in the nucleus, while NF kB ensures a DNA binding interaction.

3.4.2. Stat3 and mitochondria

Whereas pY705 is responsible for its transcriptional activation, pS727 is known for its regulation of mitochondria metabolism by interaction of various mitochondrial proteins and gene expression via non-canonical pathway (Macias et al., 2014; Wegrzyn et al., 2009). Mitochondria serve as key regulators of cellular metabolic activity. It has been reported that Stat3 can translocated also in the MAM (mitochondria associated endoplasmic reticulum membrane) fraction and into mitochondria (Fig. 4). At the MAM fraction it is able to promote IPR3 degradation and prevent cytosolic Ca^{2+} accumulation (Su et al., 2020). For translocation into mitochondria pS727 Stat3 is acting as a monomerize protein with GRIM19 and TOM20 (Fig. 4) (Tammineni et al., 2013). It is suspected to enhance electron respiratory chain activity, calcium release, ATP production and regulating ROS by interacting with complexes I and II (Gough et al., 2013; Meier et al., 2017; Yang et al., 2016). Multiple kinases are responsible for S727 phosphorylation, depending on the nature of the activating signal. Mitogen activated protein kinase (MAPK) family members are mainly reported to induce this phosphorylation in

response to different extracellular stimuli. The MAPK family is composed of extracellular signal-regulated kinase (ERK), induced by growth factors and cytokines (Fig. 4) (Gough et al., 2013). Moreover, the mitochondrial translocation of Stat3 suppresses autophagy induced by oxidative stress and may effectively preserve mitochondria from being degraded by mitophagy (You et al., 2015).

3.4.3. Stat3 and the microtubule dynamics

Through non-canonical pathway, STAT3 is also involved in microtubule dynamics. Once phosphorylated, Stat3 (pStat3) can interact via protein-protein interaction locally with Stathmin1 (Selvaraj et al., 2012; Verma et al., 2009; Wareham et al., 2021). Stathmin1 is a small protein of 17 kDa binds the α- and β-tubulin heterodimers of which microtubules are comprised which can lead to microtubule catastrophe. Together, they controlled the phases of growth and disassembly (Gavet et al., 1998; Selvaraj et al., 2012; Yadav et al., 2016), a process called “dynamic instability”.

Microtubules are the most highly conserved sequence in evolution and in mammalian cells one of the most abundant proteins. α- and β-tubulin heterodimers polymerize polar to so-called protofilaments (Bryan et al., 1971), which by interaction form the hollow cylinder known as the microtubule with a diameter of 25 nm (Erickson, 1974). Posttranslational modifications (PTM) and binding of a variety of MAPs can stabilize microtubules thereby preventing depolymerization (Bartolini et al., 2005), while microtubule-destabilizing proteins can promote depolymerization (Cassimeris et al., 2001) via Stathmin1. The variety of tubulin modification are expected to play an important role in the generation of functionally distinct of microtubules.

Many of the well-characterized tubulin PTMs occur on the C-terminus of α- and β-tubulin, which is located on the outer surface of microtubules and thus accessible to microtubule interactors. Tubulin PTMs can also influence the stability of microtubules by affecting the speed at which they are polymerized and depolymerized (Aillaud et al., 2016).

The C-terminal amino acid of most α-tubulins is tyrosine (Valenzuela et al., 1981), which is also called non-modified tubulin. Detyrosinated tubulin can be further modified to irreversible Δ2-tubulin (Paturle-Lafanechere et al., 1991; Rudiger et al., 1994). Tyrosinated tubulin is predominantly found in dynamic microtubules (Webster et al., 1987). In the inner ear, tyrosinated tubulin is found in supporting cells and the sensory hair cells, while stable detyrosinated and Δ2-tubulin is found in supporting cells of the organ of Corti (Fig. 5 blue) (Juergens et al., 2020). The absence of tyrosinated tubulin prevents the depolymerization of microtubules (Infante et al., 2000; Peris et al., 2009).

Acetylation of α -tubulin takes place at lysine (K) 40 of α-tubulin, which lies on the luminal side of the microtubule, which makes microtubules more resistant to mechanical damage (Portran et al., 2017) is found in cells with long-lived and stable microtubule (Janke et al., 2020) (Fig. 5, yellow). In the organ of Corti, acetylated microtubules are present in supporting cells like Deiters cells (Juergens et al., 2020).

Polyglutamylation are linked to glutamic acids within the C-terminal tails of α- and β-tubulin, and consist in the addition of a single, or several glutamic or glycine residues, thus creating polyglutamate chains (Fig. 5, red or green). Polyglutamylation is assumed to regulate interactions between microtubules and their interacting proteins. It is found in a variety of cells and tissues; however, it is particularly enriched in neurons as well as in cilia and flagella, but also in the Deiters and pillar cells (Juergens et al., 2020).

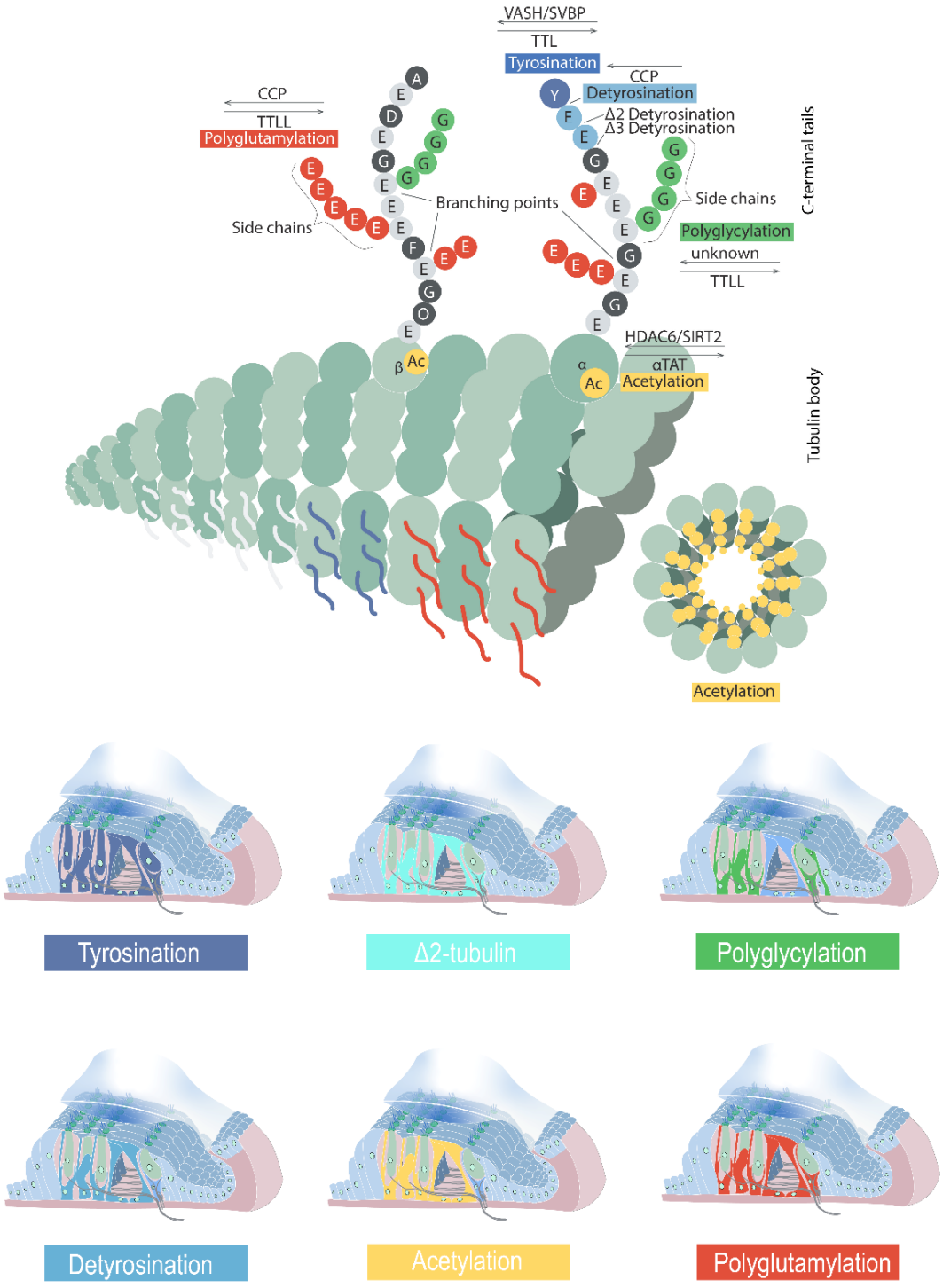

Figure 5: Posttranslational modifications of microtubules and the distribution in the Organ of Corti.
C-terminal chains of α and β tubulin can be modified by various enzymes. Both, α- and β-tubulin are modified by polyglutamylation and polyglycylation at glutamate residues within the primary peptide chain of the protein, the so-called branching points. Both PTMs are catalyzed by enzymes from TTLL family, and polyglutamylation is removed by enzymes from the CCP family. Detyrosination enzymatically removes the C-terminal tyrosine residue of α-tubulin with enzymes from the VASH family, which can be re-added by TTL. Detyrosinated tubulin can be further processed by removal of penultimate glutamate residues by CCP-family enzymes, giving rise to Δ2- and Δ3-tubulin. Acetylation of K40 on α-tubulin, located inside microtubules, is catalyzed by αTAT1, and removed by either HDAC6 or SIRT2. Acetylation of β-tubulin has been reported but is little explored. All modifications of microtubules were found in Deiters, the inner and the outer pillar cells, but so far only tyronisated tubulin was found in outer and inner hair cells. αTAT: α-tubulin N-acetyltransferase, CCP: cytosolic carboxypeptidase; HDAC6: histone deacetylase 6, SIRT2: sirtuin2; TTL: tubulin tyrosine ligase; TTLL: TTL-like. Adapted from Bieniussa et al. (2023).

4. Hypothesis and aim of the thesis

Stat3 is a critical component of cell growth, survival and differentiation, but also apoptosis, and inflammation. While Stat3 has bright range of essential roles in several cell types, little is known about Stat3 in sensory epithelia of the cochlea and hearing. Therefore, the Cre/loxp system was intended to be used to verify the role of a correct protein folding of Stat3 in sensory hair cells and epithelia cells in the inner ear of mammalian cochleae.

By this technology a conditional knock out (cKO) of Stat3 in the organ of Corti was induced, resulting in a non-functional protein. The cKO was induced either in outer hair cells (OHCs) or Deiters cells. Additionally, two time points were chosen for cKO. On the one hand before hearing onset, altering the process of postnatal development, and on the other hand after hearing onset, understanding the function of Stat3 in differentiated cells. To evaluate the importance of correct Stat3 in the organ of Corti different experimental investigations were performed. Audiological measurements including distortion productive otoacoustic emissions (DPOAE) as wells as click and tone auditory brainstem responses (ABRs) were performed to evaluate the hearing performance of cKO mice compared to control littermates. Additionally, cochleae were dissected and stained with various protocols for histomorphology examination of affected mice. Moreover, molecular analysis including OHC selection, mRNA extraction and its sequencing were performed.

5. Material

5.1. Technical equipment

name	article	company
amplifier	RA4PA 4-Channel Medusa Preamp	Tucker-Davis Technologies
confocal microscope	OlympusFluoview 1000IX81	Olympus
cryostat	CM 1950	Leica
Electron microscope		Leica
fluorescence microscope	DMi 8	Leica
heating pad	Rodent Warmer 53810	Stoelting
I/O processor	RZ6 Multi I/0 Prozessor	Tucker-Davis Technologies
Magnetic beads separator	MACS multistand, separator	Miltenyi Biotec
Cell separation columns	MACS LS separator	Miltenyi Biotec
microphone	ER-10 B+ Low Noise DPOAE Microphone	Etymotic Research
PCR thermocycler	Biometra Trio	Analytik Jena
rotator	Mini Rocker-Shaker	Hartenstein
speaker	MF1Multi-Field Magnetic Speakers	Tucker-Davis Technologies
tissue preparation microscope	Stemi 508	Zeiss

Table 1: Technical equipment

5.2. Preparation set

name	article	company
decapitation scissor	14200-21	Fine Science Tools
Insulin-syringe	U-40 Insulin, 30Gx5/16“	Braun
syringe	Omnifix F	Braun
Liquid Blocker	Pap-Pen Mini	Science Services
Perfusion	Venofix Safety	Braun
Cryomold	small	Sakura
Dumont Forceps	t #5 11252-20	Fine Science Tools
Fine Iris Scissors	Hardened,14090-09	Fine Science Tools
Vannas Spring Scissors	15000-03	Fine Science Tools
Sichel Knife	10073-14	Fine Science Tools

Spatel	10091-12	Fine Science Tools
weighing machine	Digital Platform Scale I-2000	Superior Mini
24-well plate	24 well Cellstar	Greiner Bio-One

Table 2: preparation set

5.3. Anaesthesia

name	**Authorization number**	**company**
Ursotamin 100mg/ml	3100370.00.00	Serumwerk Bernburg
Xylavet 20mg/ml	401510.00.00	cp-pharma

Table 3: anaesthesia

5.4. Chemicals

name	**article**	**company**
aceton	32201	Sigma-Aldrich
agarose, universal	9012-36-6	VWR Life Science
aqua polymount	18606	Polysciences
chloroform	2445	Merck
DNA Gel Loading Dye (10X)	R0611	ThermoFisher Scientific
ethanol	64-17-5	Fisher BioReagents
GeneRuler 1 kb DNA Ladder	SM0311	ThermoFisher Scientific
Medunasal Heparin 500 I.U.	67771	Sintetica
Midori Green Advance	617004	Biozym
NaCl 0,9%	2737756	Braun
Natriumchlorid	31434	Sigma-Aldrich
Propan-2-ol	67-63-0	Fisher Chemical
Red HS Taq Mastermix	331126XL	Biozym
saccharose	A2211,1000	PanReac AppliChiem
SDS (Sodium dodecyl sulfate solution)	71736	Sigma-Aldrich
TissueTek	4583	Sakura
Tris(hydroxymethyl)aminomethane	77-86-1	Merck

Table 4: chemicals

5.5. Solutions

name	**ingredients**
aneasthesia 5ml	0.6 ml Ketamin 100mg/ml 0.2 ml Xylazin 20mg/ml ad 5 ml 0,9% NaCl
antibody solution	3% NGS 1% BSA 0.5% TritonX100 0.1% Tween20 in 1M PBS
blocking solution	10% NGS 1% BSA 0.5% Triton X100 0.1% Tween20 in 1M PBS
cacodylate buffer 0.15M	50 mM cacodylate 50 mM KCl 2.5 mM MgCl2 2 mM CaCl2 in ddH_2O, pH 7.4
EM fixation	2.5% glutaraldehyde 2% formaldehyde 2 mM calcium chloride in 0.15 M cacodylate buffer, pH 7.4
Eosin	0.1 % Eosin in ddH20
Fixation solution	4% PFA in 1M PBS
Tissue lysate buffer	1mg/ml Collagenase VI 1mg/ml Papain 1mg/ml Thermolysin In HBSS
PBS 10x	80 g NaCl 2 g KCl 2 g KH_2PO_4

	11.75 g Na_2HPO_4 ad 1l ddH_2O
PFA 4%	10 g Paraformaldehyde 205 ml 0.2 M Na_2HPO_4 45 ml 0.2 M $Na_2H_2PO_4$ ad 500 ml ddH_2O, pH = 7.4
Rinsing buffer	1% BSA In 1M PBS
washing solution	0.3% Triton X100 0.1% Tween20 in 1M PBS

Table 5: solutions

5.6. Kits

name	**arcticle**	**company**
Basecope		Advanced
PicoPure RNA Isolation Kit	12204-01	Arcturus
In situ Cell Death, POD	684817910	Roche
MACS IgG rabbit beads separation	130-048-602	Miltenyi Biotec

Table 6: Kits

5.7. Antibodies and dyes

name	**Conc.**	**Info/gene**	**host**	**clone**	**No.**	**company**
Alexa 488 Phalloidin	1/800	F-actin	-	-	8878S	Cell Signaling
Alexa 555 Phalloidin	1/800	F-actin	-	-	8953S	Cell Signaling
Alexa 647 Phalloidin	1/800	F-actin	-	-	8940S	Cell Signaling
Alexa Fluor Plus™ 488	1/1000	anti-mouse	donkey	-	A32766	invitrogen
Alexa Fluor Plus™ 488	1/1000	anti-rabbit	donkey	-	A32690	invitrogen

Alexa Fluor Plus™ 555	1/1000	anti-rabbit	donkey	-	A32794	invitrogen
Alexa Fluor Plus™ 555	1/1000	anti-mouse	donkey	-	A32773	invitrogen
Alexa Fluor 555	1/1000	anti-rat	donkey	-	ab150154	abcam
Alexa Fluor Plus™ 647	1/1000	anti-mouse	donkey	-	A32787	invitrogen
Alexa Fluor Plus™ 647	1/1000	anti-rabbit	donkey	-	A32795	invitrogen
α-tubulin acetyl., K40	1/1000	TUBA1A	mouse	6-11B-2	T7451	Sigma
α-tubulin tyr.	1/2000	C-terminal -GEEF	rat	TUB1A2	SAB4200776	Sigma
α-tubulin detyr.	1/2000	C-terminal -GEE	rabbit	1	AB3201	Millipore
βIII-tubulin	1/1000	TUBB3	mouse	Tuj1	801201	Biolegend
ßIII-tubulin	1/1000	-	rabbit	-	Ab18207	abcam
CtBP2	1/1000	-	mouse	6	612044	BD
DAPI	1/5000	-	-	-	D9542	Sigma
HistoGreen	1/1000	POD	-	-	E109	Biozol
Slc26a5	1/1000	aa 128-177	rabbit	-	LS-C199978	LS Bio
Synaptophysin	1/2000	555 conjug.	mouse	101-OP	101004	SySy
Parvalbumin	1/2000	-	rabbit	-	Ab181086	abcam

Table 7: Antibodies and dyes

5.8. Mouse lines

Nomenclature	**ID**	**ZEMM-name**	**genotype**
C57BL/B6J;129SV-Tg(Slc26a5$^{tm4\text{-}cre/ERT2}$)^{Jnz}	MGI:5316514	B6.Slc26a5-Cre	Cre/Cre
C57BL/6J;CBA-Tg(Fgfr3-icre/^{ERT2})$^{4\text{-}2Wdr/J}$	Jax:025809	B6.Fgfr3-Cre	Cre/Cre
C57BL/6J;Cg (Stat3^{tm2})^{Aki}	MGI: 1926816	B6.Stat3-fl	fl/fl
B6.Cg-Gt(ROSA)26Sor$^{tm14(CAG\text{-}tdTomato)Hze/J}$	Jax:007914	B6.CAG-tdTomato	fl/fl

Table 8: mouse lines

5.9. Primer

name	5´→ 3´	bp	Δ°C
tdTom wt for	AAG GGA GCT GCA GTG GAG TA	300	68
tdTom wt rev	CCG AAA ATC TGT GGG AG TC		
tdTom mut for	GGC ATT AAA GCA GCG TAT CC	200	72
tdTom mut rev	CTG TTC CTG TAC GGC ATG G		
Fgfr3-Cre for	GAG GGA CTA CCT CCT GTA CC	550	61
Fgfr3-Cre rev	TGC CCA GAG TCA TCC TTG GC		
Prestin wt for	CAC AAG TTG TGA ATG ACC TC	300	60
Prestin wt rev	TAA CTG CTA GCA TTT CCC TT		
Prestin mut rev	GTT AAA GAG CGT AAT CTG GAA CA	230	
Stat3 for	CCT GAA GAC CAA GTT CAT CTG TGT GAC	wt: 250	56
Stat3 rev	CAC ACA AGC CAT CAA ACT CTG GTC TCC	fl: 400	

Table 9: Primers

5.10. Softwares

name	company
BioSigRZ	Tucker Davis Technologies
Graphpad Prism 7	Graphpad Software Inc.
LAS XF	Leica
ImageJ	Wayne Rasband
Fluoview Olympus	Olympus
Office 2019	Microsoft
Photoshop CS9	Adobe

Table 10: softwares

6. Methods

6.1. Animals and cKO

For this project, inducible Cre-loxp mouse system were used to create conditional Knock-out (cKO) of interested gene. The Cre recombinase-containing homozygote mouse lines used in this project were Slc26a5 (Prestin) -iCre (Cre/Cre) (Fang et al., 2012) and Fgfr3-iCreER^{T2} (Cre/Cre) (Young et al., 2010). Prestin is the contractile element of the cortical organ and is expressed postnatally exclusively at OHCs (Liberman et al., 2002). Fgfr3 is a promoter that is active in neural tube progenitors and differentiated astrocytes (Young et al., 2010). Due to their high and early postnatal recombination activity, the lines were also appropriate to induce genetic changes already from the early postnatal stage. Homozygote Slc26a5-iCre and Fgfr3-iCreER^{T2} were cross breeded with B6.CAG-tdTomato to evaluate Cre-recombinase activity of our mouse lines. For experiments, homozygote Stat3-fl mice (Takeda et al., 1998) were cross breeded with inducible Cre-mouse line for a 100% Cre/+, fl/+ F1-Generation, which were used in the study. They received an injection of tamoxifen (3mg/40g body weight) daily either from p2 to p5 (Tam 2/5) or from p16 to p19 (Tam 16/19). The earlier injection was used to study microtubule changes during postnatal development, i.e. before hearing onset. The later injection was to investigate the function of hearing might be altered by the changed microtubule dynamics. Cochleae were evaluated at p7, p14, p21, p28 and p35.

Animals were fostered and housed under controlled conditions (20–22°C, 55–65% humidity, 12:12-h light/dark cycle, food and water ad libitum) and were controlled for vitality and health daily. All mice used for audiometry were carefully matched for age and sex to minimize the confounding effects on the measurement outcomes. The experimental procedures were performed according to German regulations on animal welfare in agreement with and under control of the local veterinary authority and Committee on the Ethics of Animal Experiments (license number 55.2-DMS-2532-2-686-15).

6.2. Anaesthesia

Audiological examinations were performed on induced Cre/+, fl/+ and their uninduced littermates (control) at the age of postnatal days 21, 28 and 35. For anesthesia, a mixture of ketamine hydrochloride (75 mg/kg body weight, Ketavet 100, Pharmacia) and xylazine hydrochloride (5 mg/kg body weight, Rompun 290, Bayer) was injected intraperitoneal with an injection volume of 1 ml/kg body weight. Anesthesia was maintained by application of 10% of the initial dose, typically in 30 minutes intervals. A temperature-controlled heating pad maintained the body temperature to 37°C.

6.3. Audiometric Assessment

Hearing function assessment was performed via Tucker-Davis Technologies Inc. (TDT, USA) setup using the programming SigGenRZ software and the TDT BioSigRZ performing platform. The equipment loudspeaker control, microphone (378C01, PCB Pieztronics Inc., N.Y., USA), acquisition, processing, averaging, and data management were further coordinated using the RZ6 Multi I/O Processor System.

6.3.1. Distortion Product Otoacoustic Emissions

A total of two pure tones (f1 and f2, f2/f1 = 1.2) were used to measure distortion product otoacoustic emissions (DPOAEs). The primary tone f1 is 0.894 times and the primary tone f2 is 1.118 times the fundamental frequency. Through a low noise recording microphone, primary tones produced by two separate loudspeakers were introduced into the closed ear canal of the animal and emissions were recorded. If a peak in the spectrum at 2x(f1–f2) exceeded the background noise by 3 dB µV, then it was defined as a positive DPOAE. Fixed test frequencies ranged from 8 to 24 kHz in 4 kHz steps and a stimulus level of 90 to 20 dB sound pressure level (SPL) in 5 dB steps were performed and averaged from 128 responses. DPOAEs were always performed prior to ABR, since the reverse procedure can result in a temporary reduction of DPOAEs.

6.4.2. Auditory Brainstem Response

For recording of monaural bioelectrical auditory brainstem potentials, subdermal stainless-steel electrodes (27GA 12 mm, Rochester Electro-Medical, USA) were inserted subcutaneously to the ventrolateral side of the ear (active), on the vertex (negative), and on the body (neutral) and connected to a preamplifier (RA4PA, TDT, USA) with 20-fold amplification. To verify proper electrode positioning or conductivity, impedance measurements of all electrodes (<5 kΩ) were taken prior to each ABR recording. The bioelectrical ABR signals recorded from the subdermal electrodes were transferred to a head stage (RA4LI, TDT, USA). The sounds were applied via a microphone that was inserted into the external auditory canal (active ear). For ABR threshold recordings and wave latency, click stimuli and tone bursts between 4 and 24 kHz were applied. The stimuli started at a sound pressure level of 90 dB and decreased in 5 dB steps to 20 dB. The responses were amplified 20-folds and filtered with a bandpass filter set at 0.3–3.0 kHz. Responses were sampled over a 10-ms period and averaged from 512 responses to determine the minimum threshold. The responses were sampled over a period of 10 ms and averaged from 512 responses. The minimum threshold was assumed to be the last wave that could still be reproduced. Wave I represent the distal part of the auditory nerve, whereas wave II portions the proximal of the auditory nerve (AN) in

the cochlear nucleus (NC) in the brainstem. The superior olivocochlear (SOC) is presented by wave III, respectively. Waves IV and V are produced by evoked neural responses in the inferior colliculus (IC) and the nucleus lemniscus lateralis (NLL) (Davies, 2016; Young et al., 2020).

6.4. Tissue Preparation

For immunohistochemical analysis, mice were deeply anesthetized with CO_2 and intracardially perfused with 4% PFA in 1M PBS pH 7.4 by the force of gravity at room temperature. Cochleae were post-fixated for 1 h and decalcified in 125 mM EDTA overnight on a 3D rotator at room temperature. Once decalcification was complete, the cochleae were stored in 1M PBS pH 7.4 until use or immediately dissected for whole-mount staining. For electronic microscope evaluation, mice were intracardially perfused with 0.9% NaCl with 0.66 ml Heparin/100ml in A. bidest for 2 minutes followed by electronic microscope fixation at RT for 5 minutes. Cochleae were post-fixated in 4% PFA in 1M PBS pH 7.4 over night at 4°C on a 3D rotator.

6.5. mRNA bulk sequencing of OHCs

mRNA of OHCs from Slc26a5-Cre/+; B6.Stat3-fl/+ induced Tam 2/5 and Tam 16/19 at the age of p28 and p35 were sequenced via Bioanalyzer Pico at the Core Unit SysMed at the Rudolf-Virchow Center Würzburg. Therefore, the organ of Corti were carefully separated out of the cochlea and digested in single cells with a lysis buffer containing 1mg/ml Collagenase IV, 2 mg/ml Papain and 1mg/ml Thermolysin for 10 min at 37°C in a thermo cycler and triturated. Afterwards, OHCs were incubated with a Slc26a5 antibody and secondly with IgG anti-rabbit microbeads (Miltenyi Biotec) for indirect selection of OHCs. The cell suspension was flown through MACS® Separator columns (Miltenyi Biotec) to separate and enrich magnetic labeled OHCs. After elution of OHCs, the mRNA was extracted via Pico Pure Isolation Kit and sequenced with Takara smart-seq v4 library prep protocol by Core Unit System (RVZ, Würzburg). Gene expression under log2foldexchange of -1 were seen as downregulated with a significance with $p<0.05$, whereas gene expression over 1 with $p<0.05$ was seen as upregulated compared to control mice.

6.6. Immunohistochemistry

6.6.1. Whole Mount and cryosection staining

After decapitation, left cochlea were used for whole mount staining and the right cochlea were set up cryosections. Therefore, right cochleae were incubated in ascending concentration of 10%, 20% and 30% sucrose with additional suspension of Compound Tissue Tek and 30% sucrose in relation of 1:3, 1:1 and 3:1. Finally, cochleae were embedded in pure Compound

Tissue Tek and frozen at -80°C until 9 µm cryosections were performed. Cochlear turns of the left tissue were separated in a 24-well plate submerged with 1% PFA in 1M PBS pH 7.4. For the following steps, the tissue was always covered in liquid. After blocking and permeabilization with 10% normal horse serum (NHS), 1% bovine serum albumin (BSA), 1% Triton X100, and 0.1% Tween20 in 1M PBS pH 7.4 for 1 h, the cochlear tissue was incubated with antibody solution (3% NHS, 1% BSA, 0.3% TritonX100, 0.1% Tween20 in 1M PBS pH 7.4) containing primary antibodies for 3 h at room temperature. Cochlear turns or cryosections were washed three times with 0.3% TritonX100 and 0.1% Tween20 in 1M PBS pH 7.4. Primary antibodies were detected with secondary fluorochrome-conjugated antibodies for 1 h at room temperature. In addition, labeling with phalloidin-conjugated Alexa and DAPI were performed.

6.6.2. Hematoxylin/Eosin

After washing cryosections with 1M PBS, tissues were incubated with filtered Hematoxylin for 2 minutes and washed carefully out with ddH_2O before Eosin incubation were performed. Eosin were rinsed with dd H_2O after 3 minutes and were incubated at first shortly in 96% ethanol and afterwards 2 times with 100% ethanol for 5 minutes. At last, cryosections were bathed in Xylol and finally embedded in Entellan. Cryosections were scanned and analyzed with a Leica microscope with an LAS AF epifluorescence and scanned. The images were captured with a 10x objective.

6.6.3. TUNEL assay

For TUNEL assay, in situ Death Detection Kit, POD were used to detect cell apoptosis of spiral ganglia. Therefore, cryosections of cochleae were post-fixated with 4% PFA in 1M PBS and washed with 1M PBS. Afterwards, cryosection were blocked with 3% H2O2 for 10 minutes and permeabilized with 1M PBS containing 0.1% Triton X100 and 0.1% natrium citrate for 2 minutes at 4°C. The TUNEL reaction solution were prepared after description and incubated on the tissue for 1h at 37°C and labeled with HistoGreen substrate for 10 minutes at RT. Positive controls were preincubated with 10 mg/ml DNAse I, whereas negative controls were not incubated with TUNEL reaction solution. Cryosections were embedded in Entellan, scanned and analyzed via a Leica light microscope with a 10x objective.

6.7. Microscopy

6.7.1. Light microscopy

Cryosections stained by in situ hybridization, Hämalaun/Eosin and TUNEL assay were scanned and analyzed via a Leica microscope in brightfield. Cryosection were scanned with an 10x objective and analyzed via Image J.

6.7.2. Confocal Microscopy

Immunolabeling with posttranslational modifications of microtubules, whole mounts and in situ hybridization were analyzed using an Olympus IX81 microscope equipped with an Olympus FV1000 confocal laser scanning system, an FVD10 SPD spectral detector, and diode lasers of 473, 559, and 651 nm. The images were acquired with an Olympus UPLSAPO 40X objective (oil, numerical aperture: 1.3). For high-resolution confocal scanning, a pinhole aperture setting was used, which represented a diffraction disk. Whole-mount images of the organ of Corti were taken in about 300-nm steps in the z-axis. Cryosection images were taken of 9µm Z-stacks, brightness, and contrast of the images were adjusted using ImageJ for better visualization.

6.7.3. Electron microscopy

For electronic microscopy, animals were deeply anesthetized with CO_2 and intracardially perfused with 0.9% NaCl containing 0.66 ml Heparin/100ml for 2 minutes followed by 0.15 cacodylate buffer pH 7.4 containing fresh 2.5 % glutaraldehyde, 2%formaldehyde with 2mM calcium chloride by force gravity for 5 minutes at room temperature. Cochleae were post-fixated over night at 4°C and washed afterwards 5 times in cold cacodylate buffer. Cochleae were decalcified in an aqueous solution containing 4% paraformaldehyde, 0,85% NaCl and 10% acetic acid. After washing with 10x 5 minutes with ddH20, cochleae were incubated in 1% osmium tetroxide buffered in 1M PBS pH 7.4 at room temperature for 1 hour and subsequently washed 5x 3 minutes with ddH_20 before they were incubated in 8% UAR-EMS uranylacetate replacement stain for 1 hour. Cochleae were dehydrated in an ascending ethanol series each 10 minutes of 30%, 50% 70%, 80%, 90%, 96% and 2 times with 100% ethanol. Cochleae were incubated in propylene oxide for 30 minutes and set overnight in a 1:1 mixture of propylene oxide and Epon. On the following day, cochleae were incubated in pure Epon for 2 hours and finally embedded at 60°C for 48 hours. Cochleae were cutted via an ultramicrotime till the right level of OHCs and supporting cells was available. For ultrathin sections, 60 nm sections were cutted and collected on nickel grids. For microscopy, sections were poststained with 8%UAR-EMS uranylacetate replacement stain for 30 minutes and 0.2% lead citrate for 7 minutes before analyzing with a LEO AB912 transmission electron microscope (Carls Zeiss).

6.8. Data Analysis and Statistics

The values of the DPOAE measurements were converted before analysis. The RZ6 processor is a +/– 10V device, and therefore, the described levels of the TDT system are inherently interpreted as dB Volt (dBV). DPOAEs thresholds are defined as the last positive SPL value. The following equation after TDT is used to convert dBV to dB SPL:

$$20\log\left(\frac{10^{\left(\frac{dBV}{20}\right)}}{0.05}\right)+93.9$$

Auditory brainstem response thresholds were set at the last reproducible waveform. Values of all animals of each group were averaged and are presented as hearing thresholds ± standard errors of mean, respectively. ABR analysis included latency and the maximum height of wave I and II of click ABR. Statistical analysis and graphic display were performed in GraphPad Prism software (GraphPad, San Diego, CA, USA). A column analysis was performed to determine normal distribution. In the case of a Gaussian distribution, an ANOVA and Tukey's multiple comparison post hoc test or Holm-Sidak's multiple comparisons test was performed, where mean and standard error of the mean (SEM) were determined. A p-value of <0.05 was considered as significant. Significances were always determined by comparison to control littermates, if not otherwise noted. All data are presented in mean ± SEM unless otherwise noted. Control littermates are illustrated in black, whereas each cKO with its age are represented in constant color in this manuscript. Final processing of images was performed with ImageJ and Photoshop CS9 (Adobe).

Slc26a5-iCre x Stat3-fl	Tam 2/5	Tam 16/19		**Fgfr3-iCre x Stat3-fl**	Tam 2/5	Tam 16/19
p21				p21		
p28				p28		
p35				p35		

Table 11: Color code

7. Results

7.1. Basic evaluations

7.1.1. Stat3 mouse model analyzation

The Transcript ID of murine Stat3 (Stat3-203) is ENSMUST00000127638.8 by MGI: 103038. The location of Stat3 is on Chromosome 11 100.777.636 – 100.830.366 at reverse strand. The spanning of 24 exons with introns is 744.444 bp. The total length of 5´->3´translated sequence is 4.516 bp long. The mRNA length (without UTR) for protein translation is 2.310 bp.

The protein sequence of murine STAT3a (UniProt: P42227-1, NP_998824.1) consist of 770 amino acids with a mass of 88,54 kDa. Amino acid sequence of Stat3 was separated in its Exon translation (Fig. 6A). Features of Stat3 regions and sites were highlighted and marked with colored lettering (Fig. 6B). Used mouse model (MGI:1926816) has Exon 22 flanked by loxp sites (Takeda et al., 1998), which included the phosphorylation site of Tyr (Y) 705 important for p-Stat3 heterodimerization. Through Cre activation and a deletion of exon 22, the frame shifts of the last exons, which resulted in a non-functionality of the last residue of Stat3 including the phosphorylation site of Ser (S) 727.

A

B

Amino acid position	Features
2 – 120	Protein- Protein interaction domin
139 – 318	Coiled Coil domain with coiled coil motif at aa: 142-165, 213-239, 263-284
150 - 162	essential for nuclear import
321 - 484	DNA binding domain
	Linker domain
554 - 715	SH2-domain
637, 653	Hydrophobic polypeptide binding pocket
591, 609, 636, 638	phosphotyrosine polypeptide binding pocket
601, 615, 631, 685	N6- acetyllysine alternate
705	tyrosine phosphorylation site
707	N6-acetyllysine
714	Phosphothreonine
727	serine phosphorylation site

Figure 6: Protein sequence of Stat3 with flanked Exon 22.

The protein of Stat3 possess 770 aa out of 24 Exons including a protein-protein interaction domain (2-120aa) at the N-terminal, a coiled coil domain (139-318aa) with its nuclear import sequence (150-162aa) to act as transcriptional factor

followed by DNA binding domain (321-484aa) and an SH2 domain (554-715aa). After deletion of exon 22, the frame shifts and caused a dysfunctionality of the last residue.

7.1.2. Antibody validation

Expression of posttranslational modification (PTM) of microtubules in the cochleae have been investigated at the p1, p7 and p14 (Juergens et al., 2020). For this thesis, antibody for PTM of microtubules were investigated in adult cochleae.

Tyronisated tubulin was expressed in nerve fibers, IHCs, Deiters cells and at the membrane of OHCs, whereas detyronisated and acetylated tubulin was detected in IHCs, the inner pillar cells and the Deiters cells, especially at the cup and the phalangeal processes (Fig. 7, detyr and acet), whereas polyglutamylated tubulin was detected only at the Deiters cell cup.

The results indicated a high specificity of antibodies against PTM of microtubules in the sensory epithelium of the organ of Corti of adult mouse. Nevertheless, there were no differences in immunostaining between p21, p28 and p35.

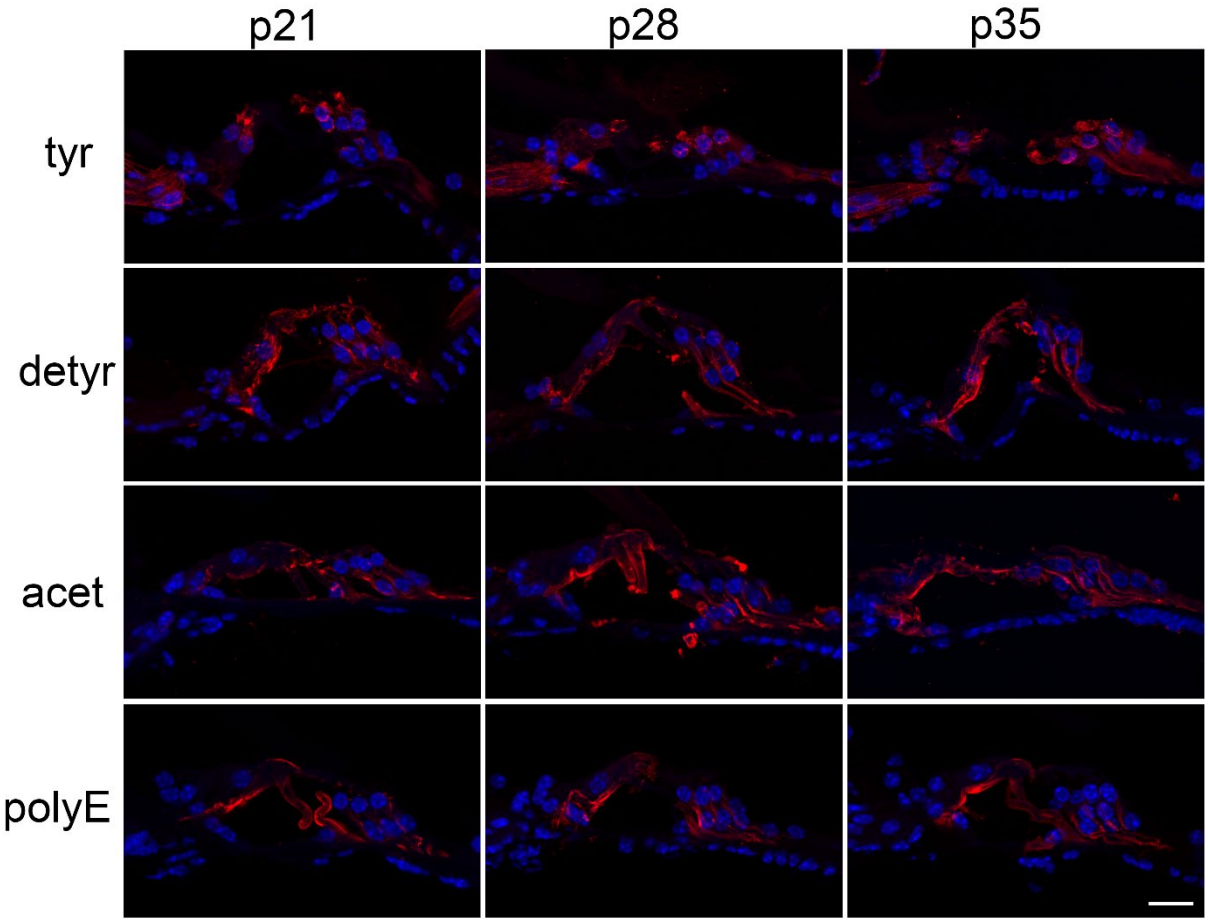

Figure 7: posttranslational modification of microtubules in adult cochleae.

Tyrosinted tubulin (tyr) expression is found in OHCs, Deiters cells, the inner pillar cell, IHCs and nerve fibers. Detyronisated (detyr) and acetylated (acet) tubulin is detected at the inner and outer pillar cells and the Deiters cells especially at the OHC-

cup and the phalangeal extension. Polyglutamylated (polyE) tubulin is highly expressed in pillar cells and the cup of Deiters cells. Scale bar: 20 µm.

7.1.3. Evaluation of mouse lines, Cre-loxp-system and the cKO

7.1.3.1. Audiological tests indicate phenotype of homozygote, but not heterozygote mice

Transgenic mouse models usually show various phenotypes, which might influence the hearing function Therefore, the used transgenic mouse models for this project were evaluated in auditory measurements at p35.

Homozygote Slc26a5-iCre mice has a significant decrease of DPOAE level from 8 kHz to 24 kHz compared to B6J mice (Fig. 8A), whereas tone-ABR indicated a hearing impairment of homozygote Fgfr3-iCre and Stat3-fl mice at high frequencies between 16 kHz and 24 kHz (Fig. 8B). Moreover, click-ABR analysis showed an increased hearing threshold for all homozygote mice compared to the wildtype background (Fig. 8C), which implicated a cKO of both alleles showed a hearing phenotype.

In addition, heterozygous transgenic mice were evaluated regarding their hearing function. Results implicated no hearing phenotypes in DPOAE and ABR measurements (Fig. 8D-F). Moreover, F1-generation Slc26a5-iCre Cre/+ or Fgfr3-iCre Cre/+, Stat3-fl fl/+ heterozygous mice were audiological analyzed. All cross breeding had no hearing impairments at p21, p28 and p35 compared to B6J (Fig. 8G-I) of Slc26a5-iCre Cre/+, Stat3-fl fl/+. Additionally, F1-generation of Fgfr3-iCre Cre/+, Stat3-fl fl/+ were audiological examined at p21, p28 and p35. The analyses implicated no differences in hearing at DPOAE, tone- and click ABR of p21, p28 and p35 compared to B6J (Fig. 8J-L).

Therefore, only heterozygote animals of F1 with Slc26a5-iCre Cre/+ or Fgfr3-iCre Cre/+, Stat3-fl fl/+ were seen as cKO. Additionally, Slc26a5-iCre Cre/+ or Fgfr3-iCre Cre/+, Stat3-fl fl/+ mice without an application of tamoxifen at the age of p21, p28 and p35 were pooled as control (ctrl) in further audiological examinations.

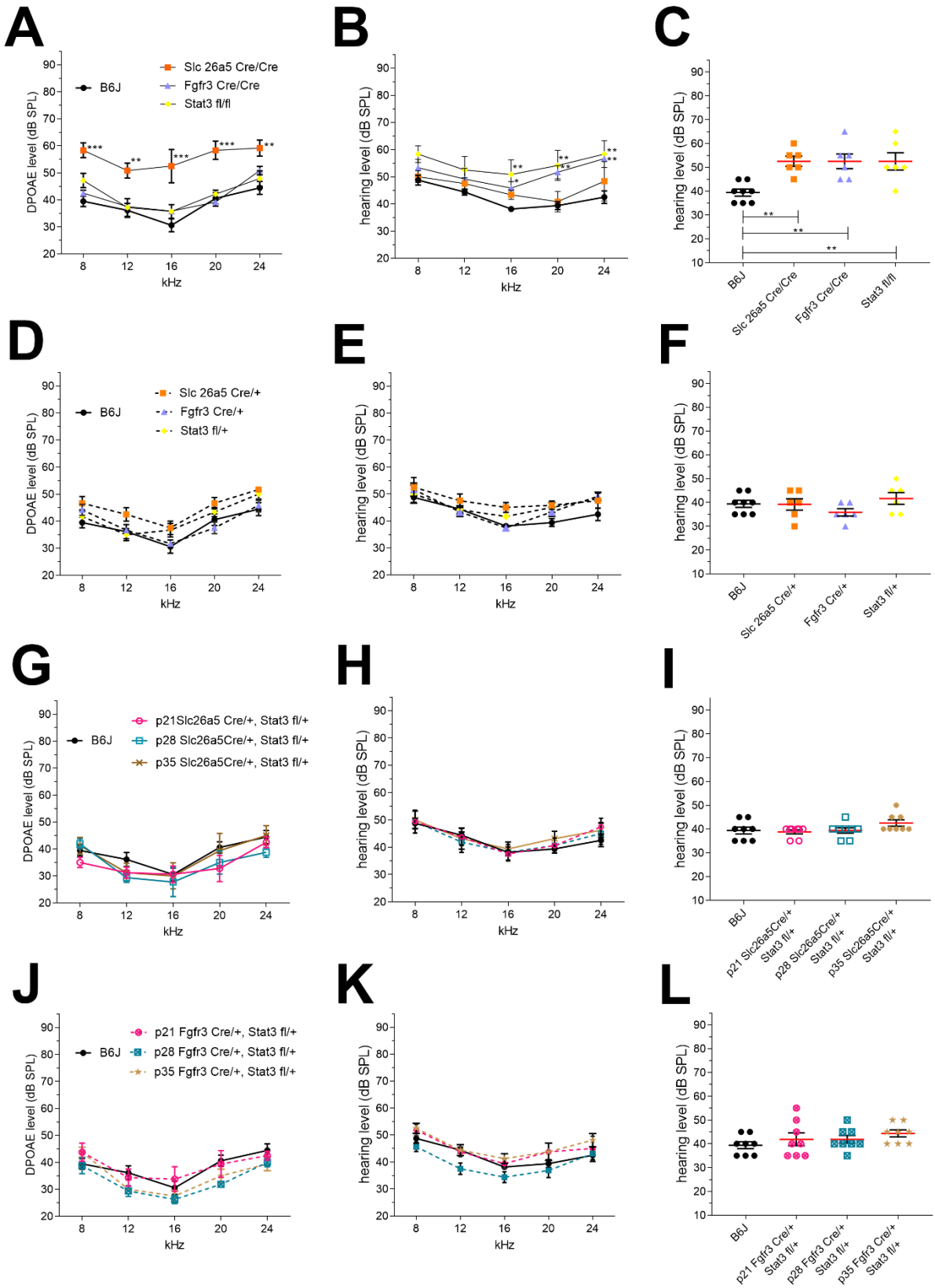

Figure 8: Electrophysiological examination of transgene mice.

(A) Homozygote Slc26a5-iCre and Fgfr3-iCre, but not Stat3-fl mice, have a significant decrease of DPOAE level to B6J at p35. (B) At tone-ABR, Fgfr3-iCre and Stat3-fl mice, but not Slc26a5-iCre, have a significant increase of hearing level at 16, 20 and 24 kHz, (C) whereas click-ABR indicates a mild hearing impairment of each mouse line. This effect leaks with heterozygote mice at the age of p35 (D) at DPOAE level and (E-F) ABR measurement. (G-L) F1-generation of Cre-loxp mice have no differences in DPOAE level, tone- or click-ABR at p21, p28 and p35.

7.1.3.2. Cell-specific activity of Cre-recombinase of Slc26a5-iCre and Fgfr3-iCre mouse line

The Cre-loxp system is used to control or manipulate DNA genomics and its gene expression. In this project, the recombinase of used mice lines should be inducible and cell specific. To evaluate the cell-specificity and the precise inducibility, Cre- mice lines were cross breed with a mouse line containing a flanked autofluorescence tdTomato cassette.

F1- generation of Slc265-iCre tg/+ and CAG-tdTomato fl/+ with no application of tamoxifen showed no expression of tdTomato in OHCs (Fig. 9A, ctrl). After inducing tamoxifen at Slc26a5-iCre Cre/+, CAG-tdTomato fl/+ mice between p2 and 5 (Tam 2/5) tdTomato is highly expressed in OHCs starting at p7 until p35 (Fig. 9A, Tam2/5). A late application of tamoxifen after hearing onset between p16 and p19 (Tam 16/19) showed a specific expression in OHCs beginning at p21 followed at p28 and p35 (Fig. 9A, Tam 16/19). Fgfr3-iCre Cre/+, CAG-tdTomato fl/+ mice with no application of tamoxifen had no expression of autofluorescence tdTomato in OHCS (Fig. 9B, ctrl). Mice with an injection at Tam 2/5 had a high expression of tdTomato starting at p7 until p35 at Deiters cells and pillar cells (Fig. 9B, Tam 2/5). Inducing tamoxifen between p16 and p19, autofluorescence td Tomato is activated and expressed in Deiters and pillar cells (Fig. 9B, Tam 16/19).

Recombinase from Slc26a5-iCre and Fgfr3-iCre mice were highly cell-specific and long active until p35. Moreover, heterozygote expression of recombinase was effective.

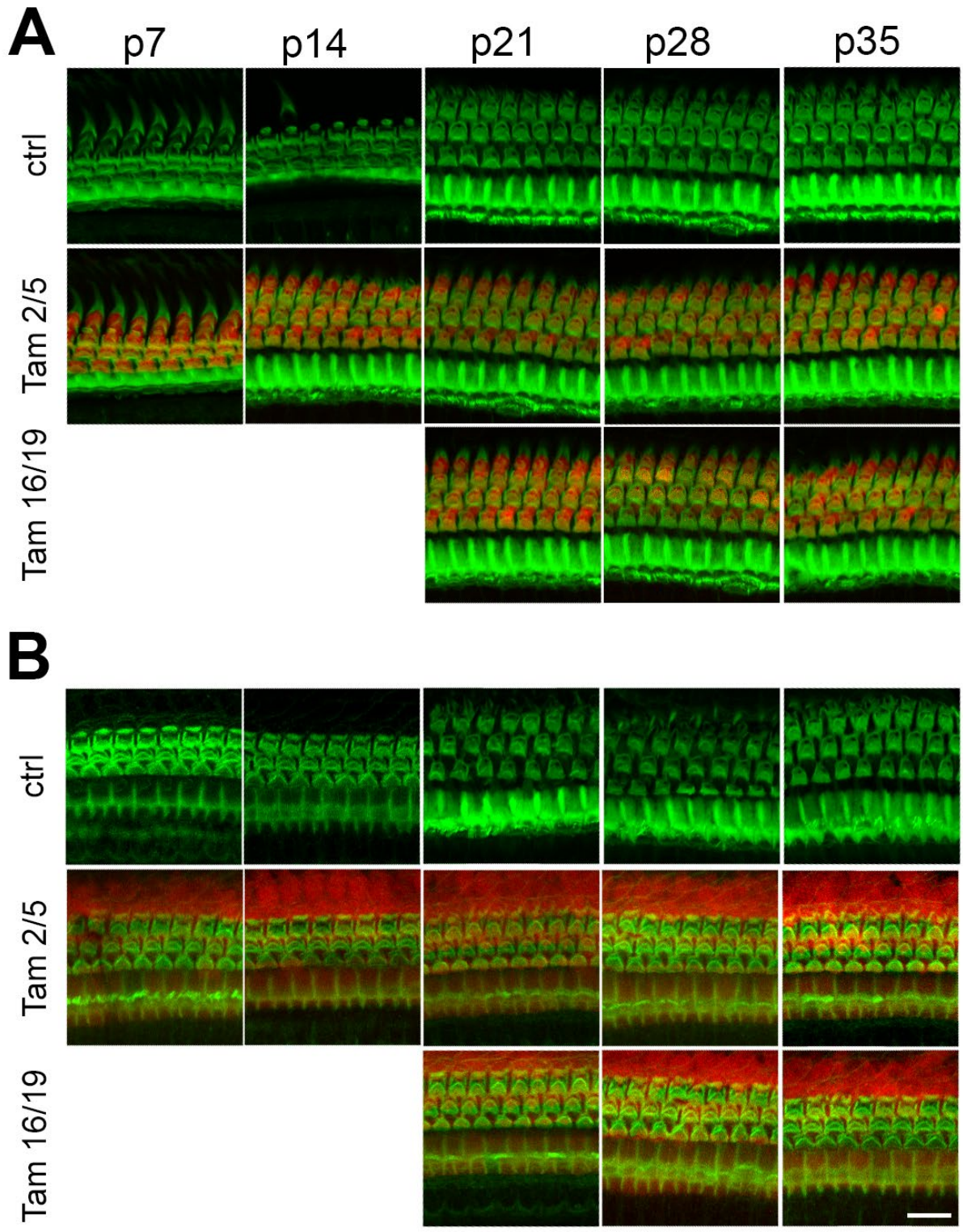

Figure 9: Cre-recombinase activity of Slc26a5-iCre and Fgfr3-iCre mice.
F1-generation with an injection of Tamoxifen between p2 and 5 show a specific activity in OHCs beginning at p7 and an injection of Tamoxifen at p16 and 19 beginning at p21 with (A) Slc26a5-iCre and (B) Fgfr3-iCre mice. At every time point, tdTomato is highly selected expressed.

7.2. Analyzation of Slc26a5-iCre Cre/+, Stat3-fl fl/+ mice

7.2.1. cKO of Stat3 in outer hair cells has a mild effect on hearing function.

Stat3 is highly expressed in sensory hair cells in the organ of Corti. To test whether a cKO of Stat3 influenced hearing, electrophysiology examination was performed via small-animal audiometry. cKO was induced between p2 and 5 (Tam 2/5) in postnatal development and between p16 and 19 (Tam 16/19) after hearing onset for functional assessment.

With an application of Tam 2/5, mice had a significant increase of DPOAE and tone-ABR hearing level over the whole frequency spectra at p28 ($p<0.001$) (Fig. 10A-B). Additionally, click-ABR showed an increasing hearing threshold at p28 with 66 ± 3 dB SPL (Fig. 10C) compared to control mice with 41 ± 1 dB SPL. At p35, the hearing level normalized with 46 ± 2 dB SPL (Fig. 10A-C). Additional analyses were assessed of distal and proximal regions of the auditory nerve. Wave I and wave II implicated a latency shift and a decrease of amplitudes at p28 (Figure 10D-G). At wave II, p35 amplitude is also decreased at higher dB level (Fig. 10G).

Inducing cKO between p16 and p19 (Tam 16/19), DPOAE level at p35 were significantly increased at 8 kHz ($p<0.05$), but also at higher frequencies between 12 kHz and 24 kHz ($p<0.001$) (Fig. 8 A). Noticeable was a relative higher DPOAE level at p28 (Fig. 11A, pink line), Tone-ABR showed no differences in hearing level compared to the control (Fig. 11B), but click-ABR indicated a significant higher hearing threshold at p28 with 54 ± 3 dB SPL and p35 with 57 ± 3 dB SPL compared to control animals (Fig. 11C). At wave I no difference latency was recorded (Fig. 11D), whereas the amplitude was significantly reduced at p28 and p35 compared to control animals (Fig. 11E). At p28, the latency of wave II had a latency shift starting at 65 dB (Fig. 11F), whereas the amplitude of p28 and p35 animals with an cKO application at p16 and p19 was significantly reduced (Fig. 11G). Audiological investigation implicated a mild effect on the hearing level of Tam 2/5 and Tam 16/19 mice at the age of p28 and p35.

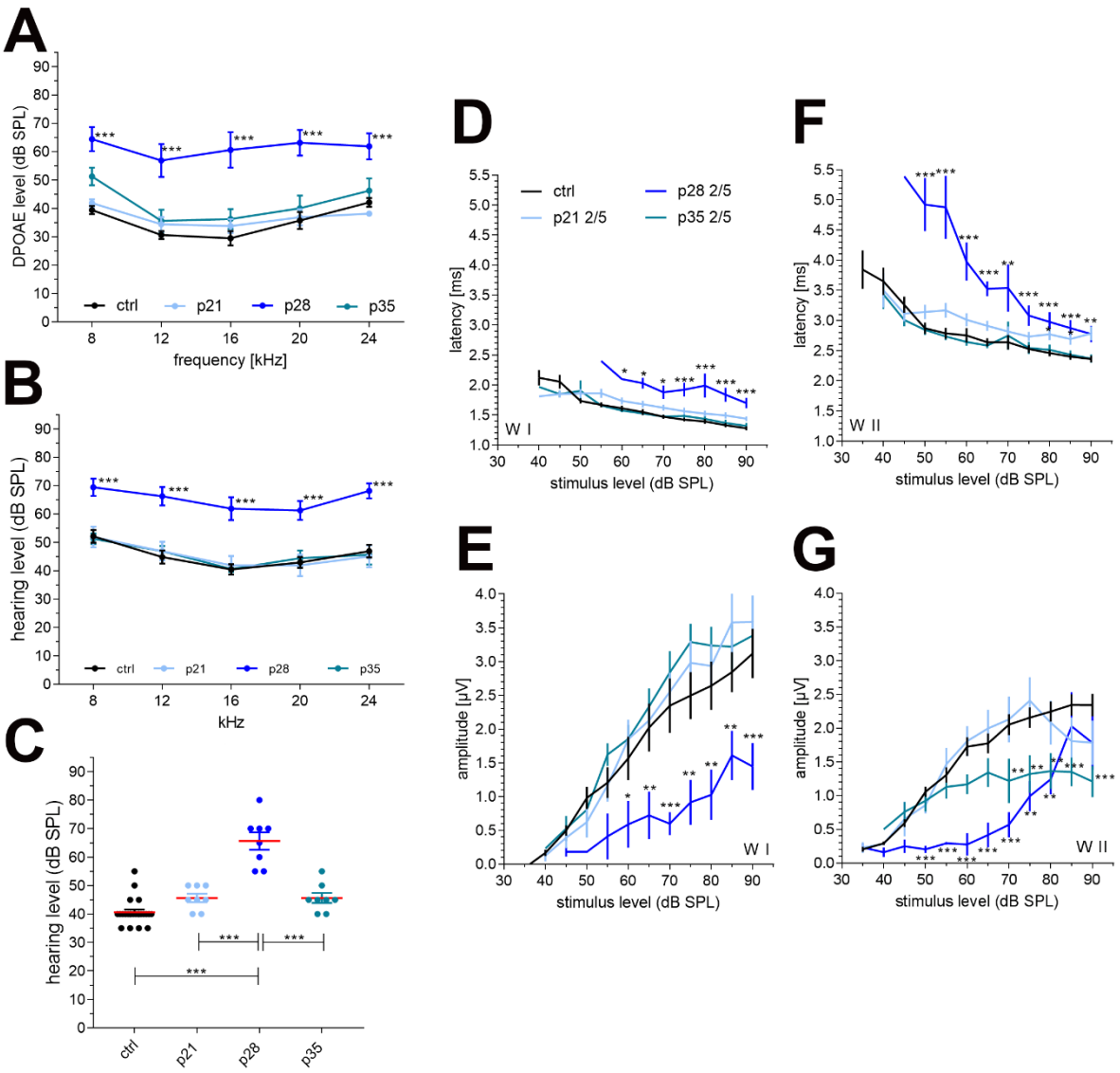

Figure 10: Audiological examination after Tam 2/5 from Slc26a5-iCre Cre/+, Stat3-fl fl/+.

(A) DPOAE level of p28 is significantly increased at 8, 12, 16, 20 and 24 kHz ($p<0.001$) compared to control. (B) Hearing level of tone specific ABR at the age of p28 is significantly decreased in 8, 12,16, 20, 24 kHz and (C) hearing threshold of click ABR indicates a significant hearing impairment. (D) Wave I of affected mice showed a latency shift and (E) a significantly reduced amplitude starting at 90 dB SPL. (F) Additionally, wave II indicates a latency shift and (G) amplitude reduction compared to control animals. DPOAE and tone ABR: Regular two-way ANOVA with multiple comparison tests and Tukey post hoc analysis. Click ABR: Ordinary one-way ANOVA with multiple comparison test and Hold-Sidak post hoc analysis. Latency and amplitude: Ordinary one-way ANOVA with multiple comparison tests and Tukey post hoc analysis. Significances: *$p<0.05$, **$p<0.01$, ***$p<0.001$.

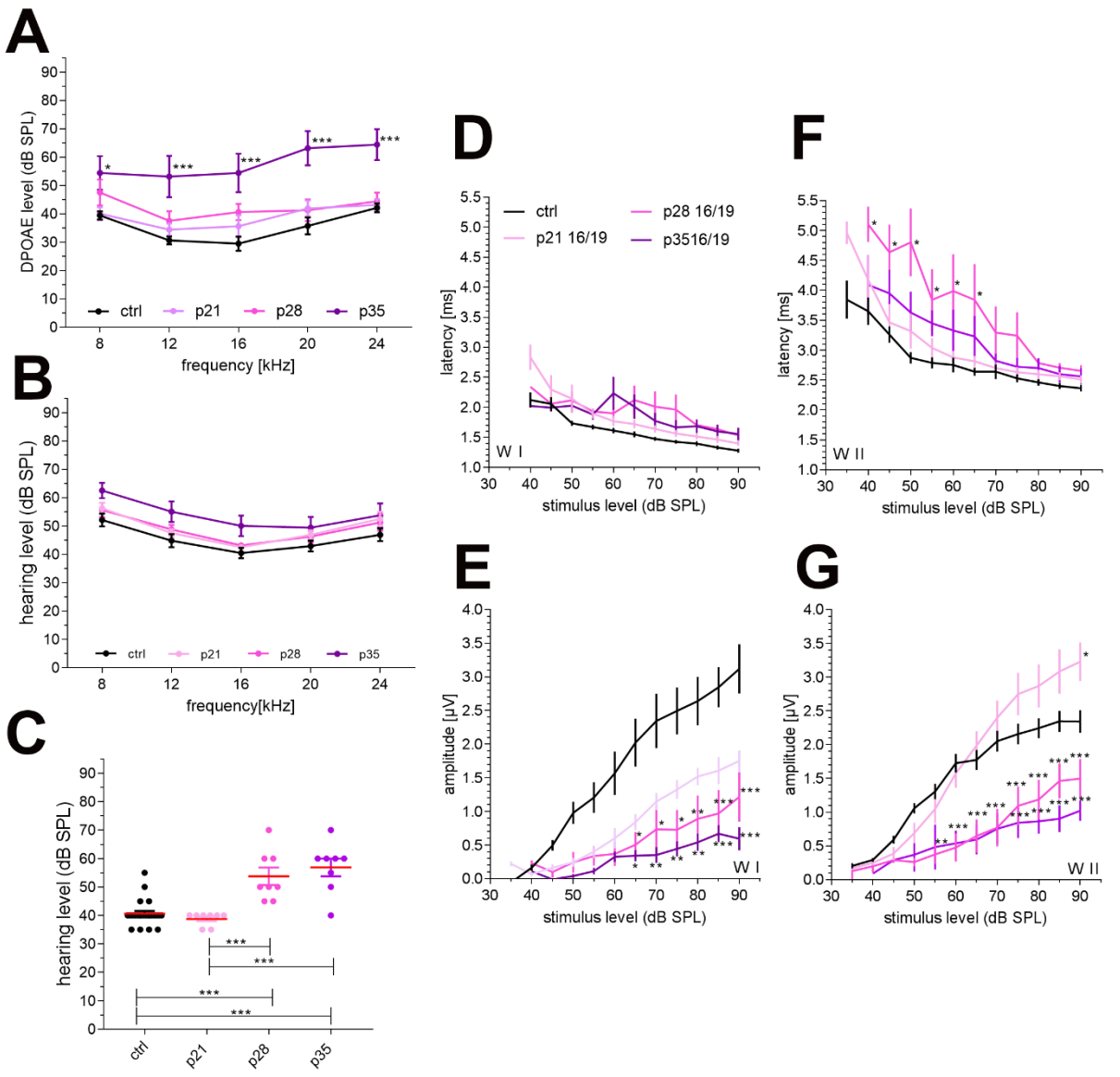

Figure 11: Audiological examination after Tam 16/19 from Slc26a5-iCre Cre/+, Stat3-fl fl/+.

(A)DPOAE level at the age of p35 is significantly reduced at 8 kHz ($p<0.05$), 12, 16, 20 and 24 kHz ($p<0.001$). (B) Hearing level of tone specific ABR showed no differences, but (C) the hearing threshold at the age of p28 and p35 ($p<0.001$) is significantly increased. (D) Wave I of cKO mice showed no latency shift, (E) but an amplitude decreasing at p28 and p35. (F) Additional analyzation of wave II implicated a latency shift at p28 starting at 65 dB SPL to 40 db SPL, but an amplitude decreasing at p28 and p35. DPOAE and tone ABR: Regular two-way ANOVA with multiple comparison tests and Tukey post hoc analysis. Click ABR: Ordinary one-way ANOVA with multiple comparison test and Hold-Sidak post hoc analysis. Latency and amplitude: Ordinary one-way ANOVA with multiple comparison tests and Tukey post hoc analysis. Significances: *$p<0.05$, **$p<0.01$, ***$p<0.001$.

7.2.2. cKO of Stat3 in outer hair cells implicates no morphological alternations of the Cochlea and the organ of Corti.

After auditory examination, the morphology of the organ of Corti and OHCs was further analyzed. Therefore, histological examination was performed to investigate the strucuture of the cochlea and the organ of Corti. Cryosections of cochlea were stained with Hämalaun/Eosin and Whole Mounts were immunolabelled with Phalloidin to visualize the cuticular plate of the organ of Corti.

Histological cryosections implicated normal development and structure of the Cochlea (Fig. 12A, C) and the organ of Corti (Fig. 12A, C Zoom) at p28 and p35. Whole Mount staining showed normal formation of one raw IHC and three raws of OHCs at p28 (Fig. 12B, D) with all sensory hair cells. Noticable was a loosing epithelium at Tam 2/5 (Fig. 12B, middle), but no loss of OHCs. At p35, the epithelium was still tight (Fig. 12D, middle).

This results implicated no significant morphology changes in the cochlea and the organ of Corti.

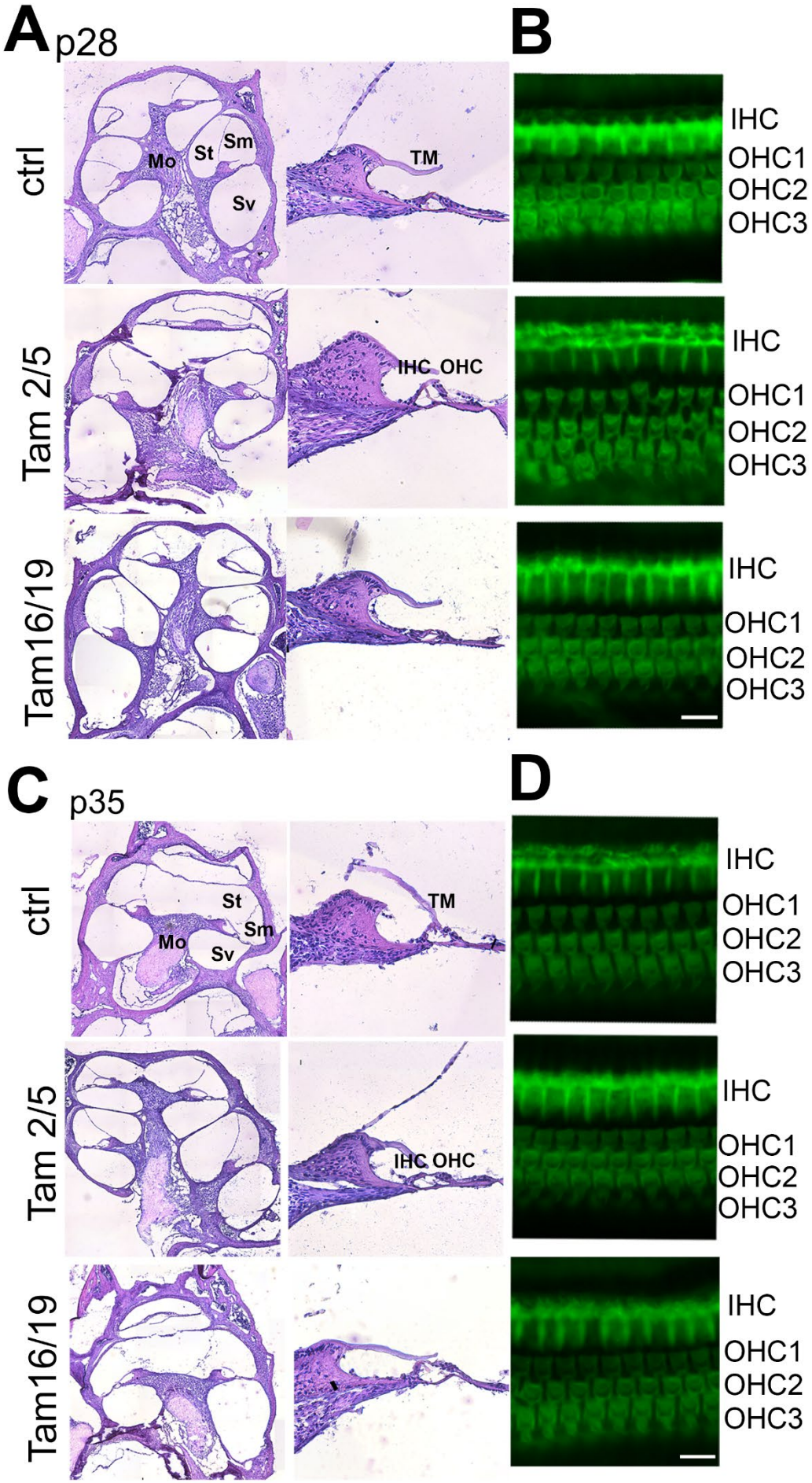
A
p28
ctrl
Mo
St
Sm
Sv
TM
Tam 2/5
IHC OHC
Tam16/19
B
IHC
OHC1
OHC2
OHC3
C
p35
ctrl
St
Sm
Mo
Sv
TM
Tam 2/5
IHC OHC
Tam16/19
D
IHC
OHC1
OHC2
OHC3

Figure 12: Histomorphological examination of affected Cochlea and organ of Corti at p28 and p35.
(A) Cryosections of cochlea at the age of p28 stained via Hämalaun/Eosin implicates normal development of the Cochlea with a modiolus (Mo) and Rosenthal canal, tectorial membrane (TM), scala vestibuli (Sv), tympani (St), media (Sm) and a normal organ of Corti with inner hair cell (IHC) and outer hair cells (OHCs)(Zoom). (B) Immunohistochemistry of the organ of Corti showed a normal cuticular plate with one raw IHC and three rows of OHCs at p28. Moreover, the epithelia tightness of Tam 2/5 is reduced. (C) Cochleae at the age of p35 had a normal development and the present of full organ of Corti (Zoom). (D) Whole mount staining showed a normal organ of Corti with one raw of IHC and three rows of OHCs. Scale bar: 20 µm.

7.2.3. cKO of Stat3 in outer hair cells indicates disturbed cell homeostasis.

Because a hearing impairment, but a normal morphology of the organ of Corti, OHCs of affected cKO mice were analyzed via bulk sequencing to identify possible irregulation in the functionality of OHCs. Therefore, housekeeping genes of OHCs, as well as important Jak/Stat3-pathway were analyzed. Regarding microtubules, PTM enzymes, MAPS, TBCs, isotypes and important regulator of the microtubule dynamic were analyzed. Additionally, gene analyzation via KEGG (Kyoto encyclopedia of genes and genomes) and GO (Gene Ontology) database were performed.

Housekeeping OHCs genes were normally expressed in cKO mice with Tam 2/5 at p28 and p35 or at p35 with Tam 16/19 compared to control animals with a high rate of *Coch* and *Myo6,* but also *Stat3* (Fig. 13A). Due to the JAK/Stat3- pathway, *Jak3* ($p<0.001$) was significantly upregulated at p28 Tam 2/5 and 035 Tam 16/19, whereas *PIAS3* is significant upregulated at all analyzed cKO models (Fig. 13B). *Cavin2* ($p<0.001$) was significantly downregulated at p35 Tam 2/5. At p28 and p35 with Tam 2/5, *Kpna1* ($p<0.05$) is significant upregulated ($p<0.05$), while *Ccl5* is upregulated in cKO Stat3 at p35 with Tam 16/19 (Fig. 13B).

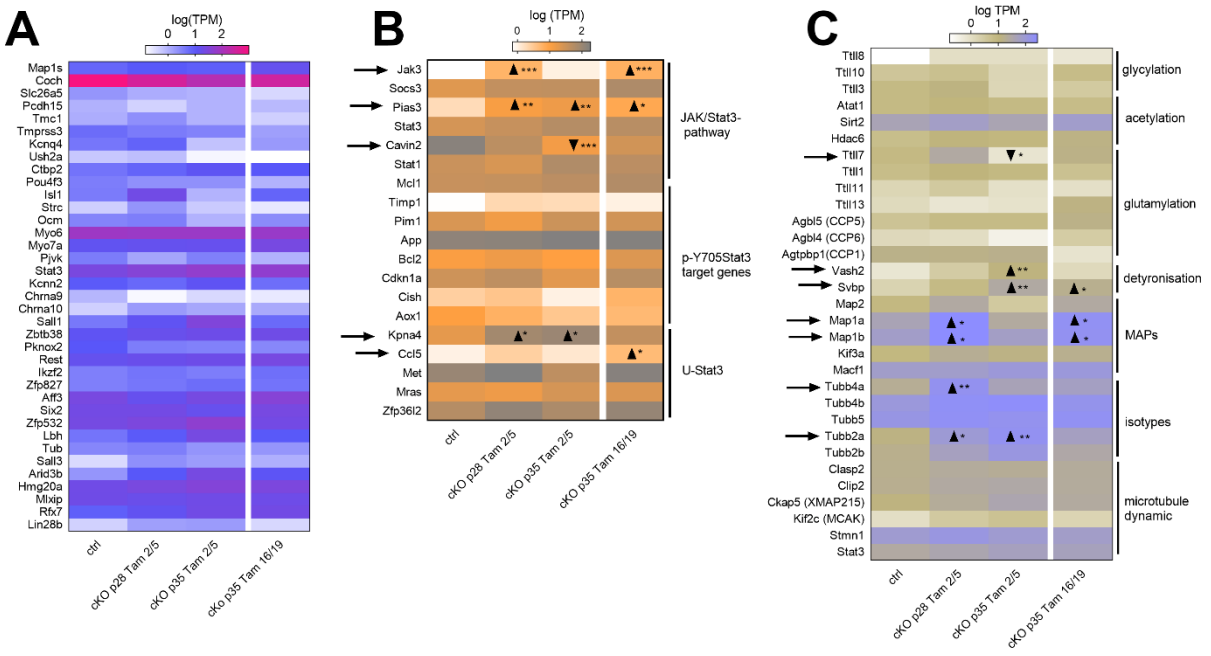

Figure 13: mRNA expression of OHC, Stat3 and microtubule related genes at p28 and p35.

(A)mRNA expression of housekeeping OHC genes were constant at each cKO mice with a high rate of Cochlin (*Coch*), Myosin VI (*Myo6*) and Stat3. (B) Regarding to Jak/Stat-pathway, *PIAS3*, an inhibitor of pY705-Stat3 is significantly higher expressed at p28 and p35 ($p<0.01$) with Tam 2/5 and at p35 Tam 16/19 ($p<0.05$) compared to control animals. Janus Kinase 3 (*Jak3*) is significantly upregulated at p28 with Tam 2/5 and at p35 with Tam 16/19 ($p<0.001$), whereas *Cavin2* is only upregulated at p35 with Tam 2/5 ($p<0.001$). Due to pY705-Stat3 regulator genes, no differences were found at gene expression, whereas importin α3 (*Kpna4*) nuclear transport of unphosphorylated (U-Stat3) is significantly upregulated at p28 and p35 with Tam 2/5 ($p<0.05$) and gene expression of RANTES (*ccl5*) at p35 with Tam 16/19. (C) For microtubule PTM, detyronisation with *vash2* and *svbp* ($p<0.01$) is upregulated at p35 with Tam 2/5 as well as with Tam 16/19 ($p<0.05$) compared to control animals. For glutamylation, *Ttll7* is downregulated for p35 with Tam 2/5 ($p<0.05$). Map1a and Map1b is significantly upregulated at p28 with Tam 2/5 and at p35 with tam 16/19 ($p<0.05$). Regarding tubulin isotypes, Tubb4a is significantly upregulated at p28 with Tam 2/5, while Tubb2a is upregulated at p28 ($p<0.05$) and p35 with Tam 2/5 ($p<0.01$). mRNA expression of proteins regarding microtubule dynamics were not affected compared to control animals. TPM = transcript per millions.

The Microtubule PTM enzyme *Ttll7* ($p<0.05$) responsible for glutamylation was significant downregulated at p28 Tam 2/5, whereas *Vash2* with *Svbp* ($p<0.01$) responsible for detyronisation was significant high regulated at p35 with Tam 2/5 and Tam 16/19. Regarding the MAPs, *Map1a* and *Map1b* ($p<0.05$) gene expression were significantly increased at p28 with Tam 2/5 and p35 with Tam 16/19. Microtubules isotype *Tubb4a* was significant ($p<0.01$) increased only at p28 with Tam 2/5, while an increase of *Tubb2a* expression was measured at p28 ($p<0.05$) and p35 ($p<0.01$) compared to control animals. Tubulin binding cofactors and microtubule dynamic genes were not affected (Fig. 13C)

mRNA expression analyzation indicated 29 significant upregulated genes and 49 downregulated genes at cKO mice at p28 with Tam 2/5 (Fig. 14D), while at p35, 781 upregulated genes and 1441 downregulated genes were identified (Fig. 14E). At p28, pathways of phagosome, calcium signaling and cytoskeletal organization and transport were upregulated, whereas ABC transporters and homeostasis pathways were downregulated (Fig. 14F). At p35, genes for ABC transporters, calcium and membrane associated pathways were downregulated, whereas RNA catabolic processes were upregulated (Fig. 14G).

mRNA expression analyzation identified 58 significant upregulated genes and 476 significant downregulated genes at p35 with Tam 16/19 (Fig. 14E). After KEGG and GO, upregulated pathways were phagosome and harmful pathways like IL17, cytokine metabolic process and NF-kB. Downregulated genes with RNA transcription and translation with nuclear transport were upregulated, whereas ECM receptor interaction, protein digestion and potassium ion transport were downregulated (Fig. 14F).

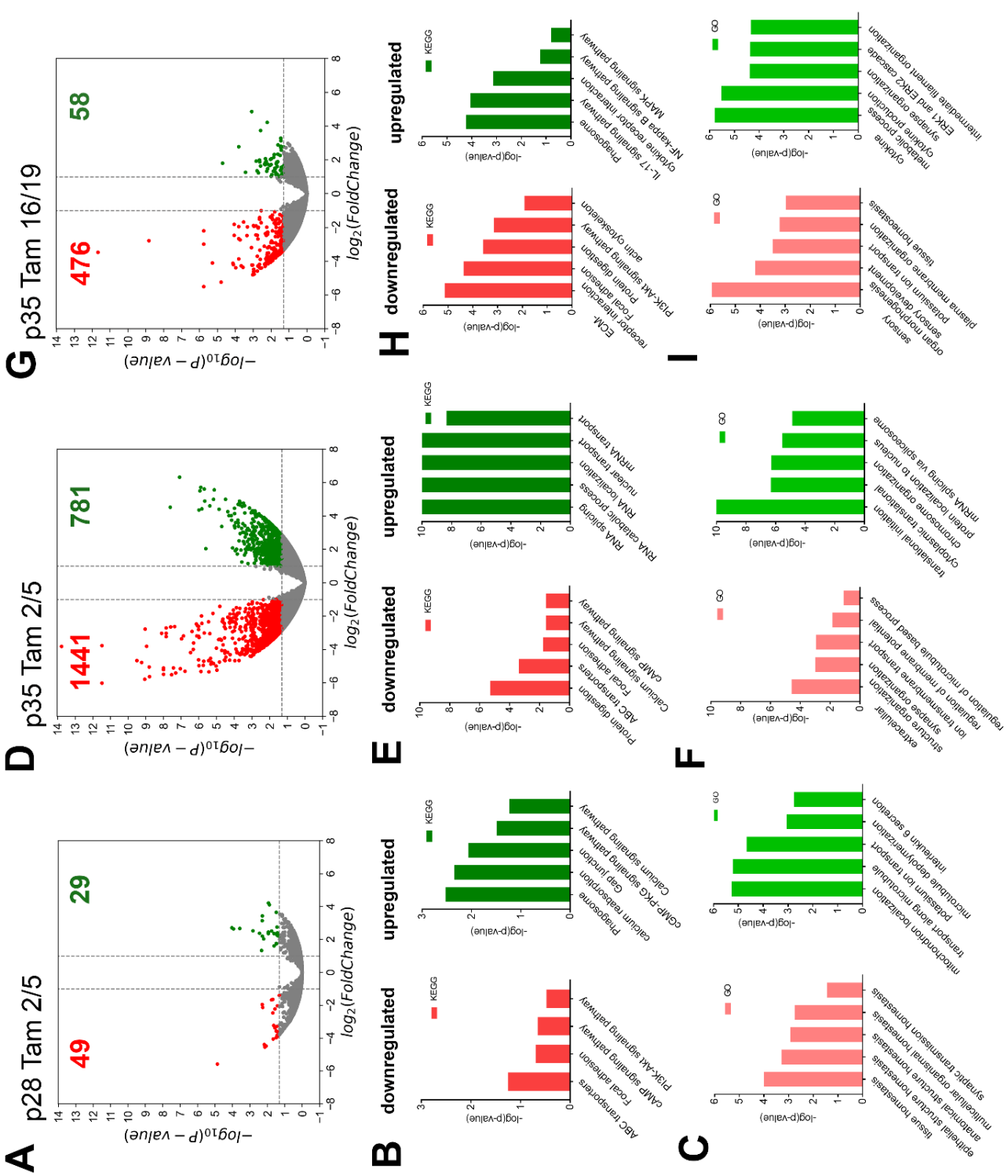

Figure 14: Up- and downregulated genes and pathways of cKO at p28 and p35.

(A) OHCs at p28 with Tam 2/5 showed significant upregulation of 29 genes and 49 upregulated genes compared to control animals. (B) After KEGG, upregulated pathways were Phagosome, the cGMP-PKG and calcium signaling with reabsorption, whereas ABC transporters, cAMP and PI3K-Akt pathway were downregulated. (C) GO analyzation resulted in a upregulation of microtubule transport, depolymerization, mitochondrion localization and potassium ion transport with IL-6 secretion, whereas cellular homeostasis were downregulated. (D) OHCs at p35 with Tam 2/5 indicated significant upregulation of 781 genes and 1441 downregulated genes compared to the control animals. (E) After KEGG, upregulated pathways included RNA localization, splicing and transport, whereas protein digestion, ABC transporters with calcium and cAMP were downregulated. (F) After GO, translation, chromosome organization with protein localization in the nucleus were upregulated, whereas

regulation of membrane potential, organization and transport were downregulated. (G) OHCs at p35 with Tam 16/19 indicated 58 upregulated genes and 476 downregulated genes, which were involved in (H) Phagosome, cytokine receptor interaction like IL-17 signaling and NF-kB and MAPK signaling. Downregulated pathways were ECM receptor interaction with protein digestion, PI3K-Akt pathway and actin cytoskeleton organization. (I) GO analyzation showed an upregulation of cytokine metabolic process with cytokine production and ERK cascade as well as synapse and intermediate filament organization. GO downregulation included sensory morphology and development, potassium transport and homeostasis.

7.2.4. cKO of Stat3 in outer hair cells has no effect on mitochondrial formation and synaptic regulation.

Due to cKO of Stat3 in OHCs caused mild hearing impairment with homeostatic imbalance and high cytokine interaction, with downregulated calcium signaling and ion transmembrane transport, mitochondria morphology was analyzed. As mentioned before, phosphorylated Stat3 on S727 is also involved in mitochondrial activity, which cKO of Exon 22 resulted in a dysfunction of Stat3. Therefore, the ultrastructure of the apical and basal structure of OHCs and mitochondria were analyzed via electron microscopy.

The images indicated a normal development of OHCs at the apical part with an intact cuticular plate, stereocilia and mitochondria at p28 and p35 with Tam 2/5 as well as with Tam 16/19 (Fig. 15A). Basally, the position of nuclei of OHCs was normal and the plasma membrane was not perforated. Also, the OHCs were lying in the cup of Deiters cells (Fig. 15A).

Because DPOAE of cKO mice at the age of p28 and p35 were increased, the OHCs were stained with parvalbumin for activity and CtBP2 to investigate the synaptic ribbon structure. Parvalbumin is a calcium-binding protein, which indicated calcium signaling in cell processes. CtBP2 is a marker for presynaptic ribbons of sensory cells. Both markers showed no different labelling in affected groups with hearing impairment compared to control littermates (Fig. 15B).

The results indicated no effect in cKO mice due to mitochondria or synaptic ribbons on the presynapses, but a lower activity of calcium signaling in OHCs.

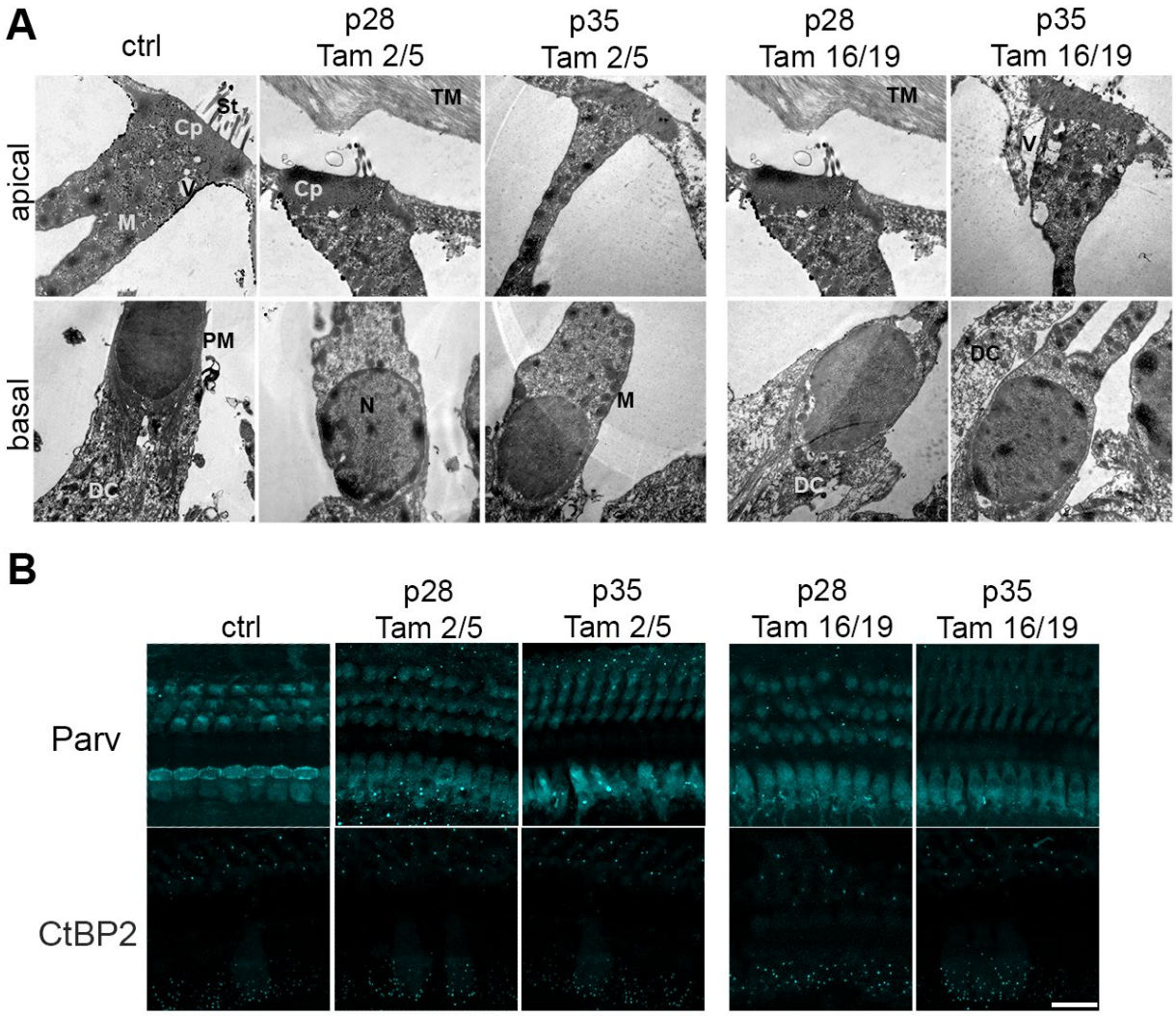

Figure 15: Ultrastructure and activity of OHCs at p28 and p35.
Images indicates normal morphology of OHCs (A) at p28 and (B) p35 on the apical part with stereocilia rooted in the cuticular plate and vacuoles at Tam 2/5 and Tam 16/19 comparted a control animal. Basally, OHCs sits on the cup of the Deiters cells with normal distances of plasma membranes and the position of the nucleus is in the lowest point. Magnification: 10000. Cp= cuticular plate, DC= Deiters cell, M = mitochondria, N = nucleus, PM= plasma membrane, St = stereocilia, TM= tectorial membrane, V= vesicles.

7.2.5. cKO of Stat3 in outer hair cells implicated no synaptopathy or neuropathy.

Since the bulk sequencing showed evidence of disturbed homeostasis in OHCs, affected groups were further analyzed in postsynaptic morphology. Therefore, different histological examinations were prepared. Synapses and nerve fibers were stained via immunohistochemistry. At the postsynapses, synaptophysin is a vesicle protein, which can be detected in synapses. Immunostaining with this protein in cKO mice indicated no different sizes of synapse or innervation of sensory cell of the organ of Corti compared to control mice. Additionally, ßIII-tubulin, which is a highly conserved neuronal fiber marker, showed no differences in neuronal fibers crossing the tunnel of Corti. Immunohistochemical analysis of

cKO mice implicated no differences in synapse formation and indicated no synaptopathy in affected cKO mice with hearing impairment.

Another reason for hearing impairment can be an auditory neuropathy. The characteristics are neuronal loss, latency shifts and reduced amplitudes. To understand the increased hearing threshold with latency shifts and amplitude reduction in the cKO mice the spiral ganglia were evaluated. For this, spiral ganglia death and changes myelin sheet were considered. Cryosections of p28 and p35 of Tam 2/5 and Tam 16/19 were labelled via TUNEL assay. This assay indicated early apoptosis in cell by labelling the nucleus (Fig. 16, positive). Spiral ganglia nuclei were not labelled by TUNEL assay at p28 and p35 (Fig. 16A), which implicated no initial cell death in these cells.

Changes in latency and amplitudes can be connected to a pathology of the myelin sheet Therefore, the g-ratio of spiral ganglion neurons was measured in proportion to the axon diameter. Therefore, semi-thin sections of p28 Tam 2/5 and p35 16/19 were analyzed by electron microscopy. The g-ratio of p28 Tam 2/5 with 0.74 and of p35 Tam 16/19 with 0.73 is not significant changed to the g-ratio of control animals with 0.71 (Fig. 16B). The results implicated no pathology in spiral ganglia of cKO mice. Therefore, the hearing impairment is caused by sensory cells.

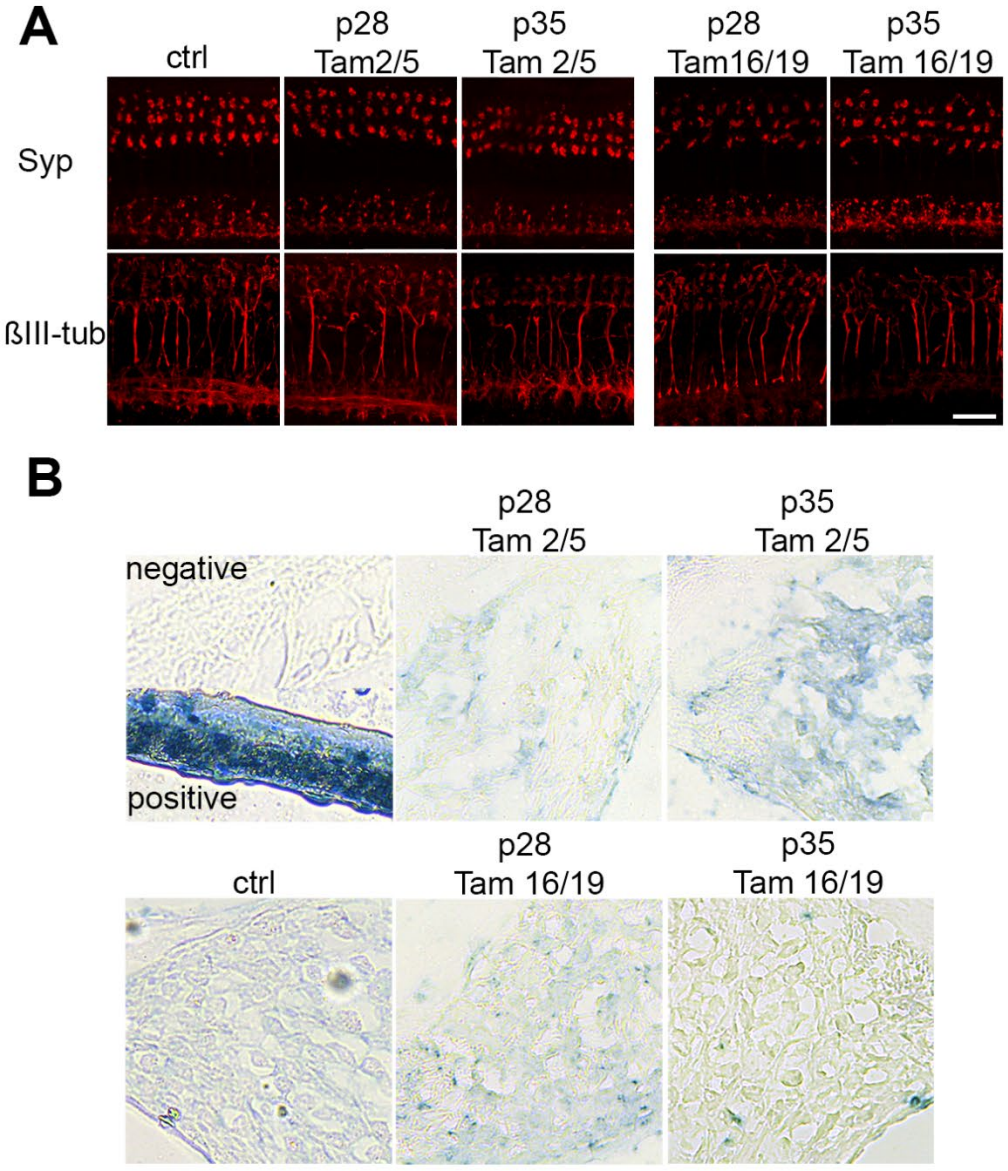
A
ctrl
p28 Tam2/5
p35 Tam 2/5
p28 Tam16/19
p35 Tam 16/19
Syp
ßIII-tub
B
p28 Tam 2/5
p35 Tam 2/5
negative
positive
ctrl
p28 Tam 16/19
p35 Tam 16/19
C
ctrl
p28 Tam 2/5
p35 Tam 16/19
g-ratio
axon diameter [µm]
ctrl
p28 2/5 distal
p35 Tam 16/19

Figure 16: Analyzation of synapses and nerve fibers at p28 and p35.
(A) Examination group with hearing impairment were stained with synaptophysin and ßIII-tubulin. However, no differences were marked including no synaptopathy or neuron fiber loss. Scale bar: 20 µm. (B) TUNEL assay of spiral ganglia at the Rosenthal canal of affected cKO mice showed no labelled nuclei compared to positive TUNEL assay control at the age of p28 and p35. (C) The myelin thickness of spiral ganglia showed no changes in the g-ratio of cKO mice at p28 Tam 2/5 and p35 Tam 16/19. Magnification of electron microscopy: 1000. Scale bar: 20 µm

7.3. Analyzation of Fgfr3-iCre Cre/+, Stat3-fl fl/+ mice

7.3.1. cKO of Stat3 in supporting cells has a mild effect on the hearing function.

Stat3 is highly expressed in supporting cells in the organ of Corti. To test whether a cKO of Stat3 in supporting cells influences hearing, electrophysiology examination was performed at p21, p28 and p35. cKO of Stat3 was induced either postnatally between p2 and p5 (Tam 2/5) or after hearing onset between p16 and p19 (Tam 16/19).

With an application of Tam 2/5, mice had no significant increase of DPOAE, tone-ABR or hearing threshold in click-ABR compared to control animals with dB SPL (Fig. 17A-C). Analyzation of Wave I in latency and amplitude showed no changes compared to control animals (Fig. 17D-E). Nevertheless, Wave II has partly significantly changed in latency (Fig. 17F) with 80 and 75 dB SPL at p28 and a reduction of amplitudes at 90 dB SPL ($p<0.001$), 85, 80 and 75 dB SPL ($p<0.05$) compared to control animals.

Mice inducing a cKO between p16 and p19 (Tam 16/19), had no significant changes in the DPOAE level, but a higher level in tone-ABR at 12, 16, 20 kHz ($p<0.05$) and 24 kHz ($p<0.01$) at p35 (Fig. 18, dark red line). Moreover, the hearing threshold of mice at the age of p35 was significantly reduced with 57 ± 4 dB SPL ($p<0.001$) compared to control mice with 43 ± 1 dB SPL. Additionally, a latency shift, but not amplitude changes, of Wave I at the age of p35 was implicated starting from 90 dB SPL to 75 dB SPL ($p<0.05$) and 70 to 65 dB SPL ($p<0.01$) (Fig. 18D-E). Analyzation of Wave II implicated no changes in latency or amplitudes (Fig. 18F-G).

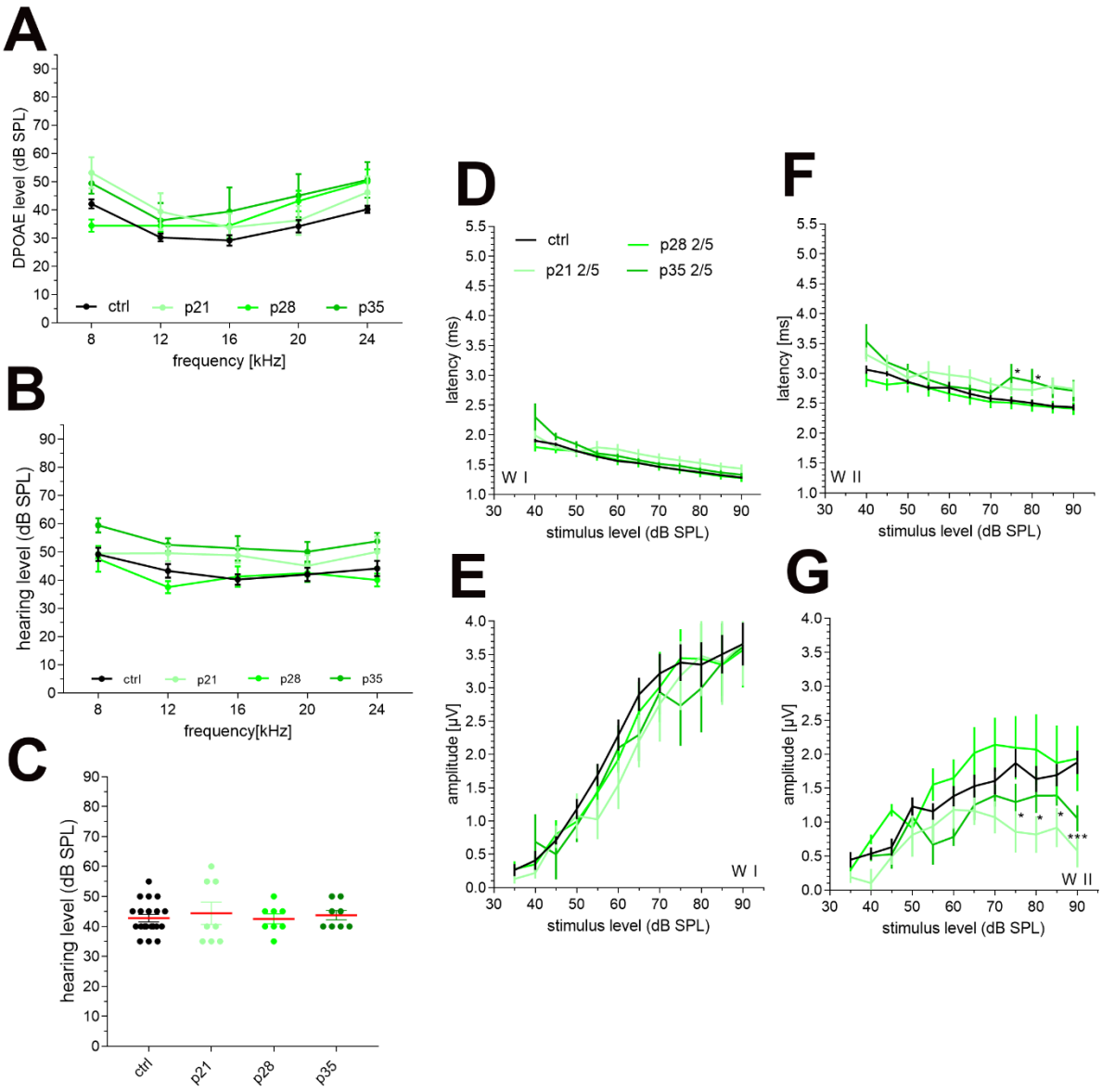

Figure 17: Audiological examination after Tam 2/5 from Fgfr3-iCre Cre/+, Stat3-fl fl/+.

(A) DPOAE level and (B) hearing level of tone specific ABR of cKO mice had no significant differences compared to control. (C) Hearing threshold of click ABR indicates no hearing impairment of cKO mice. (D) Wave I of cKO showed no differences on latency shift and (E) amplitudes. (F) Wave II indicates no differences in latency, but (G) amplitude reduction at the age of p21 compared to control animals, which effect leaks at p28 and p35. DPOAE and tone ABR: Regular two-way ANOVA with multiple comparison tests and Tukey post hoc analysis. Click ABR: Ordinary one-way ANOVA with multiple comparison test and Hold-Sidak post hoc analysis. Latency and amplitude: Ordinary one-way ANOVA with multiple comparison tests and Tukey post hoc analysis. Significances: *p<0.05, **p<0.01, ***p<0.001.

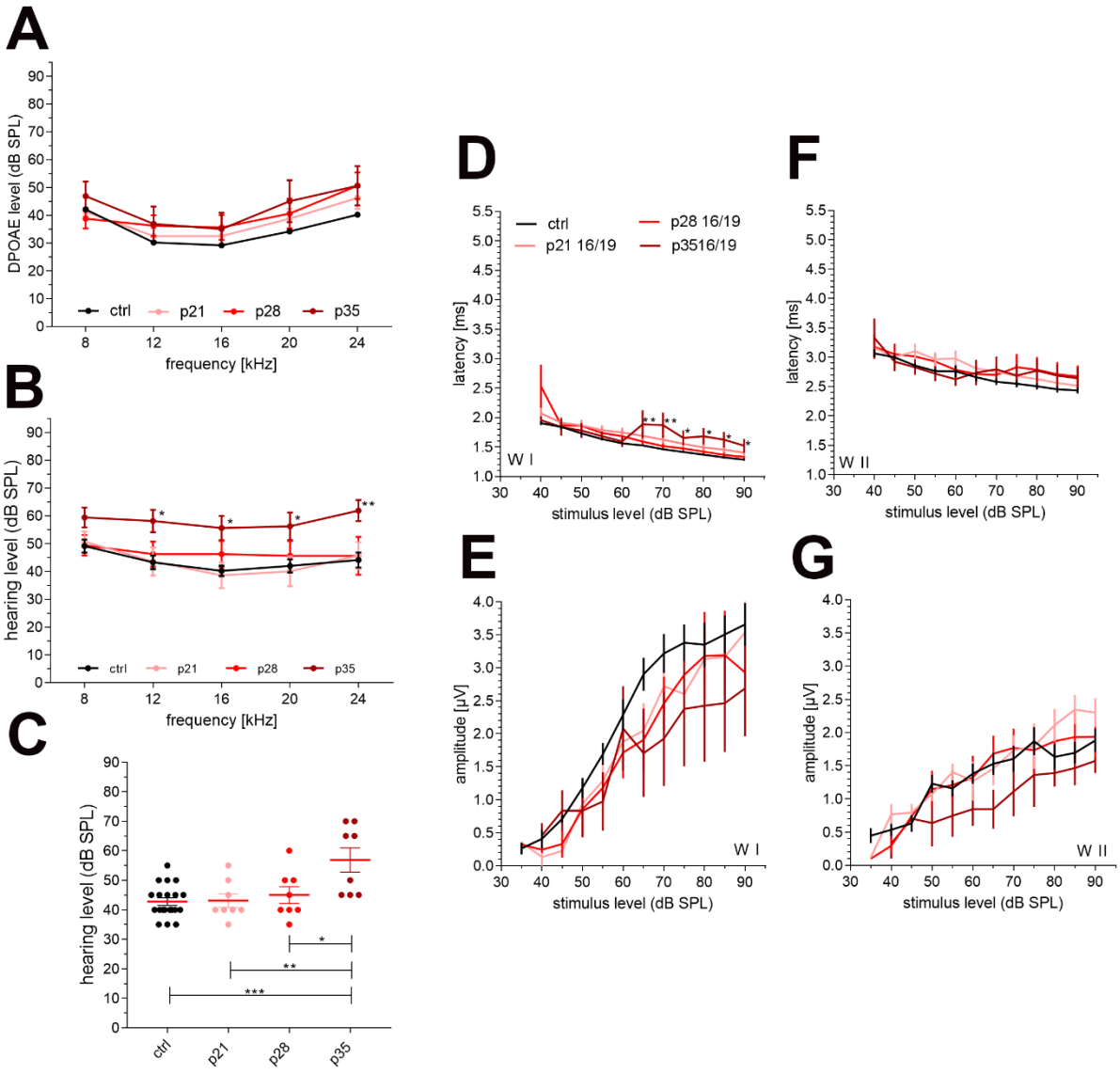

Figure 18: Audiological examination after Tam 16/19 from Fgfr3-iCre tg/+, Stat3-fl fl/+.
(A) DPOAE level showed no differences in cKO mice compared to control animals. (B) Hearing level of tone specific ABR at the age of p35 is significantly decreased in 12, 16, 20, ($p<0.01$) and 24 kHz ($p<0.001$). (C) Additionally, hearing threshold of click ABR indicates a significant hearing impairment at p35 ($p<0.001$) compared to control animals. (D) Wave I of affected mice showed a latency shift starting at 90 dB SPL until 65 dB SPL, but (E) no differences in amplitudes. (F) Wave II showed no latency or (G) amplitude differences in cKO compared to control animals. DPOAE and tone ABR: Regular two-way ANOVA with multiple comparison tests and Tukey post hoc analysis. Click ABR: Ordinary one-way ANOVA with multiple comparison test and Hold-Sidak post hoc analysis. Latency and amplitude: Ordinary one-way ANOVA with multiple comparison tests and Tukey post hoc analysis. Significances: *$p<0.05$, **$p<0.01$, ***$p<0.001$.

7.3.2. cKO of Stat3 in supporting cells effects not the microtubule bundle formation

Due to high density of acting and microtubule bundles, the ultrastructure were analyzed in semithin section via electron microscope. In the Deiters cells of Tam 16/19 mice at the age of p35 implicated a high ratio of microtubules at the apical supporting OHCs on the lateral side (Fig. 19A apical). The medial part of Deiters cells, which forms a cup, holding synapses and the OHCs. Therefore, microtubules and actin had a high density as control animals (Fig. 19A

medial). Basally, the microtubules anchored the Deiters cells at the basilar membrane as Deiters cells of control animals (Fig. 19A, basal) with a high amount of intact mitochondria.

Pillar cells are the scaffold of the organ of Corti. The density of microtubules of mice at the age of p35 with Tam 16/19 were as high as control mice at the apical, medial and basal part (Fig. 19B). Moreover, the anchoring of pillar cells at the basilar membrane with a high amount of mitochondria was not different to control animals.

Electron microscopy of Deiters and pillar cells implicated no differences in microtubule density at apical, medial of basal regions.

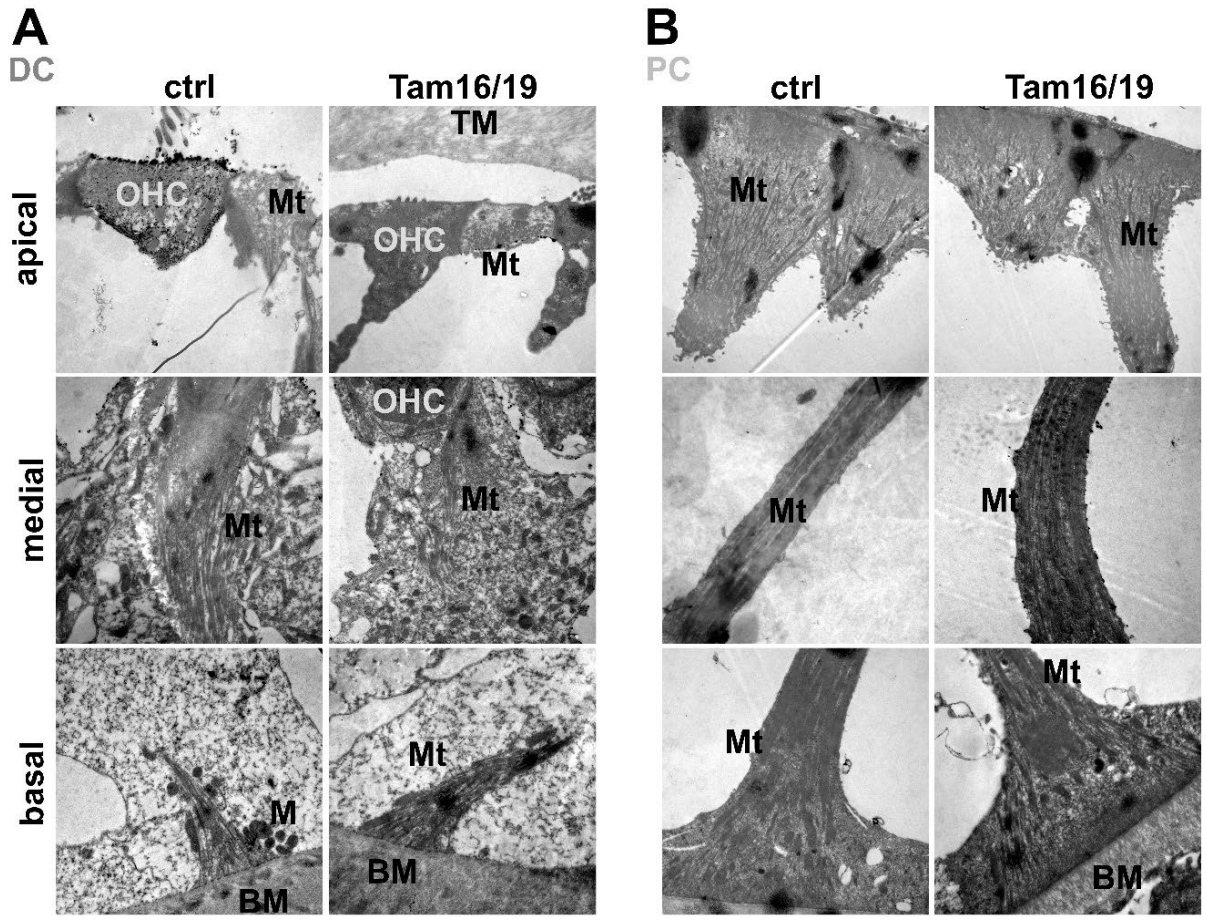

Figure 19: Ultrastructure of Deiters and pillar cells at p35.
Images indicates normal morphology of Deiters (A) and pillar cells (B) at the age of p35 with Tam 16/19. The apical part of Deiters and pillar cells had a high density of microtubules supporting the sensory cells. The medial part contains a high amount of actin and microtubules were scaffold the organ of Corti. Basally, microtubule bundles anchored Deiters cells and pillar cells at the basilar membrane. Magnification: 10000. BM = basilar membrane, DC = Deiters cell, M = mitochondria, Mt = microtubules, OHC = outer hair cell, PC = pillar cell, PM = plasma membrane, St = stereocilia, TM = tectorial membrane

7.3.3. cKO of Stat3 in supporting cells implicated changes in posttranslational modifications of microtubules.

Beside a normal distribution of microtubule bundles in Deiters and pillar cells, posttranslational modifications (PTM) of microtubules can be affected. Therefore, cryosections and whole mount of the organ of Corti were analyzed by PTM immunostaining of cKO mice at p28 and p35 with Tam 16/19.

In cryosections, tyrosinated tubulin was found in the sensory hair cells of the cochlea, the nerve fibers and Deiters cells in control mice as well as with Tam 16/19 at p28 and p35 (Fig. 20, tyr). Polyglutamylated tubulin was found in the cup-structure at the Deiters cells and the inner pillar cell, whereas defragmentation was found at cKO mice at p28 and p35 with Tam 16/19 (Fig. 20 polyE). Acetylated and detyronisated tubulin was partially defragmented in p28 Tam 16/19 cochleae and complete destroyed in the phalangeal processes of Deiters cells and especially in the outer pillar cells compared to the control cryosections (Fig. 20, acet and detyr). Whole Mount staining of detyronisated tubulin also implicated an instability of microtubule bundles starting at p28 with Tam 16/19 to a high tortuosity at p35 (Fig. 20, Whole Mount detyr).

The results indicated a different modification rate of microtubule bundles in cKO mice starting at p28 with Tam 16/19, which results in an instability of the cytoskeletal structure.

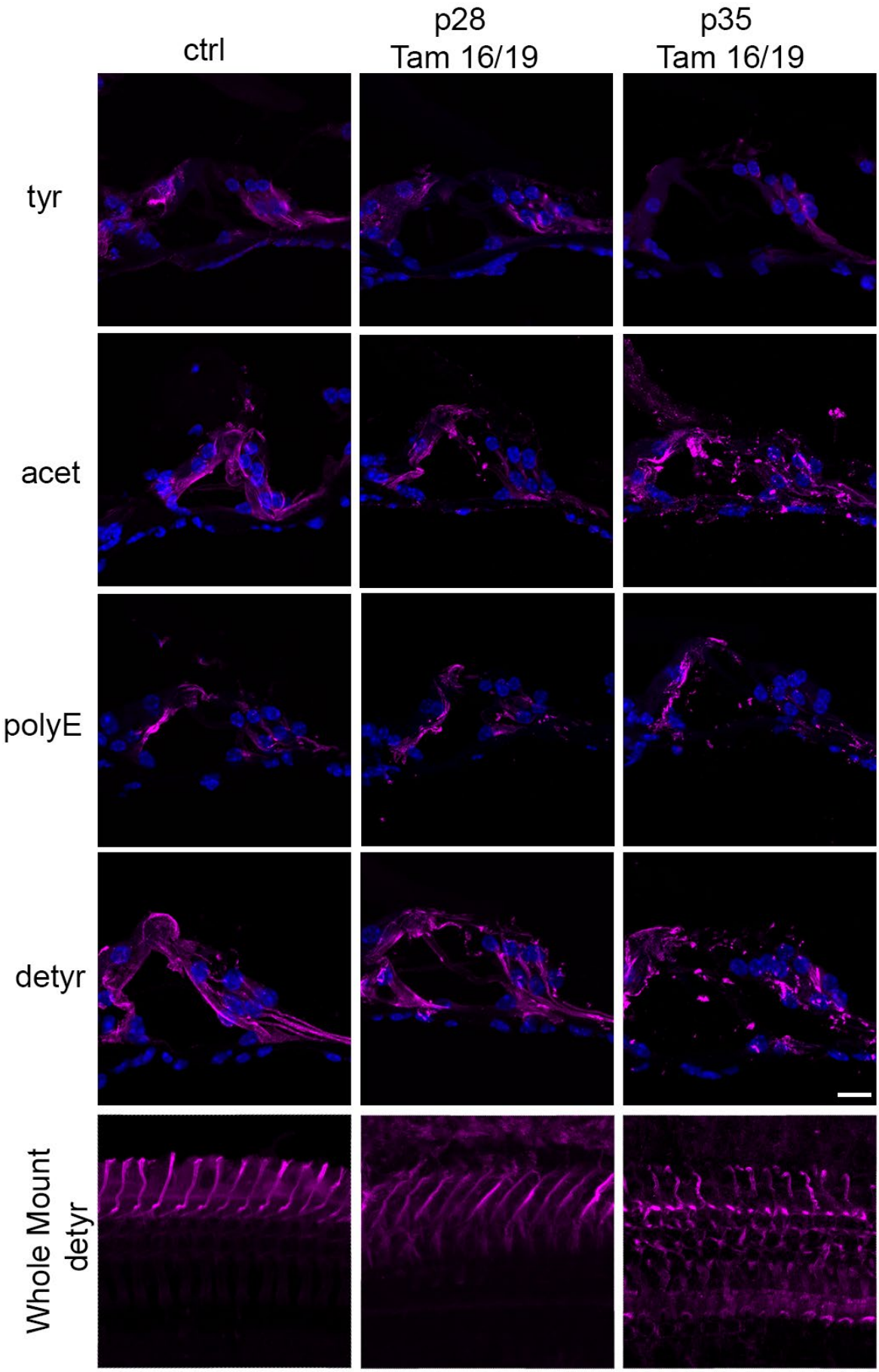
ctrl
p28
Tam 16/19
p35
Tam 16/19
tyr
acet
polyE
detyr
Whole Mount
detyr

Figure 20: Posttranslational modifications of tubulin at p28 and p35 Tam 16/19.
Tyrosinated tubulin (tyr) is normal expressed in the Deiters cells of cKO mice at p28 and p35. Stable tubulin posttranslational modification like acetylated tubulin (acet), polyglutamylated (polyE) and detyronisated tubulin (detyr) is rarely found in the phalangeal processes of the Deiters cells at p28 and were complete defragmented at p35. Whole Mount staining with detyronisated tubulin of the organ of Corti showed well defined structure of detyronisated microtubule bundles in control animals, whereas these modified bundles indicate on the one hand a decrease of detyronisated tubulin and a progressive instability with high tortuosity starting at p28 to p35. Scale bar: 20 µm.

7.3.4. cKO of Stat3 in supporting cells implicated no synaptopathy or neuropathy.

Deiters cells forming a cup out of actin and microtubules holding OHCs and synapses for optimal vesicle transfer. Pillar cells have a high density of actin and microtubule to ensure the conserved structure of the organ of Corti by hearing processes. Therefore, histological staining of synapses and neuronal fibers were analyzed. Immunolabelling of synaptophysin indicated no different sizes or dysregulation of synapse in the organ of Corti compared to control animals (Fig. 21A, Syp). Additionally, βIII-tubulin showed no differences in neuronal fibers crossing the tunnel of Corti (Fig. 21A, βIII-tub).

Immunohistochemical analysis of cKO mice implicated no differences in synapse formation, displacement and indicated no synaptopathy in mice at the age of p28 and p35 with Tam 16/19.

Additionally, analyzation of spiral ganglia and the myelin sheet were prepared to exclude a neuropathy. Cryosections of p28 and p35 of Tam 2/5 and Tam 16/19 were labelled via TUNEL assay. This assay indicated early apoptosis in cell by labelling the nucleus (Fig. 21B, positive). Here, no spiral ganglia nuclei were labelled by TUNEL assay at p28 and p35 (Fig. 21B), which implicated no initial cell death in these cells.

Moreover, the g-ratio of spiral ganglia was measured in proportion to the axon diameter of semi-thin sections at the age of p28 and p35 16/19. The g-ratio of and of p35 Tam 16/19 with 0.73 is not significant changed to the g-ratio of control animals with 0.71 (Fig. 21B). The results implicated no pathology in spiral ganglia of cKO mice.

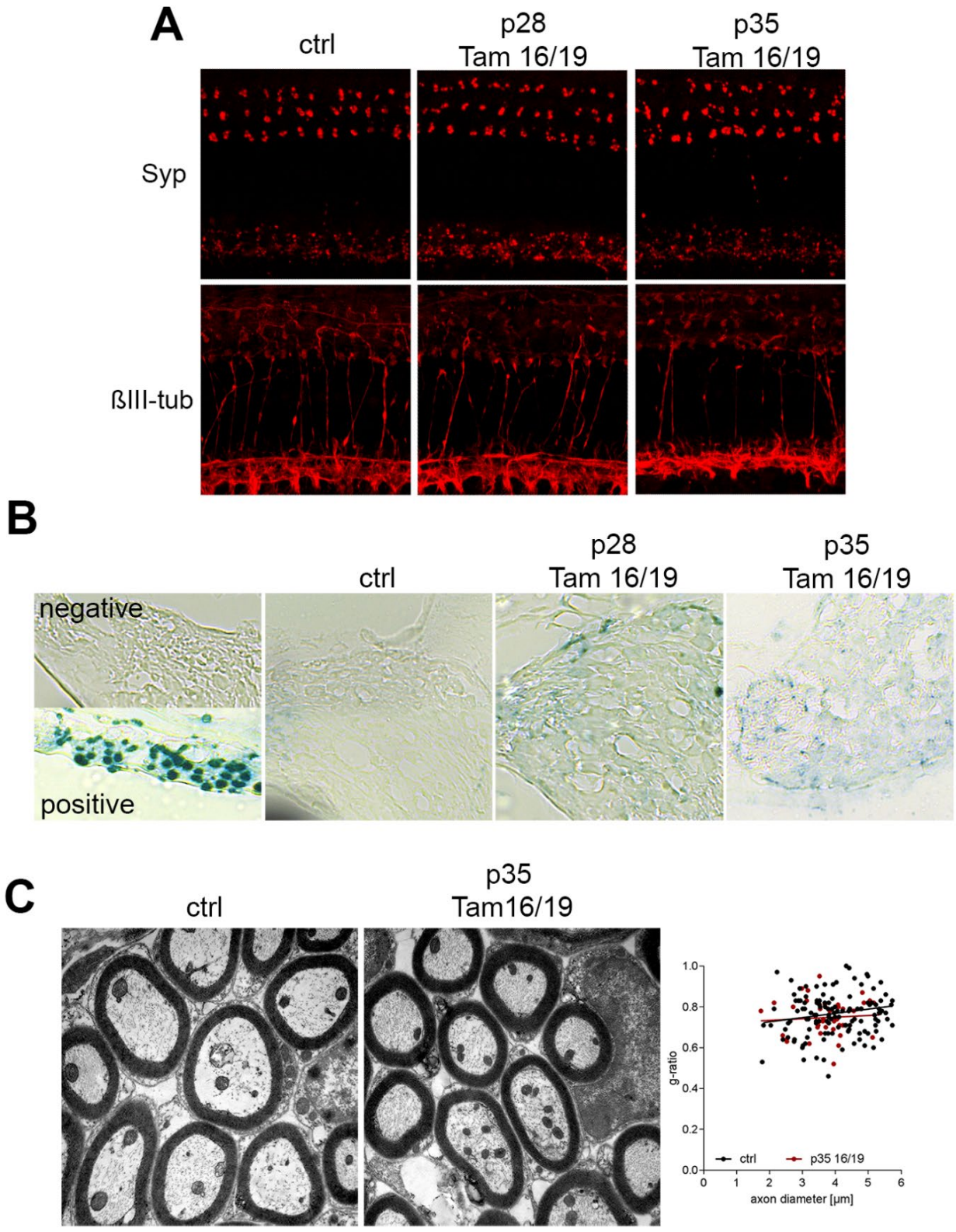

Figure 21: Analyzation of synapses and nerve fibers at p28 and p35.
(A)Examination group with hearing impairment were stained with synaptophysin and βIII-tubulin. However, no differences were marked including no synaptopathy or neuron fiber loss in the organs of Corti. Scale bar: 20 µm. (B) TUNEL assay of spiral ganglia at the Rosenthal canal of affected cKO mice showed no labelled nuclei compared to positive TUNEL assay control at the age of p28 and p35. (C) The myelin thickness of spiral ganglia showed no changes in the g-ratio of cKO mice at p35 Tam 16/19. Magnification of electron microscopy: 1000. Scale bar: 20 µm

8. Discussion

Stat3 with its canonical and non-canonical pathway regulates various processes in a cell-specific manner. In the cochlea, Stat3 has been shown to be highly expressed in sensory hair cells as well as epithelia cells and is crucial for embryonic cell development and proliferation (Wilson et al., 2014). However, Stat3 is an oncogene and is also important in the adult stage to balance cell survival and apoptosis, as well as the microtubule dynamics. Through phosphorylations at the C-terminal, Stat3 manage cellular processes in various associations with other proteins and structures.

To investigate the importance of Stat3 in the sensory epithelium of the cochlea and the process of hearing, cKOs were elicited in OHCs and supporting cells by the Cre/loxp system. These were induced either before hearing onset to study postnatal development or after hearing onset to evaluate the functionality of the cells during hearing.

The results showed that a cKO of Stat3 in OHCs before and after hearing onset leads to hearing impairment. This was indicated by an increase of DPOAE and hearing levels with a moderate latency shift and a decrease of amplitudes of nerve fiber potentials. Bulk sequencing analyses of cKO OHCs before hearing onset showed a disturbance of cellular homeostasis and extracellular signals. A cKO of Stat3 in the OHCs after hearing onset resulted in an upregulation of inflammatory related signaling and NF-κB pathways. However, histomorphological studies showed that OHC organelles as well as synapses, nerve fibers were not affected.

In supporting cells, a cKO of Stat3 after hearing onset resulted in a hearing impairment, but not before hearing onset. This was evidenced by an increase of hearing level and latencies, but no DPOAE level increase. Electron microscopical studies showed no structural changes. However, immunohistochemical investigations indicated a reduction of detyronisated tubulin, a posttranslational modification of microtubules. This modification is known for its longevity and structural strength for microtubules. In addition, phalangeal processes of Deiters´ cells showed an instability and increased tortuosity, which could result in an instability of the organ of Corti during hearing.

In summary, these results suggest that the function of Stat3 is cell-specific in the Organ of Corti. While a cKO of Stat3 leads to alternations of signaling pathways in OHCs, microtubule modifications are altered in supporting cells.

8.1. Homozygote Cre and flox- mouse line with hearing impairment

The Cre-loxp system has been developed to control or manipulate DNA genomics and its gene expression. For the presented work, two Cre-mouse lines were used for cKO in the organ of Corti. A recombinase mouse line only active in OHCs by *Slc26a5*-gene integration (Fang et al., 2012) and a recombinase mouse line, which is active in supporting cells by *Fgfr3*-gene integration (Young et al., 2010). Used Stat3-flox mouse line has the exon22 flanked by flox to be deleted by a recombinase activation. The altered Stat3-protein is characterized by a non-sense C-terminal of the Stat3 protein (Takeda et al., 1998), whereby the important phosphorylation sides of tyrosine (Y)705 and serine (S)727 are also lost.

Hearing examination of homozygote Cre and flox mice indicated a hearing impairment. While homozygote Slc26a5-iCre mice displayed increased DPOAE and ABR click levels, homozygote Fgfr3-iCre and Stat3-fl showed only increased ABR click thresholds. In the heterozygote mouse, of each mouse line, no hearing impairment was measured. Consequently, these mice were used for further experiments.

Previous studies of homozygote Slc26a5-iCre animals have shown normal hearing. (Fang et al., 2012). These differences might be due to different reasons. For example, different technical equipment used in the measurements and individual subjective manual evaluations. In addition, the environment in which the mice are kept must be taken into account, as hair cells are very sensitive to noise, e.g. from monotonous background or the noise of work in animal facility (Barden et al., 2012).

8.2. Effective Recombinase activation with heterozygote allelic

To investigate the Cre recombinase inducible activity and tissue specificity of Slc26a5-iCre and Fgfr3-iCre mice, these mice were bred with mice from reporter lines CAG-tdTomato.

The investigations approved the cell specific Cre-activity of Slc26a5-iCre line in OHCs and Fgfr3-iCre line in supporting cells of the organ of Corti. Since homozygous animals had revealed a hearing phenotype, only heterozygous descendants were also examined when crossed with the reporter lines. The results show that heterozygous Cre and flox mice exhibit highly potent Cre activity and expression. Additionally, immunohistological examination indicated recombinase activity was stable starting at p7 up to p35. Moreover, recombinase was highly effective for heterozygote Cre allelic.

These results verified prior investigation of these Cre-lines (Anttonen et al., 2012; Cox et al., 2012; Fang et al., 2012; Young et al., 2010). These indicated a high activity of recombinase of

and until 10 weeks for Slc26a5-iCre (Chessum et al., 2018) and Fgfr3-iCre until 8 months (Young et al., 2010).

Both our own and previous results show that the recombinase has cell-specific expression through the *Slc26a5* gene in OHCs and through *Fgfr3* in the supporting cells of the sensory epithelium in the organ of Corti.

8.3. Hearing loss without structural changes in Slc26a5-iCre Cre/+, Stat3-fl fl/+ mice

To investigate whether Stat3 influences OHCs in the process of hearing, Slc26a5-iCre were crossed with Stat3-flox mice. The cKO before hearing onset was induced with tamoxifen between p2 and p5 (Tam 2/5) and a cKO after hearing onset between p16 and p19 (Tam16/19). Audiological studies were performed using DPOAE and click-ABR and tone-ABR. Additionally, immunohistological investigation of the organ of Corti were performed.

The results indicated a significant increased level of DPOAE, tone ABR from 8 to 24 kHz and click ABR of Slc26a5-iCre Cre/+, Stat3-fl fl/+ at the age of p28. Additionally, a latency shift and amplitude reduction of Slc26a5-iCre Cre/+, Stat3-fl fl/+ were seen at the age of p28 with Tam 2/5. Moreover, mice with Tam 16/19 showed an amplitude reduction of spiral ganglia neurons at the age of p28 and p35, but only a latency shift at the age of 28 were measure. However, Slc26a5-iCre Cre/+, Stat3-fl fl/+ with Tam 2/5 or Tam 16/19 showed no OHC loss or degeneration of the organ of Corti. Additionally, synaptic structures were complete and no synaptopathy, neuropathy or myelinopathy were found in these mice.

Alterations in electrophysiological properties caused by sensory hair cell defects have been described for example in DFNB59 knock in mice (Delmaghani et al., 2006). DFNB59 is caused by a mutation of pejvakin, a protein of unknown function in sensory hair cells and spiral ganglia. Interestingly, mutant mice and affected patients display ABR abnormally decreased wave amplitudes and increased latencies (Delmaghani et al., 2006; Delmaghani et al., 2015; Starr et al., 2015) with an absence of DPOAEs, but no OHC loss (Schwander et al., 2007). Pejvakin mutants displayed features of marked oxidative stress and impaired antioxidant defenses. Moreover, peroxisomes in hair cells show structural degeneration, while the redox homeostasis is disturbed by overproduction of ROS (Delmaghani et al., 2015). Similar audiological and immunohistological results from our experiments suggest a related hypervulnerability of OHCs and a sensory processing failure.

Another example of sensory hearing impairment is the MANF-deficiency mouse model. MANF (mesencephalic astrocyte-derived neurotrophic factor) resides in the endoplasmic reticulum (ER), where it promotes protein folding homeostasis. Together with an ER-chaperone, BiP (binding immunoglobulin protein or GRP78) regulates the calcium release from the ER store and the activation of unfolded protein response (UPR), which is required for OHC survival. A cKO of MANF caused an upregulation of ER stress marker CHOP, ABR threshold shifts and late OHC loss (Herranen et al., 2020). Interestingly, it was recently published, that Stat3 localizes at the ER (Avalle et al., 2019) and that p-Stat3 Y705 inhibition activates ER stress by promoting the expression of CHOP (Song et al., 2020; Zhang et al., 2014) and upregulates ccl5 expression (Zhang et al., 2014). Therefore, further investigations of OHCs and cell organelles with a cKO of Stat3 might reveal further inside into these connections.

8.4. Altered gene expression in OHCs of Slc26a5-iCre Cre/+, Stat3-fl fl/+ mice

Since Slc26a5-iCre tg/+, Stat3-fl fl/+ mice with Tam 2/5 and Tam 16/19 displayed a hearing impairment, but no OHC loss or neuronal alteration, bulk sequencing was performed to further examine the sensory processing failure. Therefore, a protocol was developed to separate OHCs from other cells of the organ of Corti. Here, OHCs were marked with a specific antibody and selected by magnetic activated cell sorting technology. In the end, mRNA was isolated and sequenced.

Sequencing analysis of Slc26a5-iCre Cre/+, Stat3-fl fl/+ at p28 with Tam 2/5 showed a homeostasis disturbance with alternations of the ABC transporters. In addition, phagocytosis, microtubule depolymerization, but also calcium signaling were highly upregulated. After one week, p35 mice at Slc26a5-iCre Cre/+, Stat3-fl fl/+ with Tam 2/5 displayed a higher rate of RNA catabolic processes and a downregulation of calcium and ABC transporters and membrane regulations. Additionally, in Slc26a5-iCre Cre/+, Stat3-fl fl/+ with Tam 2/5, importin a3 (*Kpna*) was significantly upregulated. Slc26a5-iCre Cre/+, Stat3-fl fl/+ with Tam 16/19 at the age of p35 showed an upregulation of *RANTES* gene (*ccl5*), NF-κB-signaling pathway and cytokine metabolic and a downregulation of extracellular membrane interaction and plasma membrane organization.

ATP-binding cassette (ABC) transporters form one of the largest known protein families at the plasma membrane. By consuming ATP, they actively transport substrates out of the cell. In our cKO OHCs cells, ABC transporter are downregulated, while the homeostasis of OHCs is disturbed. Recently a publication could show that blocking of Stat3 in osteosarcoma cell lines leads to a decreased activity of ABC-transporter (Yang et al., 2023). In the cochlea, ABC

transporter were not identified in the OHCs yet, but in supporting and spiral ganglia cells (Savary et al., 2007), where a defect can also cause non-syndromic hearing loss (Li et al., 2019). This provides evidence that ABC transporters are important in the sensory epithelium of the cochlea and further investigation is needed to determine the role of these in OHCs.

While ABC transporter are more downregulated, phagocytosis and microtubule transport are upregulated in cKO OHCs. Phagocytosis is a form of endocytose, which build phagosome and is a central mechanism in the tissue remodeling, recycling of protein and cell defense. Previous publications found phagocytosis in intact OHCs and suggested being a part of the homeostatic regulation process of specific proteins (Harasztosi et al., 2021; Parker et al., 2022) . According to Stat3, phagocytosis was increased by Stat3-blocking in several cell types (He et al., 2016; Li et al., 2022; Liu et al., 2021). How exactly phagocytosis of intact OHCs occurs and which proteins might be recycled for homeostasis according to Stat3 should be explored in further electrophysiological and molecular biological studies.

Beside phosphorylated Stat3, unphosphorylated Stat3 play a major role in cells. Unphosphorylated Stat3 (U-Stat3) interacts with importin-α3 (*Kpna*), which transports U-Stat3 into the nucleus. Subsequently, NF-κB binds U-Stat3 and promotes oncogenesis such as, among others, the expression of *RANTES* (*ccl5*) gene (Yang et al., 2008). Both genes are higher expressed in our cKO OHCs and could explain on the one side the higher rate of RNA catabolic process and on the other side the NF-κB signaling pathway and cytokine metabolic process. Related results were seen in vascular smooth muscle cells, where *ccl5* and *Kpna* were upregulated after Stat3/NF-κB activation and caused cytokine production and inflammation (Kovacic et al., 2010). Additionally, patients with a Stat3 gain-of-function syndrome develop an early onset autoimmunity due to disturbance of phosphorylation of Stat3 (Vogel et al., 2022). Molecular biological studies of the OHCs can provide information about the concentration of several Stat3-forms in the OHCs and which binding partners of Stat3 exist to identify and analyze possible signaling pathways.

For this purpose, an immortalized cell line such as HEI-OC1 is useful to perform a similar knock-out via CRISPR/Cas9 can be used to perform a similar KO like our mice. This cell line was derived from the auditory organ of an H-2kb-tsA58 transgenic mice used for tumorigenesis due to unlimited cell division. Incubation of these at 33°C and 10% CO2 (permissive conditions) induces expression of an immortalizing gene that triggers de-differentiation and accelerated proliferation; moving the cells to 39°C and 5% CO2 (non-permissive conditions) lead to decreased proliferation and differentiation to cochlear hair cells. Therefore, molecular studies are easier to perform due to the large amount of cells, where binding proteins and signaling pathways of Stat3 in OHCs can be studied in detail.

8.5. Normal morphology and activity of mitochondria in Slc26a5-iCre Cre/+, Stat3-fl fl/+ mice

Beside the main role as transcriptional factor, Stat3 is also integrated in mitochondria, where it functions is a positive regulator of electron transport chain, mitochondrial DNA transcription and calcium homeostasis (Wegrzyn et al., 2009) and represents a major source of ROS (Szczepanek et al., 2012a) via S727 p-Stat3. Therefore, mitochondria in the OHCs were analyzed for morphological structure via electron microscopy.

No mitochondrial loss or defragmentation of the intracellular membrane was detected in OHCs of Slc26a5-iCre Cre/+, Stat3-fl fl/+ mice with Tam 2/5 or Tam 16/19.

This is in difference to other studies, in which KO of Stat3 has resulted changes of the mitochondrial function and morphology. For example, cardiomyocytes of Stat3 -/- mice displayed a significant decreased activity of co electron respiratory chain in mitochondria (Wegrzyn et al., 2009), which resulted in a significant increase in ROS (Szczepanek et al., 2012b). ROS is inducing mitophagy, a selective autophagic degradation of mitochondria (Scherz-Shouval et al., 2007), which can be suppressed by correct Stat3 expression (Szczepanek et al., 2011). Therefore, specific assays are needed to investigate mitochondrial activity and concentration of ROS in OHCs.

Moreover, mitochondria interact tightly with the endoplasmic reticulum by mitochondria-associated endoplasmic reticulum membranes (MAM), which is the functional contact between these organelles (Su et al., 2020). Another study of cardiac dysfunction showed that Stat3 influenced FUNCD1, a protein of MAM, which regulates intracellular calcium level via IP3R. A knock down of Stat3 caused a decreasing of FUNCD1, which leads to an increase of intracellular calcium, but a decrease of mitochondrial membrane potential and intracellular ATP levels (Jiang et al., 2021). In OHCs, little is known about the endoplasmic reticulum (ER) and the calcium homeostasis. However, it could be shown that ER stress leads to an OHC loss in the organ of Corti (Herranen et al., 2020).

Further investigations are needed to understand the role of Stat3 and mitochondrial and ER interaction in OHCs and the hearing process.

8.6. Hearing impairment without structural changes in Fgfr3-iCre Cre/+, Stat3-fl fl/+ mice

After the investigation of cKO of Stat3 in OHCs, the next step was to examine a cKO of Stat3 in supporting cells. Therefore, Fgfr3-iCre mice were crossed with Stat3-fl to induce a cKO of Stat3 in supporting cells before hearing onset (Tam 2/5) and after hearing onset (Tam16/19).

Audiological experiments included DPOAE, click-ABR and tone-ABR. Moreover, immunohistological and morphological investigation of the organ of Corti were performed.

Fgfr3-iCre Cre/+, Stat3-fl fl/+ mice with Tam 2/5 showed no hearing pathology. However, Fgfr3-iCre Cre/+, Stat3-fl fl/+ mice with Tam 16/19 displayed a latency shift at p35 at wave 1 of click ABR as well as an increasing level of tone and click ABR, but not altered DPOAE level. Histological examinations of OHCs and synapses indicated no sensory cell loss, synaptopathy, neuropathy or myelinopathy in these mice.

Similar hearing impairments have been reported in a mouse model with a cytoskeleton disturbance in supporting cells (Chen et al., 2021). Due to a lack of Gas2, a cytoskeletal regulatory protein, hearing loss accompanied by disorganization and destabilization of microtubule bundles in supporting cells. Gas2 mutant mice showed a reduced stiffness of supporting cells, which in turn altered cochlear micromechanics during amplification and propagation of sound waves in the cochlea.

Further mouse models are needed to understand the role of supporting cells due to OHC amplification and mechanoelectrical hearing processes.

8.7. Alteration of posttranslational modification rate of microtubules in supporting cells of Fgfr3-iCre Cre/+, Stat3-fl fl/+

To further investigate the cause of the hearing impairment, the cytoskeleton of supporting cells was analyzed. Therefore, histomorphological examinations of the organ of Corti were performed to analyze the microtubule bundle formation in supporting cells and to evaluate posttranslational modifications of microtubules.

Electron microscopy indicated normal microtubule bundle formations in the base, middle and apex of supporting cells of Fgfr3-iCre Cre/+, Stat3-fl fl/+ mice at the age of p35 with Tam16/19. In contrast to the cochlear supporting cells of control mice, in which detyrosinated, acetylated and polyglutamylated tubulin was expressed, Fgfr3-iCre Cre/+, Stat3-fl fl/+ at the age of p35 with Tam 16/19 showed a reduction of detyrosinated tubulin, especially in its phalangeal processes of Deiters cells. Additionally, the stability of microtubules bundles in pillar and Deiters cells at p28 and p35 seemed reduced, since these structures in immunohistochemical staining were broken.

Posttranslational modifications of microtubules influence the stability of microtubules by affecting the speed of polymerization and depolymerization (Aillaud et al., 2016). While tyrosinated tubulin supports depolymerization, detyrosination maintains polymerization

(Infante et al., 2000; Peris et al., 2009). Decreasing rate of detyronisated tubulin can cause an imbalance of microtubule dynamic and a higher rate of depolymerization of microtubule. If the changes of expression of detyrosinated tubulin effect the stability of the supporting cells can be for example investigated by atomic force microscopy, like it has been performed in another microtubule deficient model in the organ of Corti (Chen et al., 2021). This results underly the hypothesis, that supporting cell stiffness is required for correct cochlear mechanics and that an instable architecture of supporting cells leads to an OHC disfunction and hearing impairment.

Moreover, phosphorylated Stat3 is the antagonist of depolymerization phosphorylated protein Stathmin1 (Moreno et al., 1998; Verma et al., 2009). Together, they controlled the phases of growth and disassembly of microtubules. Therefore, a cKO of Stat3 could prevent depolymerization of tubulin via stathmin1 and an instability of the cytoskeletal in supporting cells. Own initial immunohistochemical examination revealed, that Stathmin1 is highly expressed in Deiters cells of wildtype mice (data not shown). Previous studies showed a disturbance of microtubule dynamics and a defective MTOC polarization by stathmin1 deficiency (Filbert et al., 2012; Machado-Neto et al., 2015; Silva et al., 2013; Tian et al., 2012). Accordingly, investigation of the KO of Stathmin1 in supporting cells should be performed to analyze the role of stathmin1 and Stat3 in the microtubule dynamic in these cells.

8.8. Conclusion

Stat3 has a broad interaction spectrum that is most likely interact in a cell-specific and function-specific manner in cells of the organ of Corti. Whereas a cKO of Stat3 in OHCs before hearing onset results in a severe hearing impairment with disturbance of cell homeostasis a cKO after hearing onset results in a moderate hearing impairment and cytokine metabolism as well as proinflammatory signaling pathway activation. Moreover, no cell or organelle degeneration was seen in the organ of Corti. In supporting cells, a cKO of Stat3 resulted in a mild hearing impairment, while posttranslational modifications of microtubules were altered, which might result in an instability of the organ of Corti. However, further molecular biology experiments should analyze the function and processes of the specific cells to make a clear statement of the function of Stat3 in the cortical organ and the hearing process.

9. Abbreviations

aa	amino acid
ABR	Auditory Brainstem Response
BM	basilar membrane
Cre	recombinase
Cre/+	heterozygote for recombinase
Cre/Cre	homozygote for recombinase
cKO	conditional Knock-Out
Cp	cuticular plate
ctrl	control
DC	Deiters cells
DPOAE	Distortion productive otoacoustic emission
dB	Dezibel
fl	flox
fl/+	heterozygote to flox
fl/fl	homozygote to flox
GO	Gene Ontology
iCre	inducible recombinase
IHC	inner hair cell
KEGG	Kyoto Encyclopedia Gene and Genomes
kHz	kilohertz
loxp	flanked by flox
M	mitochondrion
Mt	microtubule
Mo	modiolus
OHC	outer hair cells

p35	postnatal day 35
PM	plasma membrane
PTM	posttranslational modification
PC	pillar cells
p-Stat3	phosphorylated Stat3
TM	tectorial membrane
S727	serine at amino acid position 727
SC	supporting cells
Sm	Scala media
SPL	sound pressure level
St	Scala tympani
Sv	Scala vestibuli
Syp	synaptophysin
Tam 2/5	tamoxifen injection between p2 and p5
Tam 16/19	tamoxifen injection between p16 and p19
tdTom	tandem dimer Tomato fluorescent protein
tg	transgene
tg/+	heterozygote transgene
tg/tg	homozygote transgene
tub	tubulin
U-Stat3	unphosphorylated Stat3
V	vesicle
W I / W II	Wave I / Wave II of clickABR
Y705	tyrosine at amino acid position 705

10. List of Figures

11. List of Tables

Reference listLiterature

Aillaud, C., Bosc, C., Saoudi, Y., Denarier, E., Peris, L., Sago, L., Taulet, N., Cieren, A., Tort, O., Magiera, M.M., Janke, C., Redeker, V., Andrieux, A., Moutin, M.J. 2016. Evidence for new C-terminally truncated variants of alpha- and beta-tubulins. Mol Biol Cell 27, 640-53.

Anttonen, T., Kirjavainen, A., Belevich, I., Laos, M., Richardson, W.D., Jokitalo, E., Brakebusch, C., Pirvola, U. 2012. Cdc42-dependent structural development of auditory supporting cells is required for wound healing at adulthood. Sci Rep 2, 978.

Avalle, L., Camporeale, A., Morciano, G., Caroccia, N., Ghetti, E., Orecchia, V., Viavattene, D., Giorgi, C., Pinton, P., Poli, V. 2019. STAT3 localizes to the ER, acting as a gatekeeper for ER-mitochondrion Ca2+ fluxes and apoptotic responses. Cell Death & Differentiation 26, 932-942.

Bai, J.-P., Surguchev, A., Montoya, S., Aronson, P.S., Santos-Sacchi, J., Navaratnam, D. 2009. Prestin's Anion Transport and Voltage-Sensing Capabilities Are Independent. Biophys J 96, 3179-3186.

Barden, E.K., Rellinger, E.A., Ortmann, A.J., Ohlemiller, K.K. 2012. Inheritance patterns of noise vulnerability and "protectability" in (C57BL/6J × CBA/J) F1 hybrid mice. J Am Acad Audiol 23, 332-40.

Bartolini, F., Tian, G., Piehl, M., Cassimeris, L., Lewis, S.A., Cowan, N.J. 2005. Identification of a novel tubulin-destabilizing protein related to the chaperone cofactor E. J Cell Sci 118, 1197-207.

Bavi, N., Clark, M.D., Contreras, G.F., Shen, R., Reddy, B.G., Milewski, W., Perozo, E. 2021. The conformational cycle of prestin underlies outer-hair cell electromotility. Nature.

Bazwinsky, I., Hilbig, H., Bidmon, H.J., Rübsamen, R. 2003. Characterization of the human superior olivary complex by calcium binding proteins and neurofilament H (SMI-32). J Comp Neurol 456, 292-303.

Bieniussa, L., Jain, I., Bosch Grau, M., Juergens, L., Hagen, R., Janke, C., Rak, K. 2023. Microtubule and auditory function - an underestimated connection. Semin Cell Dev Biol 137, 74-86.

Boulton, T.G., Zhong, Z., Wen, Z., Darnell, J.E., Jr., Stahl, N., Yancopoulos, G.D. 1995. STAT3 activation by cytokines utilizing gp130 and related transducers involves a secondary modification requiring an H7-sensitive kinase. Proc Natl Acad Sci U S A 92, 6915-9.

Bourk, T.R., Mielcarz, J.P., Norris, B.E. 1981. Tonotopic organization of the anteroventral cochlear nucleus of the cat. Hear Res 4, 215-41.

Braun, M. 2000. Inferior colliculus as candidate for pitch extraction: multiple support from statistics of bilateral spontaneous otoacoustic emissions. Hear Res 145, 130-40.

Bryan, J., Wilson, L. 1971. Are cytoplasmic microtubules heteropolymers? Proc Natl Acad Sci U S A 68, 1762-6.

Cassimeris, L., Spittle, C. 2001. Regulation of microtubule-associated proteins. International review of cytology 210, 163-226.

Chen, T., Rohacek, A.M., Caporizzo, M., Nankali, A., Smits, J.J., Oostrik, J., Lanting, C.P., Kücük, E., Gilissen, C., van de Kamp, J.M., Pennings, R.J.E., Rakowiecki, S.M., Kaestner, K.H., Ohlemiller, K.K., Oghalai, J.S., Kremer, H., Prosser, B.L., Epstein, D.J. 2021. Cochlear supporting cells require GAS2 for cytoskeletal architecture and hearing. Dev Cell 56, 1526-1540.e7.

Chessum, L., Matern, M.S., Kelly, M.C., Johnson, S.L., Ogawa, Y., Milon, B., McMurray, M., Driver, E.C., Parker, A., Song, Y., Codner, G., Esapa, C.T., Prescott, J., Trent, G., Wells, S., Dragich, A.K., Frolenkov, G.I., Kelley, M.W., Marcotti, W., Brown, S.D.M., Elkon, R., Bowl, M.R., Hertzano, R. 2018. Helios is a key transcriptional regulator of outer hair cell maturation. Nature 563, 696-700.

Cho, T.H., Fischer, C., Nighoghossian, N., Hermier, M., Sindou, M., Mauguière, F. 2005. Auditory and electrophysiological patterns of a unilateral lesion of the lateral lemniscus. Audiol Neurootol 10, 153-8.

Chung, C.D., Liao, J., Liu, B., Rao, X., Jay, P., Berta, P., Shuai, K. 1997. Specific inhibition of Stat3 signal transduction by PIAS3. Science 278, 1803-5.

Cox, B.C., Liu, Z., Lagarde, M.M., Zuo, J. 2012. Conditional gene expression in the mouse inner ear using Cre-loxP. J Assoc Res Otolaryngol 13, 295-322.

Davies, R.A. 2016. Chapter 11 - Audiometry and other hearing tests. In: Furman, J.M., Lempert, T., (Eds.), Handbook of Clinical Neurology, Vol. 137. Elsevier. pp. 157-176.

Delmaghani, S., del Castillo, F.J., Michel, V., Leibovici, M., Aghaie, A., Ron, U., Van Laer, L., Ben-Tal, N., Van Camp, G., Weil, D., Langa, F., Lathrop, M., Avan, P., Petit, C. 2006. Mutations in the gene encoding pejvakin, a newly identified protein of the afferent auditory pathway, cause DFNB59 auditory neuropathy. Nature genetics 38, 770-8.

Delmaghani, S., Defourny, J., Aghaie, A., Beurg, M., Dulon, D., Thelen, N., Perfettini, I., Zelles, T., Aller, M., Meyer, A., Emptoz, A., Giraudet, F., Leibovici, M., Dartevelle, S., Soubigou, G., Thiry, M., Vizi, E.S., Safieddine, S., Hardelin, J.P., Avan, P., Petit, C. 2015. Hypervulnerability to Sound Exposure through Impaired Adaptive Proliferation of Peroxisomes. Cell 163, 894-906.

Diallo, M., Herrera, F. 2022. The role of understudied post-translational modifications for the behavior and function of Signal Transducer and Activator of Transcription 3. The FEBS Journal 289, 6235-6255.

Elliott, K.L., Kersigo, J., Lee, J.H., Jahan, I., Pavlinkova, G., Fritzsch, B., Yamoah, E.N. 2021. Developmental Changes in Peripherin-eGFP Expression in Spiral Ganglion Neurons. Front Cell Neurosci 15, 678113.

Erickson, H.P. 1974. Assembly of microtubules from preformed, ring-shaped protofilaments and 6-S tubulin. J Supramol Struct 2, 393-411.

Fang, J., Zhang, W.C., Yamashita, T., Gao, J., Zhu, M., Zuo, J. 2012. Outer hair cell–specific prestin-CreER(T2) knockin mouse lines. Genesis 50, 124-31.

Filbert, E.L., Le Borgne, M., Lin, J., Heuser, J.E., Shaw, A.S. 2012. Stathmin regulates microtubule dynamics and microtubule organizing center polarization in activated T cells. J Immunol 188, 5421-7.

Frolenkov, G.I., Belyantseva, I.A., Friedman, T.B., Griffith, A.J. 2004. Genetic insights into the morphogenesis of inner ear hair cells. Nat Rev Genet 5, 489-98.

Fuchs, P.A., Lauer, A.M. 2019. Efferent inhibition of the cochlea. Cold Spring Harbor perspectives in medicine 9, a033530.

Gavet, O., Ozon, S., Manceau, V., Lawler, S., Curmi, P., Sobel, A. 1998. The stathmin phosphoprotein family: intracellular localization and effects on the microtubule network. J Cell Sci 111 (Pt 22), 3333-46.

Gough, D.J., Koetz, L., Levy, D.E. 2013. The MEK-ERK pathway is necessary for serine phosphorylation of mitochondrial STAT3 and Ras-mediated transformation. PLoS One 8, e83395.

Harasztosi, C., Klenske, E., Gummer, A.W. 2021. Vesicle traffic in the outer hair cell. European Journal of Neuroscience 54, 4755-4767.

He, G.L., Luo, Z., Shen, T.T., Li, P., Yang, J., Luo, X., Chen, C.H., Gao, P., Yang, X.S. 2016. Inhibition of STAT3- and MAPK-dependent PGE(2) synthesis ameliorates phagocytosis of fibrillar β-amyloid peptide (1-42) via EP2 receptor in EMF-stimulated N9 microglial cells. J Neuroinflammation 13, 296.

Herranen, A., Ikäheimo, K., Lankinen, T., Pakarinen, E., Fritzsch, B., Saarma, M., Lindahl, M., Pirvola, U. 2020. Deficiency of the ER-stress-regulator MANF triggers progressive outer hair cell death and hearing loss. Cell Death & Disease 11, 100.

Infante, A.S., Stein, M.S., Zhai, Y., Borisy, G.G., Gundersen, G.G. 2000. Detyrosinated (Glu) microtubules are stabilized by an ATP-sensitive plus-end cap. J Cell Sci 113 (Pt 22), 3907-19.

Janke, C., Magiera, M.M. 2020. The tubulin code and its role in controlling microtubule properties and functions. Nat Rev Mol Cell Biol 21, 307-326.

Jensen-Smith, H.C., Eley, J., Steyger, P.S., Ludueña, R.F., Hallworth, R. 2003. Cell type-specific reduction of β tubulin isotypes synthesized in the developing gerbil organ of Corti. Journal of Neurocytology 32, 185-197.

Jiang, T., Peng, D., Shi, W., Guo, J., Huo, S., Men, L., Zhang, C., Li, S., Lv, J., Lin, L. 2021. IL-6/STAT3 Signaling Promotes Cardiac Dysfunction by Upregulating FUNDC1-Dependent Mitochondria-Associated Endoplasmic Reticulum Membranes Formation in Sepsis Mice. Front Cardiovasc Med 8, 790612.

Juergens, L., Bieniussa, L., Voelker, J., Hagen, R., Rak, K. 2020. Spatio-temporal distribution of tubulin-binding cofactors and posttranslational modifications of tubulin in the cochlea of mice. Histochem Cell Biol.

Kelly, M., Chen, P. 2007. Shaping the mammalian auditory sensory organ by the planar cell polarity pathway. Int J Dev Biol 51, 535-47.

Knirsch, M., Brandt, N., Braig, C., Kuhn, S., Hirt, B., Munkner, S., Knipper, M., Engel, J. 2007. Persistence of Ca(v)1.3 Ca2+ channels in mature outer hair cells supports outer hair cell afferent signaling. J Neurosci 27, 6442-51.

Kovacic, J.C., Gupta, R., Lee, A.C., Ma, M., Fang, F., Tolbert, C.N., Walts, A.D., Beltran, L.E., San, H., Chen, G., St Hilaire, C., Boehm, M. 2010. Stat3-dependent acute Rantes production in vascular smooth muscle cells modulates inflammation following arterial injury in mice. J Clin Invest 120, 303-14.

Levy, D.E., Lee, C.-k. 2002. What does Stat3 do? The Journal of Clinical Investigation 109, 1143-1148.

Li, M., Mei, L., He, C., Chen, H., Cai, X., Liu, Y., Tian, R., Tian, Q., Song, J., Jiang, L., Liu, C., Wu, H., Li, T., Liu, J., Li, X., Yi, Y., Yan, D., Blanton, S.H., Hu, Z., Liu, X., Li, J., Ling, J., Feng, Y. 2019. Extrusion pump ABCC1 was first linked with nonsyndromic hearing loss in humans by stepwise genetic analysis. Genet Med 21, 2744-2754.

Li, Y., Song, Z., Han, Q., Zhao, H., Pan, Z., Lei, Z., Zhang, J. 2022. Targeted inhibition of STAT3 induces immunogenic cell death of hepatocellular carcinoma cells via glycolysis. Mol Oncol 16, 2861-2880.

Liberman, M.C., Gao, J., He, D.Z., Wu, X., Jia, S., Zuo, J. 2002. Prestin is required for electromotility of the outer hair cell and for the cochlear amplifier. Nature 419, 300-4.

Liem, F., Zaehle, T., Burkhard, A., Jäncke, L., Meyer, M. 2012. Cortical thickness of supratemporal plane predicts auditory N1 amplitude. Neuroreport 23, 1026-30.

Lim, D.J., Anniko, M. 1985. Developmental morphology of the mouse inner ear. A scanning electron microscopic observation. Acta Otolaryngol Suppl 422, 1-69.

Liu, H., Zhou, Y.C., Song, W. 2021. Involvement of IL-10R/STAT3 pathway in amyloid β clearance by microlgia in Alzheimer's disease. Int Immunopharmacol 101, 108263.

Liu, L., McBride, K.M., Reich, N.C. 2005. STAT3 nuclear import is independent of tyrosine phosphorylation and mediated by importin-alpha3. Proc Natl Acad Sci U S A 102, 8150-5.

Machado-Neto, J.A., de Melo Campos, P., Favaro, P., Lazarini, M., da Silva Santos Duarte, A., Lorand-Metze, I., Costa, F.F., Saad, S.T., Traina, F. 2015. Stathmin 1 inhibition amplifies ruxolitinib-induced apoptosis in JAK2V617F cells. Oncotarget 6, 29573-84.

Macias, E., Rao, D., Carbajal, S., Kiguchi, K., DiGiovanni, J. 2014. Stat3 binds to mtDNA and regulates mitochondrial gene expression in keratinocytes. J Invest Dermatol 134, 1971-1980.

Maison, S.F., Adams, J.C., Liberman, M.C. 2003. Olivocochlear innervation in the mouse: immunocytochemical maps, crossed versus uncrossed contributions, and transmitter colocalization. J Comp Neurol 455, 406-16.

Meier, J.A., Hyun, M., Cantwell, M., Raza, A., Mertens, C., Raje, V., Sisler, J., Tracy, E., Torres-Odio, S., Gispert, S., Shaw, P.E., Baumann, H., Bandyopadhyay, D., Takabe, K., Larner, A.C. 2017. Stress-induced dynamic regulation of mitochondrial STAT3 and its association with cyclophilin D reduce mitochondrial ROS production. Sci Signal 10.

Mohr, A., Chatain, N., Domoszlai, T., Rinis, N., Sommerauer, M., Vogt, M., Müller-Newen, G. 2012. Dynamics and non-canonical aspects of JAK/STAT signalling. European journal of cell biology 91, 524-532.

Moralee, S.J. 1996. Rosenthal and the spiral canal of the modiolus. Am J Otol 17, 171.

Moreno, F.J., Avila, J. 1998. Phosphorylation of stathmin modulates its function as a microtubule depolymerizing factor. Mol Cell Biochem 183, 201-9.

Ota, C.Y., Kimura, R.S. 1980. Ultrastructural study of the human spiral ganglion. Acta Otolaryngol 89, 53-62.

Parker, A., Parham, K., Skoe, E. 2022. Noise exposure levels predict blood levels of the inner ear protein prestin. Scientific Reports 12, 1154.

Paturle-Lafanechere, L., Edde, B., Denoulet, P., Van Dorsselaer, A., Mazarguil, H., Le Caer, J.P., Wehland, J., Job, D. 1991. Characterization of a major brain tubulin variant which cannot be tyrosinated. Biochemistry 30, 10523-8.

Peris, L., Wagenbach, M., Lafanechere, L., Brocard, J., Moore, A.T., Kozielski, F., Job, D., Wordeman, L., Andrieux, A. 2009. Motor-dependent microtubule disassembly driven by tubulin tyrosination. J Cell Biol 185, 1159-66.

Portran, D., Schaedel, L., Xu, Z., Thery, M., Nachury, M.V. 2017. Tubulin acetylation protects long-lived microtubules against mechanical ageing. Nat Cell Biol 19, 391-398.

Rudiger, M., Wehland, J., Weber, K. 1994. The carboxy-terminal peptide of detyrosinated alpha tubulin provides a minimal system to study the substrate specificity of tubulin-tyrosine ligase. Eur J Biochem 220, 309-20.

Satir, P., Christensen, S.T. 2007. Overview of structure and function of mammalian cilia. Annu Rev Physiol 69, 377-400.

Savary, E., Hugnot, J.P., Chassigneux, Y., Travo, C., Duperray, C., Van De Water, T., Zine, A. 2007. Distinct population of hair cell progenitors can be isolated from the postnatal mouse cochlea using side population analysis. Stem Cells 25, 332-9.

Scherz-Shouval, R., Elazar, Z. 2007. ROS, mitochondria and the regulation of autophagy. Trends Cell Biol 17, 422-7.

Schwander, M., Sczaniecka, A., Grillet, N., Bailey, J.S., Avenarius, M., Najmabadi, H., Steffy, B.M., Federe, G.C., Lagler, E.A., Banan, R., Hice, R., Grabowski-Boase, L., Keithley, E.M., Ryan, A.F., Housley, G.D., Wiltshire, T., Smith, R.J., Tarantino, L.M., Muller, U. 2007. A forward genetics screen in mice identifies recessive deafness traits and reveals that pejvakin is essential for outer hair cell function. J Neurosci 27, 2163-75.

Selvaraj, B.T., Frank, N., Bender, F.L., Asan, E., Sendtner, M. 2012. Local axonal function of STAT3 rescues axon degeneration in the pmn model of motoneuron disease. J Cell Biol 199, 437-51.

Silva, V.C., Cassimeris, L. 2013. Stathmin and microtubules regulate mitotic entry in HeLa cells by controlling activation of both Aurora kinase A and Plk1. Mol Biol Cell 24, 3819-31.

Simmons, D.D. 2002. Development of the inner ear efferent system across vertebrate species. J Neurobiol 53, 228-50.

Slepecky, N.B., Cefaratti, L.K., Yoo, T.J. 1992. Type II and type IX collagen form heterotypic fibers in the tectorial membrane of the inner ear. Matrix 12, 80-6.

Song, L., Santos-Sacchi, J. 2010. Conformational State-Dependent Anion Binding in Prestin: Evidence for Allosteric Modulation. Biophys J 98, 371-376.

Song, M., Wang, C., Yang, H., Chen, Y., Feng, X., Li, B., Fan, H. 2020. P-STAT3 Inhibition Activates Endoplasmic Reticulum Stress-Induced Splenocyte Apoptosis in Chronic Stress. Frontiers in Physiology 11.

Stahl, N., Yancopoulos, G.D. 1993. The alphas, betas, and kinases of cytokine receptor complexes. Cell 74, 587-90.

Stahl, N., Farruggella, T.J., Boulton, T.G., Zhong, Z., Darnell, J.E., Jr., Yancopoulos, G.D. 1995. Choice of STATs and other substrates specified by modular tyrosine-based motifs in cytokine receptors. Science 267, 1349-53.

Starr, A., Rance, G. 2015. Auditory neuropathy. Handb Clin Neurol 129, 495-508.

Su, Y., Huang, X., Huang, Z., Huang, T., Xu, Y., Yi, C. 2020. STAT3 Localizes in Mitochondria-Associated ER Membranes Instead of in Mitochondria. Front Cell Dev Biol 8, 274.

Szczepanek, K., Lesnefsky, E.J., Larner, A.C. 2012a. Multi-tasking: nuclear transcription factors with novel roles in the mitochondria. Trends Cell Biol 22, 429-37.

Szczepanek, K., Chen, Q., Larner, A.C., Lesnefsky, E.J. 2012b. Cytoprotection by the modulation of mitochondrial electron transport chain: the emerging role of mitochondrial STAT3. Mitochondrion 12, 180-9.

Szczepanek, K., Chen, Q., Derecka, M., Salloum, F.N., Zhang, Q., Szelag, M., Cichy, J., Kukreja, R.C., Dulak, J., Lesnefsky, E.J., Larner, A.C. 2011. Mitochondrial-targeted Signal transducer and

activator of transcription 3 (STAT3) protects against ischemia-induced changes in the electron transport chain and the generation of reactive oxygen species. J Biol Chem 286, 29610-20.
Takeda, K., Kaisho, T., Yoshida, N., Takeda, J., Kishimoto, T., Akira, S. 1998. Stat3 Activation Is Responsible for IL-6-Dependent T Cell Proliferation Through Preventing Apoptosis: Generation and Characterization of T Cell-Specific Stat3-Deficient Mice. The Journal of Immunology 161, 4652-4660.
Tammineni, P., Anugula, C., Mohammed, F., Anjaneyulu, M., Larner, A.C., Sepuri, N.B. 2013. The import of the transcription factor STAT3 into mitochondria depends on GRIM-19, a component of the electron transport chain. J Biol Chem 288, 4723-32.
Tian, X., Tian, Y., Sarich, N., Wu, T., Birukova, A.A. 2012. Novel role of stathmin in microtubule-dependent control of endothelial permeability. Faseb j 26, 3862-74.
Valenzuela, P., Quiroga, M., Zaldivar, J., Rutter, W.J., Kirschner, M.W., Cleveland, D.W. 1981. Nucleotide and corresponding amino acid sequences encoded by alpha and beta tubulin mRNAs. Nature 289, 650-5.
Verma, N.K., Dourlat, J., Davies, A.M., Long, A., Liu, W.Q., Garbay, C., Kelleher, D., Volkov, Y. 2009. STAT3-stathmin interactions control microtubule dynamics in migrating T-cells. J Biol Chem 284, 12349-62.
Vogel, T.P., Leiding, J.W., Cooper, M.A., Forbes Satter, L.R. 2022. STAT3 gain-of-function syndrome. Front Pediatr 10, 770077.
Wan, J., Fu, A.K., Ip, F.C., Ng, H.K., Hugon, J., Page, G., Wang, J.H., Lai, K.O., Wu, Z., Ip, N.Y. 2010. Tyk2/STAT3 signaling mediates beta-amyloid-induced neuronal cell death: implications in Alzheimer's disease. J Neurosci 30, 6873-81.
Wareham, L.K., Echevarria, F.D., Sousa, J.L., Konlian, D.O., Dallas, G., Formichella, C.R., Sankaran, P., Goralski, P.J., Gustafson, J.R., Sappington, R.M. 2021. Interleukin-6 promotes microtubule stability in axons via Stat3 protein-protein interactions. iScience 24, 103141.
Webster, D.R., Gundersen, G.G., Bulinski, J.C., Borisy, G.G. 1987. Differential turnover of tyrosinated and detyrosinated microtubules. Proc Natl Acad Sci U S A 84, 9040-4.
Wegrzyn, J., Potla, R., Chwae, Y.J., Sepuri, N.B., Zhang, Q., Koeck, T., Derecka, M., Szczepanek, K., Szelag, M., Gornicka, A., Moh, A., Moghaddas, S., Chen, Q., Bobbili, S., Cichy, J., Dulak, J., Baker, D.P., Wolfman, A., Stuehr, D., Hassan, M.O., Fu, X.Y., Avadhani, N., Drake, J.I., Fawcett, P., Lesnefsky, E.J., Larner, A.C. 2009. Function of mitochondrial Stat3 in cellular respiration. Science 323, 793-7.
Wilson, T., Omelchenko, I., Foster, S., Zhang, Y., Shi, X., Nuttall, A.L. 2014. JAK2/STAT3 inhibition attenuates noise-induced hearing loss. PLoS One 9, e108276.
Winer, J.A. 1984. The human medial geniculate body. Hear Res 15, 225-47.
Yadav, P., Selvaraj, B.T., Bender, F.L.P., Behringer, M., Moradi, M., Sivadasan, R., Dombert, B., Blum, R., Asan, E., Sauer, M., Julien, J.-P., Sendtner, M. 2016. Neurofilament depletion improves microtubule dynamics via modulation of Stat3/stathmin signaling. Acta Neuropathol 132, 93-110.
Yang, J., Stark, G.R. 2008. Roles of unphosphorylated STATs in signaling. Cell Research 18, 443-451.
Yang, J., Liao, X., Agarwal, M.K., Barnes, L., Auron, P.E., Stark, G.R. 2007. Unphosphorylated STAT3 accumulates in response to IL-6 and activates transcription by binding to NFkappaB. Genes Dev 21, 1396-408.
Yang, R., Rincon, M. 2016. Mitochondrial Stat3, the Need for Design Thinking. Int J Biol Sci 12, 532-44.
Yang, Y., Chen, Y., Liu, J., Zhang, B., Yang, L., Xue, J., Zhang, Z., Qin, L., Bian, R. 2023. MiR-125b-5p/STAT3 Axis Regulates Drug Resistance in Osteosarcoma Cells by Acting on ABC Transporters. Stem Cells Int 2023, 9997676.
You, L., Wang, Z., Li, H., Shou, J., Jing, Z., Xie, J., Sui, X., Pan, H., Han, W. 2015. The role of STAT3 in autophagy. Autophagy 11, 729-39.
Young, A., Cornejo, J., Spinner, A.J.S. 2020. Auditory Brainstem Response.

Young, K.M., Mitsumori, T., Pringle, N., Grist, M., Kessaris, N., Richardson, W.D. 2010. An Fgfr3-iCreER(T2) transgenic mouse line for studies of neural stem cells and astrocytes. Glia 58, 943-953.

Yu, H., Pardoll, D., Jove, R. 2009. STATs in cancer inflammation and immunity: a leading role for STAT3. Nat Rev Cancer 9, 798-809.

Yu, H., Lee, H., Herrmann, A., Buettner, R., Jove, R. 2014. Revisiting STAT3 signalling in cancer: new and unexpected biological functions. Nat Rev Cancer 14, 736-46.

Zhang, Y., Liao, S., Fan, W., Wei, W., Wang, C., Sun, S. 2014. Tunicamycin-induced ER stress regulates chemokine CCL5 expression and secretion via STAT3 followed by decreased transmigration of MCF-7 breast cancer cells. Oncol Rep 32, 2769-76.

12. Curriculum vita

13. Publication list

Bieniussa L, Kahraman B, Skornicka J, Schulte A, Voelker J, Jablonka S, Hagen R, Rak K. Pegylated Insulin-Like Growth Factor 1 attenuates Hair Cell Loss and promotes Presynaptic Maintenance of Medial Olivocochlear Cholinergic Fibers in the Cochlea of the Progressive Motor Neuropathy Mouse. Front Neurol. 2022 Jun 3;13:885026. doi: 10.3389/fneur.2022.885026. PMID: 35720065; PMCID: PMC9203726.

Juergens L*, **Bieniussa L***, Voelker J, Hagen R, Rak K. Spatio-temporal distribution of tubulin-binding cofactors and posttranslational modifications of tubulin in the cochlea of mice. Histochem Cell Biol. 2020 Dec;154(6):671-681. doi: 10.1007/s00418-020-01905-6. Epub 2020 Jul 25. PMID: 32712744; PMCID: PMC7723944. (*contributed equally)

Bieniussa L, Jain I, Bosch Grau M, Juergens L, Hagen R, Janke C, Rak K. Microtubule and auditory function - an underestimated connection. Semin Cell Dev Biol. 2023 Mar 15;137:74-86. doi: 10.1016/j.semcdb.2022.02.004. Epub 2022 Feb 8. PMID: 35144861.

Engert J, Spahn B, **Bieniussa L**, Hagen R, Rak K, Voelker J. Neurogenic Stem Cell Niche in the Auditory Thalamus: In Vitro Evidence of Neural Stem Cells in the Rat Medial Geniculate Body. Life (Basel). 2023 May 15;13(5):1188. doi: 10.3390/life13051188. PMID: 37240833; PMCID: PMC10223215.

Schulte A, **Bieniussa L**, Gupta R, Samtleben S, Bischler T, Doering K, Sodmann P, Rittner H, Blum R. Homeostatic calcium fluxes, ER calcium release, SOCE, and calcium oscillations in cultured astrocytes are interlinked by a small calcium toolkit. Cell Calcium. 2022 Jan;101:102515. doi: 10.1016/j.ceca.2021.102515. Epub 2021 Dec 3. PMID: 34896701.

Voelker J, Engert J, Voelker C, **Bieniussa L,** Schendzielorz P, Hagen R, Rak K. Different Neurogenic Potential in the Subnuclei of the Postnatal Rat Cochlear Nucleus. Stem Cells Int. 2021 Apr 5;2021:8871308. doi: 10.1155/2021/8871308. PMID: 33880121; PMCID: PMC8046557.

Engert J, Rak K, **Bieniussa L**, Scholl M, Hagen R, Voelker J. Evaluation of the Neurogenic Potential in the Rat Inferior Colliculus from Early Postnatal Days Until Adulthood. Mol Neurobiol. 2021 Feb;58(2):719-734. doi: 10.1007/s12035-020-02151-6. Epub 2020 Oct 3. PMID: 33011856; PMCID: PMC7843480.

Völker J, Engert J, Völker C, **Bieniussa L**, Schendzielorz P, Hagen R, Rak K. Isolation and Characterization of Neural Stem Cells from the Rat Inferior Colliculus. Stem Cells Int. 2019 Oct 29;2019:5831240. doi: 10.1155/2019/5831240. PMID: 31781242; PMCID: PMC6875198.

14. Danksagung

Ich bedanke mich bei meinem Doktorvater, **Prof. Dr. med. Kristen Rak**, für die Möglichkeit zur Erstellung meiner Doktorarbeit in seinen Laboratorien. Gleichzeitig gab er mir die Gelegenheit über mich hinaus zu wachsen und Aufgaben zu bearbeiten, die nicht jeder Doktorand bekommt, um mich zusätzlich auf die Welt der Wissenschaft vorzubereiten. Außerdem ermutigte er mich stets die Projekte weiter zu bearbeiten, auch wenn es schlechte Zeiten gab. Durch seine Hingabe an die Forschung war es ebenfalls möglich Kooperationen zu schaffen, die mir nochmals das Potenzial gaben zu wachsen. Vielen Dank, Kristen, für deine Bemühungen, Problemlösungen, deine Menschlichkeit und dein Verständnis.

Ich bedanke mich bei **Prof. Dr. med. Dr. h.c. Rudolf Hagen** für sein großes Interesse an meinem Forschungsgebiet. Durch das Zusammenkommen an Forschungstreffen und den kleinen einfachen Fragen seinerseits zu meinem Thema, konnte ich den Fokus wieder scharf stellen und Einblicke in der die klinische Forschung der Hals-Nasen-Ohrenheilkunde zu gewinnen.

Ein besonderer Dank gilt **Prof. Dr. rer. nat. Robert Blum**, der mir die Chance gab vor langer Zeit mich als Frisch-Wissenschaftlerin zu etablieren und meine Fähigkeiten zu formen. Ich danke dir für die zusätzliche Betreuung meiner Doktorarbeit und auch **Dr. rer. nat. Annemarie Sodmann (geb. Schulte)** und **Felicitas Schlott** bei der Mithilfe der Sequenzierungsanalyse.

Vielen Dank an **Prof. Dr. rer. nat. Rudolf Martini** und **Dr. rer. nat. Dennis Klein**, dass ich im Team mitwirken konnte und an der Beteilung an Seminaren während meiner Doktorandenzeit. Dies ermöglichte meine Präsentationsskills und Auffassungsgabe zu verbessern. Auch bezüglich Auswertungen waren sie zu Rat und Tat bereit.

Zusätzlich bedanke ich mich an meine Kollegen **Dr. med. Johannes Völker, Dr. med. Jonas Engert, Baran Kahraman**, sowie **Johannes Skornicka** und **Clara Stolte**. Durch das Arbeitsumfeld mit euch konnten einige Meilensteine erzielt werden. Vielen Dank euch dafür.

Außerdem gebürt Frau **PD Dr. rer. nat. Nicole Wagner** und **Karin Reinfurt-Gehm** im Institut der Anatomie und Zellbiologie ein besonderer Dank für die tolle Unterstützung bei der Aufarbeitung von Cochlea-Proben für das Elektronenmikroskop, sowie die Betreuung bei den vielen Aufnahmestunden am Mikroskop. Genauso bedanke ich mich an **Dr. rer. nat. Tom Gräfenhan** und **Dr. rer. nat. Panagiota Arampathi** der Core Unit Systememedizin des Rudolf-Virchow-Zentrums für die Bulk-Sequenzierung.

Schlussendlich danke ich meiner **Familie** und den Menschen, die immer an mich geglaubt haben und mich all die Jahre stetig wieder ermutigt haben nicht aufzugeben.

An alle: **Vielen herzlichen Dank! Merći! Thank you! Mulţumesc!**